Technical Report Documentation Page

1. Report No.	2. Government Accession No.	3. Recipient's Catalog No.
FHWA/TX-05/0-4468-1		

4. Title and Subtitle	5. Report Date
PRELIMINARY FATIGUE ANALYSIS OF A COMMON TxDOT HOT MIX ASPHALT CONCRETE MIXTURE	May 2004 Resubmitted: January 2005 Resubmitted: June 2005
	6. Performing Organization Code

7. Author(s)	8. Performing Organization Report No.
Lubinda F. Walubita, Amy Epps Martin, Sung Hoon Jung, Charles J. Glover, Arif Chowdhury, Eun Sug Park, and Robert L. Lytton	Report 0-4468-1

9. Performing Organization Name and Address	10. Work Unit No. (TRAIS)
Texas Transportation Institute The Texas A&M University System College Station, Texas 77843-3135	11. Contract or Grant No. Project 0-4468

12. Sponsoring Agency Name and Address	13. Type of Report and Period Covered
Texas Department of Transportation Research and Technology Implementation Office P. O. Box 5080 Austin, Texas 78763-5080	Technical Report: September 2002-April 2004
	14. Sponsoring Agency Code

15. Supplementary Notes

Project performed in cooperation with the Texas Department of Transportation and the Federal Highway Administration.

Project Title: Evaluate the Fatigue Resistance of Rut Resistance Mixes.

URL: http://tti.tamu.edu/documents/0-4468-1.pdf

16. Abstract

Over the past decade, the Texas Department of Transportation (TxDOT) focused research efforts on improving mixture design to preclude rutting in the early life of the pavement, which also offered increased resistance to moisture damage, but fatigue cracking may surface in the long term particularly if the binder stiffens excessively due to aging. The primary goal of this project is to evaluate and recommend a fatigue analysis system for TxDOT designs to ensure adequate mixture fatigue performance in a particular pavement structure under specific environmental and loading conditions. A secondary goal of comparing fatigue resistance of commonly used TxDOT mixtures including investigating the effects of aging will also be realized. Two fatigue analysis approaches, the mechanistic empirical (ME) and the calibrated mechanistic (CMSE) with surface energy measurements, based on one common TxDOT mixture including the effects of aging are presented in this interim report. Results showed that both the ME and CMSE approaches were comparable in terms of predicting mixture fatigue resistance. The results also showed that aging reduces the mixture's resistance to fracture damage and its ability to heal. A preliminary comparison of the ME and CMSE approaches showed that although the ME analysis procedure is simple and straightforward, there is a relatively high variability in both the mixture air voids (AV) and the final fatigue results. The input data for the CMSE approach are very comprehensive and require numerous auxiliary tests that are necessary to account for all the HMAC mixture properties that affect fatigue performance. However, research is still ongoing to further:(1) investigate the effects of binder aging on the HMAC mixture fatigue properties, (2) review other fatigue analysis approaches including the proposed NCHRP 1-37A Pavement Design Guide, and (3) investigate the applicability and validity of the CMSE fatigue analysis approach, and finally recommend an appropriate fatigue analysis system to TxDOT.

17. Key Words	18. Distribution Statement
Asphalt, Fatigue, Aging, Fracture, Microcracking, Healing, Environment, Mechanistic Empirical (ME), Calibrated Mechanistic (CM), Surface Energy (SE), Anisotropy (AN)	No restrictions. This document is available to the public through NTIS: National Technical Information Service Springfield, Virginia 22161 http://www.ntis.gov

19. Security Classif.(of this report)	20. Security Classif.(of this page)	21. No. of Pages	22. Price
Unclassified	Unclassified	142	

Form DOT F 1700.7 (8-72) **Reproduction of completed page authorize**

PRELIMINARY FATIGUE ANALYSIS OF A COMMON TxDOT HOT MIX ASPHALT CONCRETE MIXTURE

by

Lubinda F. Walubita
Graduate Research Assistant, Texas Transportation Institute

Amy Epps Martin
Assistant Research Scientist, Texas Transportation Institute

Sung Hoon Jung
Graduate Research Assistant, Texas Transportation Institute

Charles J. Glover
Research Engineer, Texas Transportation Institute

Arif Chowdhury
Associate Transportation Researcher, Texas Transportation Institute

Eun Sug Park
Assistant Research Scientist, Texas Transportation Institute

and

Robert L. Lytton
Research Engineer, Texas Transportation Institute

Report 0-4468-1
Project 0-4468
Project Title: Evaluate the Fatigue Resistance of Rut Resistance Mixes

Performed in Cooperation with the
Texas Department of Transportation
and the
Federal Highway Administration

May 2004
Resubmitted: January 2005
Resubmitted: June 2005

TEXAS TRANSPORTATION INSTITUTE
The Texas A&M University System
College Station, Texas 77843-3135

DISCLAIMER

The contents of this report reflect the views of the authors, who are responsible for the facts and the accuracy of the data presented herein. The contents do not necessarily reflect the official view or policies of the Federal Highway Administration (FHWA) and Texas Department of Transportation (TxDOT). This report does not constitute a standard, specification, or regulation, nor is it intended for construction, bidding, or permit purposes. Trade names were used solely for information and not for product endorsement. The engineers in charge were Amy Epps Martin, P.E. (Texas No. 91053) and Charles J. Glover, P.E. (Texas No. 48732).

ACKNOWLEDGMENTS

This project was conducted for TxDOT, and the authors thank TxDOT and FHWA for their support in funding this research project. In particular, the guidance and technical assistance provided by the Project Director (PD) Gregory S. Cleveland of TxDOT, the Project Coordinator (PC) James Travis of the FHWA, and German Claros of the Research and Technology Implementation (RTI) office are greatly appreciated. Special thanks are also due to Lee Gustavus, Ricky Canatella, Scott Hubley, Sharath Krishnamurthy, Amit Bhasin, Jeffrey Perry, and Andrew Fawcett from the Texas Transportation Institute (TTI) and Texas Engineering Experiment Station (TEES) for their help in specimens/samples preparation, laboratory testing, and data analysis. The various TxDOT district offices that provided the material mix-designs and assistance in material procurement are also thanked.

TABLE OF CONTENTS

TABLE OF CONTENTS (continued)

TABLE OF CONTENTS (continued)

TABLE OF CONTENTS (continued)

LIST OF FIGURES

Figure **Page**

LIST OF FIGURES (continued)

LIST OF TABLES

Table **Page**

CHAPTER 1
INTRODUCTION

Hot mix asphalt concrete (HMAC) mixtures are designed to resist aging and distress induced by traffic loading (rutting and fatigue cracking) and changing environmental conditions (thermal cracking). Over the past decade the Texas Department of Transportation (TxDOT) focused research efforts on improving mixture design to preclude rutting in the early life of the pavement. Improvements in rutting resistance also offered increased resistance to moisture damage, but fatigue cracking may surface in the long term in stiff materials and pavement structures or materials that age rapidly. The primary goal of this project is to evaluate and recommend a fatigue mix-design and analysis system to ensure adequate performance under specified environmental and loading conditions in a particular pavement structure. A secondary goal of comparing fatigue resistance of two commonly used TxDOT mixtures will also be realized.

WORK PLAN

To accomplish these goals, researchers are utilizing four approaches to predict fatigue lives of two TxDOT mixtures commonly used for rutting resistance and overall performance under representative environmental conditions and typical loading conditions in standard pavement sections. The selected approaches include the following:

- the mechanistic-empirical approach developed during the Strategic Highway Research Program (SHRP) using the bending beam fatigue test (*1*);
- the proposed National Co-operative Highway Research Program (NCHRP) 1-37A 2002 Pavement Design Guide using the dynamic modulus test (*2*,*3*);
- a calibrated mechanistic approach developed at Texas A&M that requires strength, and repeated tests in uniaxial tension and creep tests in uniaxial compression for material characterization and monitoring dissipated pseudo strain energy (*4*); and

- an updated calibrated mechanistic approach developed at Texas A&M that also requires measuring surface energies of component materials in addition to the material characterization tests from the original calibrated mechanistic approach (5).

At the conclusion of the second year of the project in 2004, the best approach for fatigue design and analysis will be recommended based on a value engineering assessment. This comparison of the four approaches will consider variability; required resources; implementation issues; the ability to incorporate the important effects of aging, fracture, and healing; practicality; and the capability to interface with pavement design. A key element in the recommended approach is expected to stem from an investigation of the relationship between the change in mixture fatigue resistance due to aging and aged binder properties. With a better understanding of this relationship from this project, testing of aged binders and unaged mixtures will allow for prediction of the performance of aged mixtures.

In a proposed modified third year of the project, fatigue lives of up to 10 additional mixtures will be predicted using the recommended design and analysis system. These additional mixtures will include the materials used at the Texas Accelerated Pavement Testing (TxAPT) Center and possibly other rut resistant mixtures or mixtures with different materials (binders, aggregates, aggregate gradations) to facilitate comparison of performance and the effects of different mixture parameters.

SCOPE

This interim report documents: (1) detailed descriptions of two of the four fatigue analysis approaches used to predict fatigue life, (2) the effect of aging for two aging states using one of the four approaches, and (3) a preliminary comparison of two approaches using one aging state. The report describes fatigue analysis results for one selected mixture in a specific pavement structure under representative environmental and loading conditions.

DESCRIPTION OF CONTENTS

The interim report is divided into eight chapters including this chapter that provides the motivation for the project, the overall objectives and work plan, and the scope of this report. The following chapter describes the experimental design that includes selection of fatigue analysis approaches, materials, specimen preparation protocols, aging conditions, and a typical pavement structure. Next the two approaches highlighted in the preliminary results presented in this report are described in detail, followed by the testing and analysis utilized to explore the relationship between binder and mixture aging. Then the resulting fatigue lives from both approaches and the aging evaluation are described. This report concludes with a summary and work plan required to complete the project.

CHAPTER 2
EXPERIMENTAL DESIGN

The methodology for this research project involved a literature review and consultation with TxDOT project personnel to select appropriate approaches for HMAC fatigue design and analysis and materials and the corresponding specimen fabrication protocols, laboratory tests, and data analysis techniques.

LITERATURE REVIEW

A literature review consisting of an information search of electronic databases and resulting publications and a field-survey questionnaire was conducted to gather data on fatigue design and analysis approaches, related laboratory tests, materials, pavement structures and design, corresponding standards or references, and resources or methodologies used to obtain fatigue resistant HMAC mixtures. Effects of aging, healing, and fracture on mixture performance were also reviewed, and the literature found was summarized and documented. Researchers also reviewed and documented commonly used TxDOT mixtures, material characteristics, and other general input parameters including pavement structures, traffic loading, environmental conditions, mix designs, aging, and reliability levels. Results of the literature review will be discussed in more detail in the final research report. Highlights relevant to the scope of this interim report are presented in the subsequent sections of this chapter and Chapters 3, 4, and 5.

FATIGUE ANALYSIS APPROACHES

Based on the literature review and consultation with TxDOT project personnel, researchers selected the following four fatigue analysis approaches: the proposed NCHRP 1-37A 2002 Pavement Design Guide with dynamic modulus (DM) testing, Mechanistic Empirical (ME) with flexural bending beam (BB) fatigue testing, Calibrated Mechanistic (CM), and Calibrated Mechanistic with surface energy (CMSE) measurements for evaluation in this project.

In this interim report, only the ME and CMSE approaches and the effects of aging are discussed in Chapters 3, 4, and 5, respectively. The proposed NCHRP 1-37A 2002 Pavement Design Guide is briefly discussed in Chapter 8 under current and future work. Materials, aging conditions (asphalt and HMAC specimens), and the selected pavement structure are discussed in this chapter.

MATERIALS

The research team selected two commonly used TxDOT HMAC mixtures for utilization in this project. These were basic and rut resistant mixtures and defined as the Bryan and Yoakum mixtures, respectively, to represent the districts where the mix designs were obtained. Note that development of mix designs was not part of this project. In this interim report, only the Bryan mixture is discussed.

Mix Design

The Bryan HMAC mixture was designed using standard TxDOT gyratory design protocols from the Bryan District (*6*). This mixture consists of a performance-graded (PG) PG 64-22 binder mixed with limestone aggregates to produce a dense-graded TxDOT Type C mixture. The aggregate gradation curve for this mixture is shown in Figure 2-1. This mixture was used on highways US 290 and SH 47 in the Bryan District (*6*).

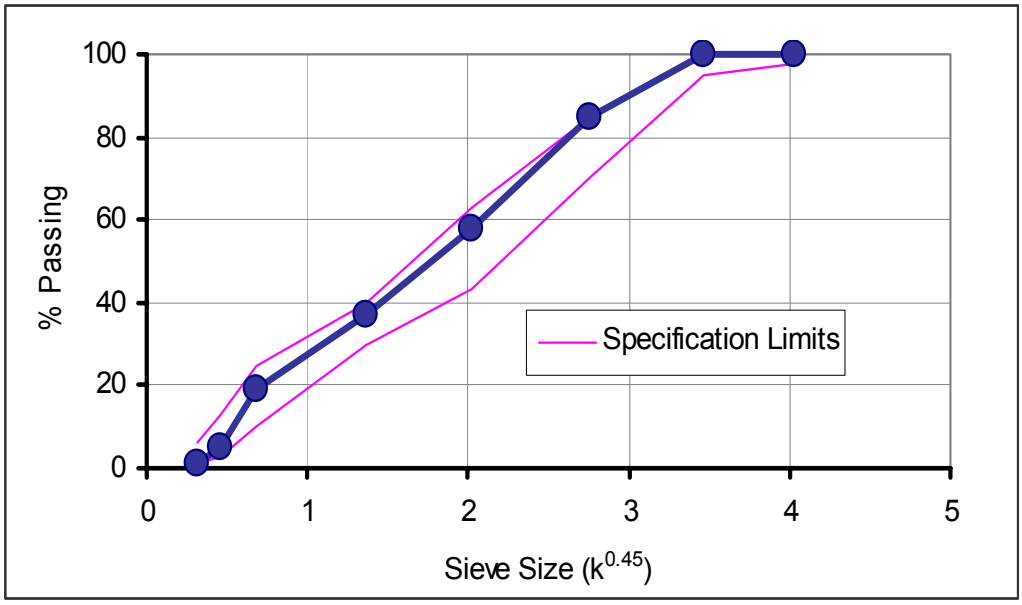

Figure 2-1. Limestone Aggregate Gradation Curve for TxDOT Type C Mixture.

The PG 64-22 binder was supplied by Eagle Asphalt, and the limestone aggregate was supplied by Colorado Materials, Inc. from its Caldwell plant. The mix design was 4.6 percent binder content by weight of aggregate (4.4 percent by weight of total mix) with a HMAC mixture theoretical maximum specific gravity of 2.419 (*6*). The HMAC specimens were fabricated with a target air void (AV) content of 7±0.5 percent to simulate in situ AV after adequate field compaction and trafficking when fatigue resistance is critical.

Material Properties

Laboratory characterization of the asphalt material based on the AASHTO PP1, PP6, T313, and T315 test protocols produced the results shown in Figures 2-2 through to 2-4 (*7*, *8*). In this interim report, the term binder is used synonymously with the term asphalt. Also note that for most of the binder test results, metric units are used consistent with the PG specifications used by TxDOT for binders (*7*, *8*). English (U.S.) units or unit conversions are provided in parentheses to meet TxDOT requirements for other units including length and temperature.

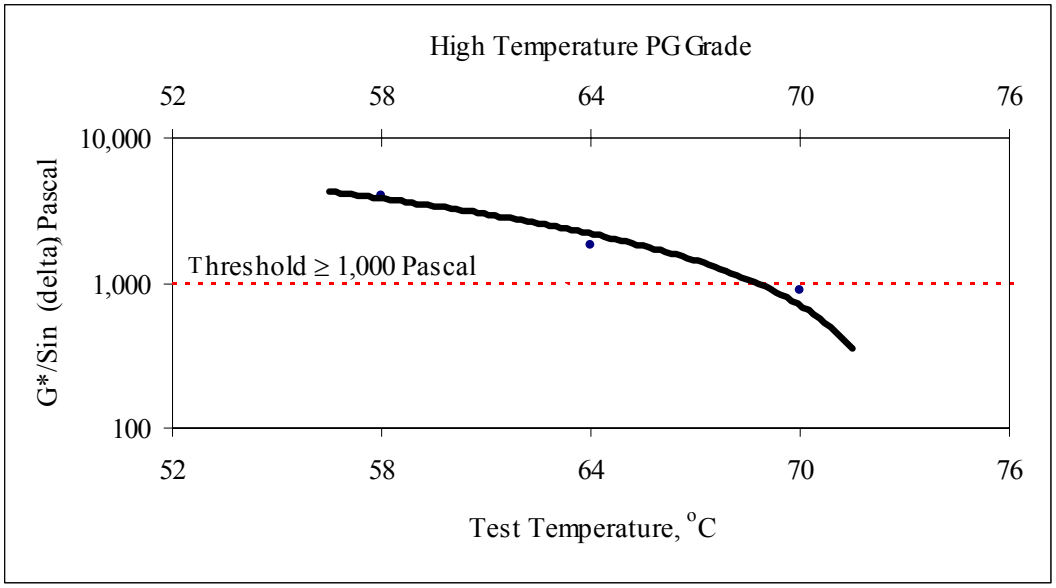

Figure 2-2. Asphalt High Temperature Properties – G*/Sin (delta), Pascal.

(delta ≅ δ)

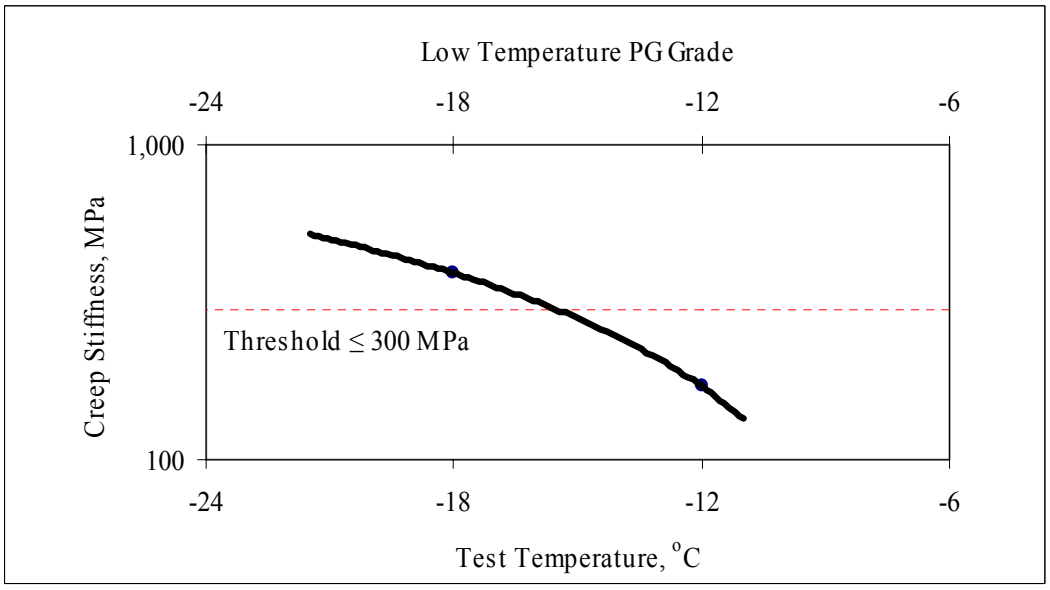

Figure 2-3. Asphalt Low Temperature Properties – Flexural Creep Stiffness, MPa.

(°F = 32 + 1.8°C)

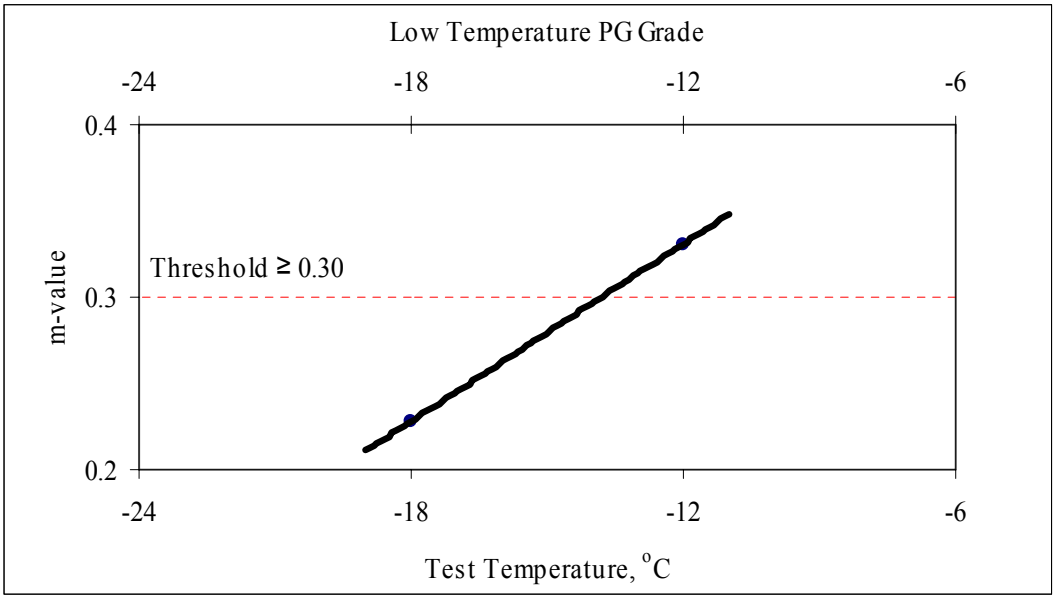

Figure 2-4. Asphalt Low Temperature Properties – m-value (°F = 32 + 1.8°C).

These verification results shown in Figures 2-2 through 2-4 indicate that the asphalt meets the PG specification consistent with the material properties for a PG 64-22 asphalt (*7*, *8*). Also, the measured intermediate temperature properties of the PG 64-22 asphalt at 25 °C (77 °F) in terms of the complex shear modulus (G*) and the phase angle (δ) met the required maximum specified threshold value of a G*× Sin δ of 5,000 kPa (*7*, *8*). The mean G*× Sin δ for three PG 64-22 replicate tests was 600 kPa with a coefficient of variation (*COV*) of 1.82 percent.

Material properties for the aggregate listed in Table 2-1 indicate that the aggregate meets the specification consistent with the respective test methods shown in Table 2-1 (*6*). The bulk specific gravity for the combined aggregates was 2.591 (*6*).

Table 2-1. Limestone Aggregate Properties (*6*).

Test Parameter	Result (%)	Specification (%)	Test Method	Comment
Soundness	18	≤ 30	Tex-411-A	Ok
Crushed faces count	100	≥ 85	Tex-460-A	Ok
LA abrasion	28	≤ 40	Tex-410-A	Ok
Sand equivalent	74	≥ 45	Tex-203-F	Ok

HMAC SPECIMEN PREPARATION

The basic HMAC specimen preparation procedure involved the following steps: aggregate batching, asphalt-aggregate mixing, short-term oven aging (STOA), compaction, sawing and coring, and finally volumetric analysis to determine AV. These steps are briefly discussed in this section.

Aggregate Batching

Aggregates were batched consistent with the gradation shown in Table 2-2, which corresponds to that shown in Figure 2-1.

Table 2-2. Limestone Aggregate Gradation.

Sieve Size	TxDOT Specification (*6*)		Percent Passing
	Upper Limit	Lower Limit	
5/8″	100	98	100.0
1/2″	100	95	100.0
3/8″	85	70	84.8
#4	63	43	57.9
#10	40	30	36.9
#40	25	10	19.0
#80	13	3	5.0
#200	6	1	1.0

Mixing, Short-term Oven Aging, Compaction, and Air Voids

The mixing and compaction temperatures were 144 °C (291 °F) and 127 °C (261 °F), respectively. These temperatures are consistent with the TxDOT Tex-205-F and Tex-241-F test specifications for PG 64-22 asphalt (*9*). Prior to asphalt-aggregate mixing, the aggregates were always pre-heated at a temperature of 144 °C (291 °F) for at least 4 hrs to remove any moisture. The asphalt was also heated for approximately 30 minutes before mixing to liquefy it.

HMAC mixture STOA lasted for 4 hrs at a temperature of 135 °C (275 °F) consistent with the American Association of State Highway and Transportation Officials (AASHTO) PP2 aging procedure for Superpave mixture performance testing. STOA simulates the time between HMAC mixing, transportation, and placement up to the time of in situ compaction in the field (*10*). Synonymous with the acronym STOA, the acronyms PP2 and AASHTO-PP2 were also used in this interim report.

All the cylindrical specimens for the CMSE tests were gyratory compacted using the standard Superpave Gyratory Compactor (SGC) shown in Figure 2-5.

Figure 2-5. Superpave Gyratory Compactor.

Researchers compacted beam specimens for the flexural bending beam fatigue tests using the linear kneading compactor, shown in Figure 2-6, up to the target AV content consistent with the specified beam thickness (*6*, *11*, *12*).

Figure 2-6. Linear kneading Compactor.

All HMAC specimens were compacted to a target AV content of 7±0.5 percent, as stated previously, to simulate in situ AV after adequate field compaction and trafficking when fatigue resistance is critical. Actual specimen AV contents after sawing and coring are reported in Chapter 6.

Sawing, Coring, Handling, and Storage

Cylindrical specimens were gyratory compacted to a size of 165 mm (6.5 inches) height by 150 mm (6 inches) diameter, while actual test specimens were sawn and cored to a 150 mm (6 inches) height and 100 mm (4 inches) diameter. Beam specimens were kneading compacted to a size of 457 mm (18 inches) length by 150 mm (6 inches) width by 63 mm (2.5 inches) thickness. Test specimens were sawn to a 380 mm (15 inches) length by 63 mm (2.5 inches) width by a 50 mm (2 inches) thickness (*11*). Figure 2-7 shows the dimensions of the final test specimens (where 1 mm ≅ 0.039 inches).

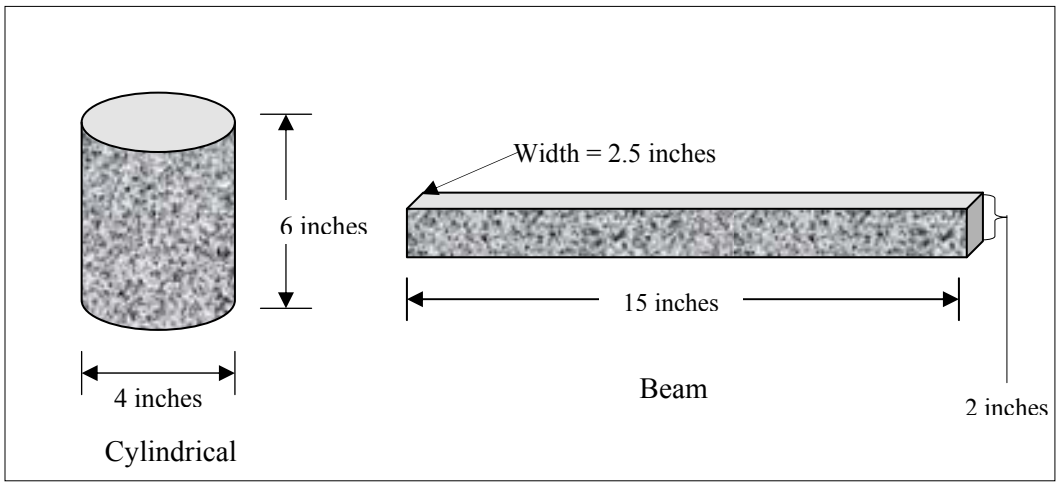

Figure 2-7. Laboratory Test Specimens (Drawing not to Scale).

(1 mm ≅ 0.039 inches)

After the specimens were sawn and cored, volumetric analysis based on the fundamental principle of water displacement was completed to determine the actual specimen AV. HMAC specimens that did not meet the target AV content were discarded and not used in the tests.

In total, a cylindrical specimen took approximately 40 hrs to fabricate while a beam specimen because of the difficultness in sawing took an additional 5 hrs. While beam specimens require delicate handling, the cylindrical specimens are not as sensitive to handling. Prior to laboratory testing, specimens were generally stored on flat surfaces in a temperature-controlled room at approximately 20±2 °C (68±36 °F).

ASPHALT AND HMAC AGING CONDITIONS

Researchers selected four aging conditions listed in Table 2-3 for this project for both the asphalt and HMAC specimens. Consistent with the Superpave procedure, all loose HMAC mixtures were subjected to 4 hrs STOA discussed previously. For this interim report, only results for 0 and 3 months aging are reported in Chapter 6.

Table 2-3. Asphalt and HMAC Aging Conditions.

Aging Condition @ 60 °C (140 °F)	Description	Comment
0 months	Simulates time period just after in situ field construction at the end of compaction	All loose HMAC mixtures (prior to compaction) were subjected to 4 hrs STOA (AASHTO PP2).
3 months	Simulates 3 to 6 years of Texas environmental exposure	
6 months	Simulates 6 to 12 years of Texas environmental exposure	
9 months	Simulates 12 to 18 years of Texas environmental exposure	

The aging process for HMAC specimens involved keeping the specimens in a temperature-controlled room at 60 °C (140 °F) and at the same time allowing the heated air to circulate freely around the specimens. This allowed for accelerated oxidative aging of the asphalt within the HMAC specimens. An aging temperature of 60 °C (140 °F) was selected to accelerate aging because this temperature realistically simulates a critical pavement service temperature in Texas for HMAC aging. Based on previous research, the process also simulates the field HMAC aging rate (*13*). The aging process for the asphalt is discussed in detail in Chapter 5.

PAVEMENT STRUCTURE, ENVIRONMENTAL CONDITIONS, AND TRAFFIC

The selected pavement structure for this preliminary analysis was a 6 inch thick HMAC (500,000 psi) layer resting on a 14 inch flex base (28,000 psi) and a subgrade with an elastic modulus of 9,000 psi and Texas triaxial value of 5.4. For this interim report, a Texas environment of wet-warm (WW) was selected to characterize the pavement materials with respect to temperature and subgrade moisture conditions. Typical traffic conditions consisted of an 18 kip axle load, 100 psi tire pressure, 60 mph speed, and 5 million equivalent single axle loads (ESALs) with about 25 percent trucks over a design life of 20 years (*14*).

To be representative of a wide spectrum of the Texas conditions, other pavement structures, environmental conditions, and traffic are being considered and will be reported in the final report. These factors are discussed in Chapter 8 of this interim report.

Stress-Strain Analysis

ELSYM5 stress-strain computations were adjusted based on Finite Element Method (FEM) simulations to account for HMAC elastic-visco-plastic behavior (*15*, *16*). The resulting strains are shown in Table 2-4. These tensile and shear strains constitute input parameters for the ME and CMSE fatigue analysis, respectively, discussed in Chapters 3 and 4. The Poisson's ratios used by the researchers in the analysis were 0.33, 0.40, and 0.45 for the HMAC layer, the base, and subgrade, respectively.

Table 2-4. Computed Design Strains.

Parameter	**Design strain**
Maximum tensile strain (ε_t) @ bottom of the HMAC layer (5.99 inches)	1.57×10^{-5}
Maximum shear strain (γ) @ edge of the tire (0 months aging)	1.56×10^{-2}

Instead of computing the strains for the 3 months aging condition, only the strains from the 0 months HMAC mixtures were used because the aging effect is postulated to be taken into account by the aging shift factor (SF_{ag}) that is being developed and will be presented in the final report. Additionally, practical implementation and application of the fatigue analysis approaches including elastic stress-strain analysis will be based on unaged HMAC mixtures while aging effects will be incorporated through the SF_{ag} determined from unaged and aged binder properties**.**

CHAPTER 3
THE MECHANISTIC EMPIRICAL APPROACH

The mechanistic empirical approach of HMAC pavement fatigue analysis including the input/output data, analysis procedure, failure criteria, and variability is discussed in this chapter. The laboratory test protocol for the required flexural bending beam fatigue test is also discussed.

THEORY

Most ME approaches for predicting the fatigue resistance of HMAC mixtures involve either controlled stress or controlled strain laboratory testing at a single representative temperature over a series of stress or strain levels, respectively, and determination of fatigue life at a stress or strain level assumed to be critical and caused by an equivalent single type of vehicle loading. These approaches predict the number of stress or strain cycles to crack initiation in flexure, direct or indirect tension, or semi-circular bending tests (*1*, *11*, *12*, *17*-*24*).

A method to determine a single representative temperature for laboratory testing and a temperature conversion factor to account for the fact that loading occurs over a temperature range is required. A shift factor is also required to account for other differences between field and laboratory conditions, including the effects of wander, healing, and crack propagation. A lengthy testing program is required with replicate tests (to account for relatively large variability) at multiple stress or strain levels to define an empirical fatigue relationship for a specific HMAC mixture.

The determination of the critical design stress or strain within the pavement structure in the HMAC layer constitutes the mechanistic part of this type of approach. The calculated stress or strain varies depending on the assumed model of material behavior; layered linear-elastic or visco-elastic, the former model being preferred because of its simplicity at the expense of possibly unrealistic simulation.

The location of the critical design stress or strain also limits the analysis to either bottom-up or top-down fatigue cracking without consideration of both. Most of the current ME approaches are based on the bottom-up mode of fatigue crack failure.

The SHRP A-003A approach utilizes the flexural bending beam fatigue test (third-point loading) and considers bottom-up cracking to determine an empirical fatigue relationship of the simple power form shown in Equation 3-1 (*25*).

$$N = k_1 \varepsilon^{-k_2} \qquad \text{(Equation 3-1)}$$

where:

N = Number of load cycles to fatigue failure,

ε = Applied tensile strain

k_i = Laboratory determined constants.

The SHRP A-003A fatigue analysis approach incorporates reliability concepts that account for uncertainty in laboratory testing, construction, and traffic prediction; and considers environmental factors, traffic loading, and pavement design. The SHRP A-003A is the ME fatigue analysis approach utilized in this project, and the BB testing to determine the HMAC mixture fatigue empirical relationship shown in Equation 3-1 was based on the AASHTO TP8-94 test protocol (*11, 12*). The AASHTO TP8-94 test protocol is discussed subsequently in this chapter.

HMAC specimen preparation by rolling or kneading wheel compaction is strongly recommended as part of this ME approach to simulate the engineering properties of extracted field pavement cores. Conditioning prior to testing to a representative or worst-case aging state is also suggested. As discussed subsequently, the AASHTO TP8-94 test protocol requires testing conditioned specimens at two different controlled strain levels under sinusoidal repeated loading to generate an empirical fatigue relationship shown in Equation 3-1.

Determination of the experimental fatigue relationship as expressed by Equation 3-1 constitutes the empirical part of the ME approach of fatigue modeling of HMAC mixtures. This empirical fatigue relationship (Equation 3-1) is then used in the design and analysis system illustrated schematically in Figure 3-1.

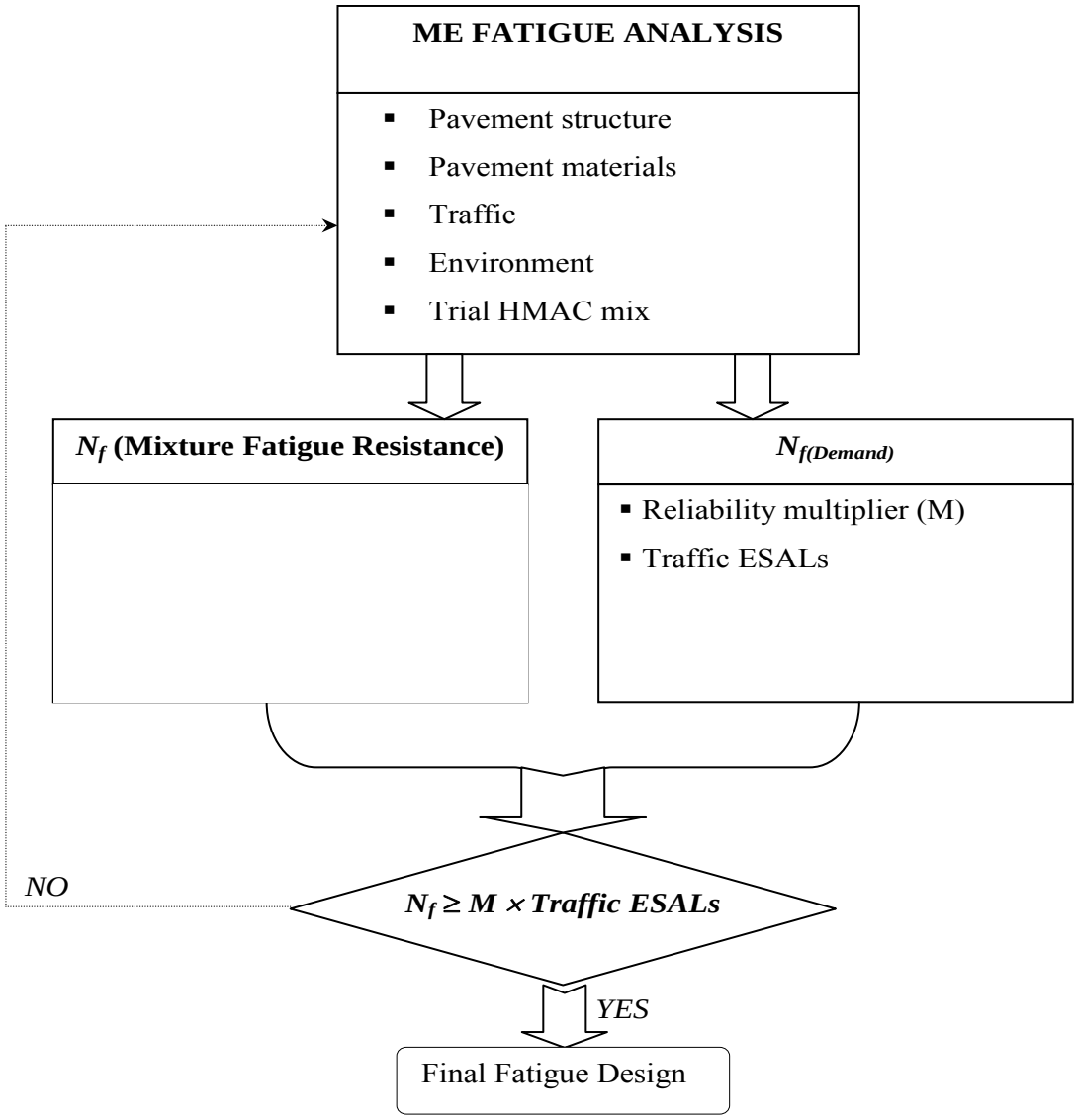

Figure 3-1. The ME Fatigue Design and Analysis System.

The fatigue system shown in Figure 3-1 evaluates the likelihood that the selected design HMAC mixture will adequately resist fatigue cracking in a specific pavement structure under anticipated in situ conditions including traffic and environment. The designer must, however, select a specific level of reliability commensurate with the pavement site for which the mixture will be utilized as well as the required level of service of the pavement structure. Under this ME approach, a HMAC mixture is expected to perform adequately in fatigue if the number of load repetitions sustainable in laboratory testing after accounting for the differences between laboratory and field conditions exceeds the number of load repetitions anticipated in service.

The design strain at which the pavement fatigue life must be estimated using the empirical fatigue relationship developed based on laboratory test results is often computed using a simple multilayer elastic theory. For this computation, the design strain of interest is the maximum principal tensile strain at the bottom of the HMAC layer in the specific pavement structure, assuming the bottom-up mode of fatigue cracking.

ME FATIGUE ANALYSIS INPUT AND OUTPUT DATA

Table 3-1 summarizes the general ME fatigue analysis input and the expected output data based on the SHRP A-003A approach and the AASHTO TP8-94 BB test protocol. These parameters and their respective components are discussed in more details in subsequent sections.

Table 3-1. Summary of ME Fatigue Analysis Input and Output Data.

Source	**Parameter**
Laboratory test data (HMAC beam specimens)	- Tensile strain (ε_t) & stress - # of fatigue load cycles (N)
Analysis of laboratory test data	- Flexural stiffness or dissipated energy - Empirical fatigue relationship ($N = f(\varepsilon_t)$)
Field conditions (design data)	- Pavement structure (layer thickness) - Pavement materials (elastic modulus & Poisson's ratio) - Traffic (ESALs, axle load, & tire pressure) - Environment (temperature & moisture conditions) - Field correction/shift factors (i.e. temperature)
Computer stress-strain analysis	- Design ε_t @ bottom of the top HMAC layer
Other	- Reliability level (i.e., 95%) - Reliability multiplier (M)
OUTPUT	- HMAC mixture fatigue resistance ($N_{f(Supply)}$) - Pavement fatigue life ($N_{f(Demand)}$) - Assessment of adequate or inadequate performance

ME FATIGUE FAILURE CRITERIA

For HMAC compacted specimens subjected to repeated flexural bending, fatigue failure is defined as the point at which the specimen flexural stiffness is reduced to 50 percent of the initial flexural stiffness (*11, 12*). This initial stiffness is generally defined as the specimen flexural stiffness measured at the 50th load cycle. With this criterion, fatigue cracking was considered to follow the bottom-up failure mode assuming a service temperature of 20 °C (68 °F).

ME FATIGUE ANALYSIS PROCEDURE

The ME fatigue analysis utilized in this project was a five step procedure involving laboratory test data analysis to determine the HMAC material N-ε_t empirical relationship expressed by Equation 3-1, computer stress-strain analysis to determine the design maximum ε_t within a selected and representative pavement structure at the bottom of the HMAC layer, statistical analysis to predict the design HMAC mixture fatigue resistance, determination of the required pavement fatigue life, and finally, a design check. These analyses, which are illustrated schematically in Figure 3-1, are discussed in this section.

Step 1: Laboratory Test Data Analysis (N-ε_t Empirical Relationship)

Laboratory test data from the BB fatigue test, which is discussed subsequently, was analyzed using the AASHTO TP8-94 calculation procedure. Equations 3-2 to 3-4 are the fundamental basis for BB test data analysis procedure (*11*).

$$S = \frac{\sigma_t}{\varepsilon_t} \qquad \text{(Equation 3-2)}$$

$$N_{50\%} = \frac{\ln\left(\frac{S_{50\%}}{A}\right)}{b} = -0.69315b^{-1} \qquad \text{(Equation 3-3)}$$

$$D = \pi \sigma_t \varepsilon_t Sin(\phi) \qquad \text{(Equation 3-4)}$$

where:

S	=	Flexural stiffness
σ_t	=	Maximum measured tensile stress per load cycle
ε_t	=	Maximum measured tensile strain per load cycle
$N_{50\%}$	=	Number of load cycles to failure
$S_{50\%}$	=	Flexural stiffness at failure
A	=	Initial peak flexural stiffness measured at the 50th load cycle, psi
b	=	Exponent constant from log S versus log load cycles (N) plot
D	=	Dissipated energy
ϕ	=	Phase angle, degrees (°)

The solution of Equation 3-3 for two different input strain levels (i.e., low and high), and a plot of the resultant $N_{50\%}$ versus the respective applied ε_t on a log-log scale will generate the required empirical fatigue relationship of the simple power form shown in Equation 3-1. Dissipated energy (D) (Equation 3-4) can also be used to determine N at failure and the empirical relationship expressed by Equation 3-1 (*12*), but this was not utilized in this project.

Step 2: Stress-Strain Analysis, $\varepsilon_{t\,(Design)}$

Following establishment of the HMAC material N-ε_t empirical relationship through laboratory test data analysis, computer stress-strain analysis was conducted to determine the actual maximum design ε_t of a given pavement structure at the bottom of the HMAC layer. Input parameters for this analysis include traffic loading, pavement structure (layer thicknesses), material properties, and the desired response location, which in this project was (t – 0.01) inches, where t is the thickness of the top HMAC layer in inches. Traffic loading data include among others the axle loabet (Design)d (e.g., 18 kip), ESALs, axle, and tire configuration. Material properties including the elastic modulus and Poisson's ratio should be defined as a function of the environment in terms of temperature and subgrade moisture conditions.

In this project, a user friendly and simple multi-layer linear-elastic software, ELSYM5, was used for ε_t computations. Ideally, a FEM software that takes into account the visco-elastic and plastic nature of the HMAC material is desired for this kind of analysis. Otherwise, adjustments can be applied to the linear-elastic analysis results.

Step 3: Statistical Prediction of the HMAC Mixture Fatigue Resistance, $N_{f(Supply)}$

$N_{f(Supply)}$ is the design HMAC mixture fatigue resistance that was statistically determined as a function of the design ε_t (ELSYM5 analysis) and the laboratory determined empirical fatigue Equation 3-1 at a given reliability level.

While $N_{f(Supply)}$ represents laboratory fatigue life, the final field fatigue life for this ME approach in this project was obtained as expressed by Equation 3-5.

$$N_f = \frac{SF\left(k_i\left[\varepsilon_t\right]^{-k_2}\right)}{TCF} = \frac{SF \times N_{f\,(Supply)}}{TCF} \qquad \text{(Equation 3-5)}$$

where:

TCF	=	Temperature conversion factor to laboratory test temperature
SF	=	Shift factor that accounts for traffic wander, construction variability, loading frequency, crack propagation, and healing

For simplicity, TCF and SF values of 1.0 and 19, respectively, were used in this project (*1*). Determination of these parameters generally requires local calibration to field conditions, which was beyond the scope of this project.

Step 4: Determination of the Required Pavement Fatigue Life, $N_{f(Demand)}$

$N_{f(Demand)}$ is the expected pavement fatigue life, which is representative of the actual applied traffic loading. It is a function of the total traffic ESALs summed over the entire pavement design life determined, as expressed by Equation 3-6.

$$N_{f(Demand)} = M \times Traffic\ ESALs_{(Design)} \quad \text{(Equation 3-6)}$$

where:

M = Reliability multiplier (for mixture and traffic estimate variability)

Step 5: Design Check

A fatigue design check for adequate performance requires that the HMAC mixture fatigue resistance be greater than or equal to the required pavement fatigue life as expressed by Equation 3-7.

$$N_f \geq N_{f(Demand)} \quad \text{(Equation 3-7)}$$

If N_f is less than $N_{f(Demand)}$, a wide range of options including the following are available:

- redesigning the mixture by changing the asphalt content and/or type, AV, aggregate type or gradation;
- redesigning the pavement structure by changing the layer thicknesses for example;
- redesigning the underlying pavement materials including the subbase, base, and/or subgrade;
- reducing the pavement design life; and/or
- allowing an increased risk of premature failure.

VARIABILITY OF FATIGUE LIFE PREDICTION BY THE ME-BB APPROACH

Precision is inversely proportional to uncertainty/variability in a testing method. If N_f is the measured fatigue life and N_{supply} is the predicted fatigue life at a given design strain level, then the precision of the method (on a log scale) can be represented by the estimated variance of $Ln\lfloor N_{\text{supply}} \rfloor$ as follows:

$$s_{y^*}^2 = s^2\left(1+\frac{1}{n}+\frac{(X-\bar{x})^2}{q\sum(x_p-\bar{x})^2}\right) \qquad \text{(Equation 3-8)}$$

where:

y^*	=	$Ln\lfloor N_{\text{supply}} \rfloor$
$s_{y^*}^2$	=	Estimated variance of $Ln\lfloor N_{\text{supply}} \rfloor$
s^2	=	$Var\lfloor Ln(N_f) \rfloor$
n	=	Number of test specimens
X	=	Ln[in situ strain] at which $Ln\lfloor N_{\text{supply}} \rfloor$ must be predicted
$\bar{x}$	=	Average Ln[test strain]
q	=	Number of replicate specimens at each test strain level
x_p	=	Ln[strain] at the pth test strain level

A prediction interval for $Ln\lfloor N_{\text{supply}} \rfloor$ is another way of assessing the precision of the prediction. If the resulting interval is narrow, there is little uncertainty in $Ln\lfloor N_{\text{supply}} \rfloor$, and the prediction is quite precise. An explicit formula for a 1-α prediction interval for the linear regression exists as follows:

$$a+bX \pm t_{1-\alpha/2,n-2}s_{y^*} \qquad \text{(Equation 3-9)}$$

where:

a, b = The estimated intercept and the estimated slope of the least squares line fitted on the $\left(Ln(strain), Ln(N_f)\right)$ data

$t_{1-\alpha/2,n-2}$ = The *t*-critical value corresponding to the right tail probability of $\alpha/2$ of the *t* distribution with *n-2* degrees of freedom

$s^2_{y^*}$ = The estimated variance of $Ln\left[N_{\text{supply}}\right]$ as given in Equation 3-8

The estimated intercept and the estimated slope, *a* and *b*, respectively, can also be given explicitly as follows:

$$a = \bar{y} + b\bar{x} \qquad \text{(Equation 3-10)}$$

$$b = \frac{S_{xy}}{S_{xx}} = \frac{q\sum\left(x_p - \bar{x}\right)\left(y_p - \bar{y}\right)}{q\sum\left(x_p - \bar{x}\right)^2} \qquad \text{(Equation 3-11)}$$

where:

y_p = $Ln(N_f)$ at the *p*th test strain level

$\bar{y}$ = Average $Ln(N_f)$

Note that the predicted fatigue life $Ln\left[N_{\text{supply}}\right]$ or the prediction interval estimate $\left[a + bX - t_{1-\alpha/2,n-2}s_{y^*}, a + bX + t_{1-\alpha/2,n-2}s_{y^*}\right]$ can be back-transformed by taking exp( ) to provide the estimates in the original scale, but the variance estimate $s^2_{y^*}$ itself cannot be transformed in the same manner.

THE FLEXURAL BENDING BEAM FATIGUE TEST

The flexural bending beam fatigue test including the test equipment, specimen setup, and data acquisition was conducted consistent with the AASHTO TP8-94 test procedure (*11, 12*). This section summarizes the BB test protocol.

BB Test Protocol

The BB fatigue test consists of applying a repeated constant vertical strain to a beam specimen in flexural tension mode until failure or up to a specified number of load cycles. In this project, the test was strain controlled, and the input strain waveform was sinusoidal shaped, applied at a frequency of 10 Hz. The BB device and the loading configuration are shown in Figures 3-2 and 3-3, respectively.

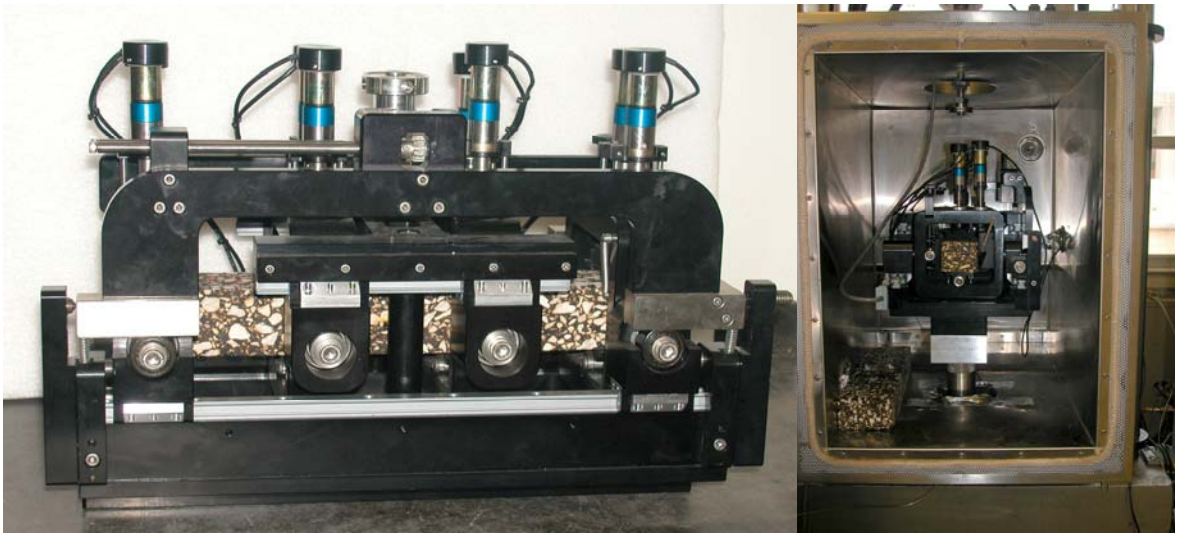

Figure 3-2. The BB Device.

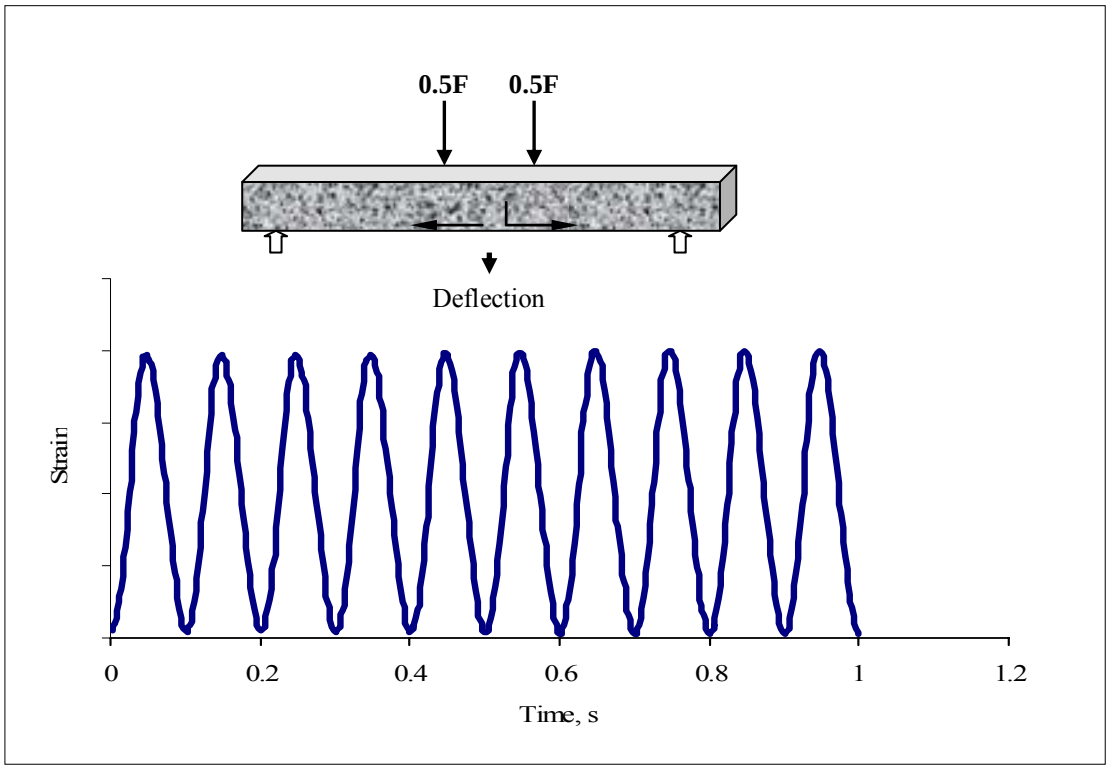

Figure 3-3. Loading Configuration for the BB Fatigue Test.

As evident in Figure 3-3, repeated vertical loading causes tension in the bottom zone of the specimen, from which cracking will subsequently initiate and propagate, thus simulating pavement fatigue failure under traffic loading. The test was conducted at two strain levels of approximately 374 and 468 microstrains (deflection of 0.20 and 0.25 mm equivalent) consistent with the AASHTO TP8-94 test protocol to generate the required material N-ε_t empirical relationship shown in Equation 3-1. These strain levels are within the recommended AASHTO TP8-94 test protocol range to reduce test time while at the same time capturing sufficient data for analysis.

A 10 Hz frequency (Figure 3-3) without any rest period was used for the test. The average duration of each test was approximately 5 hrs. Note that the BB test time is inversely proportional to the magnitude of the input strain wave. Testing can, however, be terminated either when the initial application load response (stress) recorded at the 50th load cycle decreases to 50 percent in magnitude or when a preset number of load cycles such as 100,000 is reached. The former approach was used in this project.

Test Conditions and Specimens

HMAC is temperature sensitive, so the test was conducted in an environmentally controlled chamber at a test temperature of 20±0.5 °C (68 ±32.9 °F) consistent with the AASHTO TP8-94 test procedure. The minimum specimen conditioning time was 2 hrs. However, specimens were actually preconditioned at 20 °C (68 °F) on a more convenient 12 hrs overnight-time period. The test temperature was monitored and recorded every 600 s via a thermocouple probe attached inside a dummy specimen also placed in the environmental chamber. Figure 3-4 is an example of a temperature plot captured during the BB test at 20 °C (68 °F).

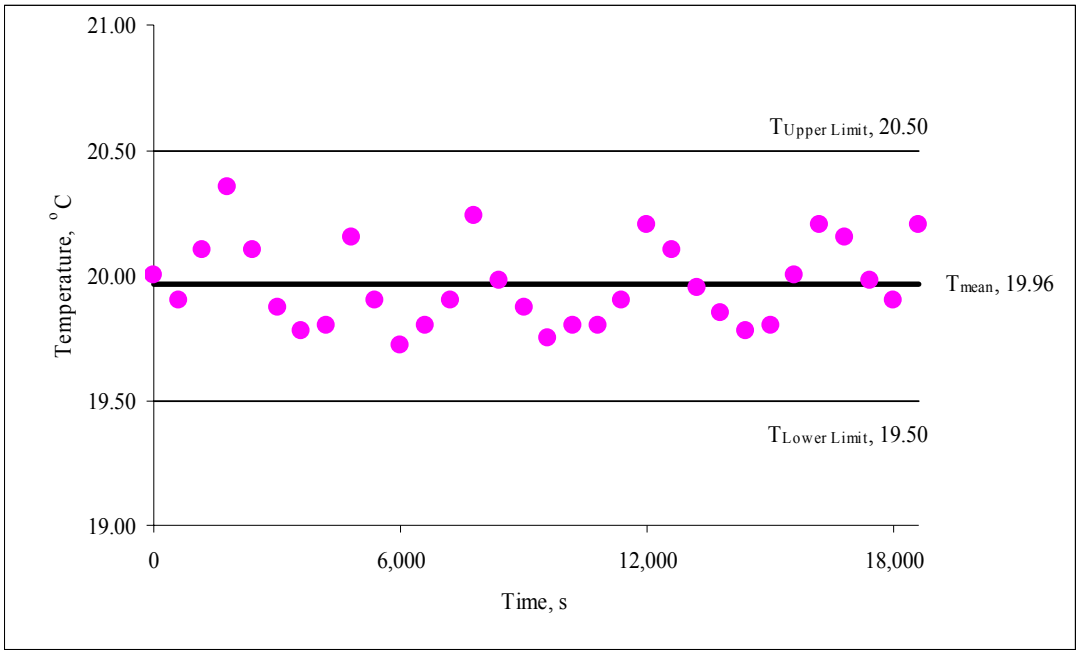

Figure 3-4. Example of Temperature Plot for the BB Test.

As evident in Figure 3-4, the average temperature for this particular test was 19.96 °C (67.93 °F) with a coefficient of variation of 0.84 percent. Three replicate beam specimens were tested for each strain level, so a complete BB test cycle for low and high strain level tests required a minimum of six beam specimens per aging condition.

Test Equipment and Data Measurement

A servo electric-hydraulic controlled material testing system (MTS) equipped with an automatic data measuring system applied the sinusoidal input strain waveform. Actual loading of the specimen was transmitted by the BB device shown in Figure 3-2, to which the beam specimen is securely clamped.

Loading data were measured via the MTS load cell, and flexural deflections were recorded via a single linear differential variable transducer (LVDT) attached to the center of the specimen. During the test, load and flexural deformation data were captured electronically every 0.002 s. Figure 3-5 is an example of the output stress response from the BB test at 20 °C (68 °F).

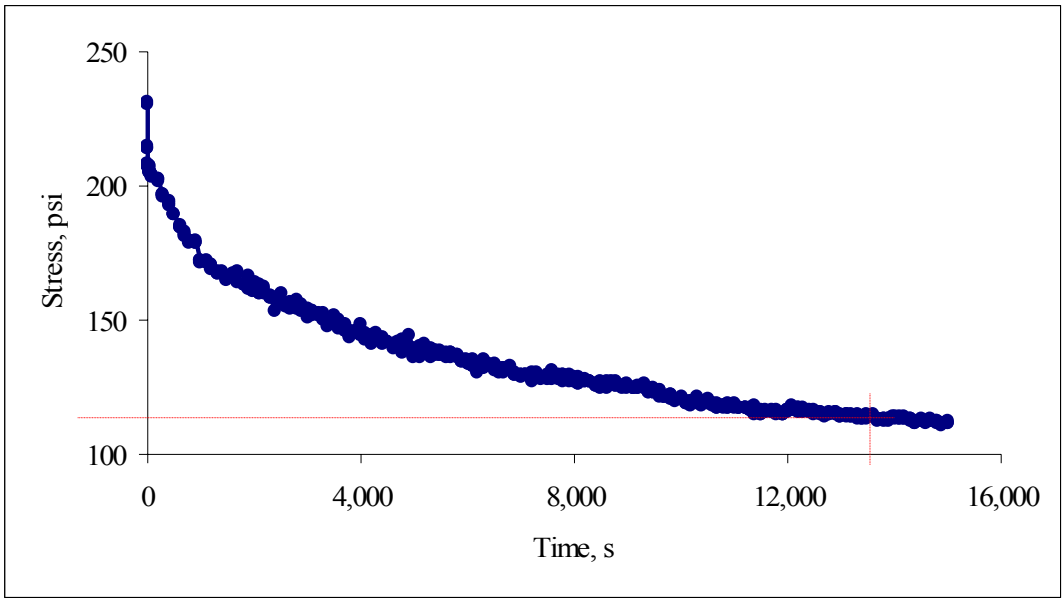

Figure 3-5. Example of Stress Response from the BB Test @ 20 °C (68 °F). (374 microstrain level).

CHAPTER 4
THE CALIBRATED MECHANISTIC APPROACH

In this chapter, the calibrated mechanistic approach including the input/output data, analysis procedure, failure criteria, and variability is discussed. The related laboratory test protocols are also discussed.

THEORY AND DEVELOPMENT

HMAC is a complex composite material that behaves in a non-linear visco-elastic visco-plastic manner, ages, heals, and requires that energy be expended to cause load-induced damage in the form of cracking. HMAC mixture resistance to fatigue cracking thus consists of two components, resistance to fracture (both crack initiation and propagation) and the ability to heal, that both change over time. Healing, defined as the closure of fracture surfaces that occurs during rest periods between loading cycles, is one of the principal components of the laboratory to field shift factor used in traditional fatigue analysis. Prediction of fatigue life or the number of cycles to failure (N_f) must account for this process that affects both the number of cycles for microcracks to coalesce to macrocrack initiation (N_i) and the number of cycles for macrocrack propagation through the HMAC layer (N_p) that add to N_f. Both components of mixture fatigue resistance or the ability to dissipate energy that causes primarily fracture at temperatures below 25 °C (77 °F), called dissipated pseudo strain energy (DPSE), can be directly measured in simple uniaxial tensile and compression tests (*4, 5, 26-28*).

The CM approach is a micromechanical approach developed at Texas A&M University based on the SHRP A-005 results *(28, 29)*. The approach characterizes HMAC materials both in terms of fracture and healing processes, and requires only creep or relaxation tests in uniaxial tension and compression, strength and repeated load tests in uniaxial tension and a catalog of fracture and healing surface energy components of asphalt binders and aggregates measured separately. In this approach, HMAC behavior in fatigue is governed by the energy stored on or released from crack faces that drive the fracture and healing processes, respectively, through these two mechanisms of fracture and healing.

DPSE and pseudo strain (PS) are defined to quantify and monitor fracture and healing in HMAC mixtures. DPSE in an undamaged non-linear visco-elastic material is expected due to the viscous lag in material response. This pseudo strain energy is represented by the area in the pseudo hysteresis loop of a measured stress versus calculated PS after correcting for non-linearity, plotted as shown in Figure 4-1. PS is determined by calculating the expected stress in a linear visco-elastic material under damaged conditions and dividing by a measured reference modulus (from the first stress cycle of a repeated load test), and a non-linearity correction factor ($\psi(t)$). This $\psi(t)$ is introduced primarily to account for any non-linearity of the undamaged visco-elastic material (*30*).

Any departure from the initial pseudo hysteresis loop requires additional dissipated energy, indicating that fracture is occurring for temperatures less than 25 °C (77 °F). As the fracture progresses with additional load cycles, DPSE will increase, while the HMAC mixture stiffness will decrease. The healing process on the other hand produces opposite results, with DPSE decreasing and the HMAC mixture stiffness increasing.

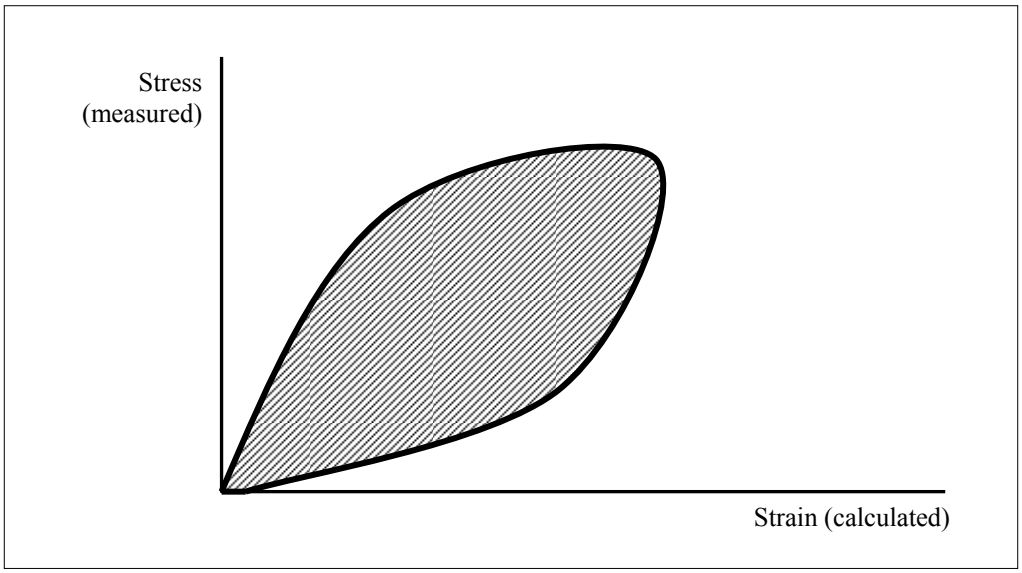

Figure 4-1. Example of Hysteresis Loop (Shaded Area is DPSE).

Monitoring of both DPSE and PS in repeated uniaxial tension tests is required in this micromechanical approach. The relationship between DPSE and N is modeled using either of two functional forms, linear logarithmic or simple power law, and calibrated using measured data. These calibration coefficients and Paris' Law fracture coefficients determined by monitoring both DPSE and PS with microcrack growth are required to determine N_i for macrocrack initiation at an average microcrack size of 0.30 inches (*29*, *31*). This calibration is required because the coefficients of the equation for microcrack growth are not widely known as compared to those for macrocrack growth. The size and shape of a microcrack is controlled by microscopic quantities such as mastic film thickness, aggregate particle size, and the degree of bonding of crack-arresting obstacles dispersed in the mastic. Nevertheless, microcrack growth is still controlled by the rate of change of DPSE and indicated by a reduction in HMAC mixture stiffness.

N_p for microcrack propagation is a function of the difference between fracture and healing speed. This N_p is primarily quantified in terms of Paris' Law fracture coefficients and the shear strain that constitute the failure load-response parameter. Fracture speed depends on material properties determined in uniaxial tensile creep or relaxation and strength tests at multiple temperatures and total fracture surface energy.

Healing occurs as a result of both short-term and long-term rates of rest periods, and depends on traffic rest periods, healing surface energy components, and the material properties measured in compression relaxation modulus tests. Because the HMAC mixture healing properties are climatic dependent, fatigue healing calibration constants must be used to account for the climatic and environmental location of a given pavement structure (*29*). In determining the final N_f, an anisotropic shift factor (discussed subsequently) is also introduced to account for the anisotropic nature of HMAC.

The surface energies are made up of contributions from nonpolar short-range Lifshitz-van der Waals forces and longer-range polar acid-base forces mainly associated with hydrogen bonding (*30*, *32*, *33*). The polar acid-base surface energy is itself also a combination of the acid surface energy and the base surface energy. These polar forces typical of hydrogen bonding take longer to form and act perpendicular to the crack faces to actively pull them together, while the nonpolar tensile short-range and short-lived Lifshitz-van der Waals forces act in the plane of the crack face to form a contractile skin that resists healing (*28*-*30*, *32*, *33*).

The difference between the total fracture and healing surface energies lies in the measurement of the individual surface energy components using carefully selected materials with known surface energy component values. Fracture components are found when dewetting, and healing components are determined when wetting (*28-30, 32, 33*).

In this CM approach, the design shear strain computed within the HMAC layer of the pavement structure for N_p analysis constitutes the failure load-response parameter. This critical design shear strain is determined at the edge of a loaded wheel-tire using either a layered linear-elastic or visco-elastic model of material behavior characterization. The utilization of calibration constants in modeling SF_h, N_i, and N_p constitutes the calibration part of the CMSE approach. This calibration simulates the field mechanism of microcrack growth in the HMAC layer thickness with respect to traffic loading and environmental conditions.

HMAC mixture characterization for the CM fatigue analysis requires uniaxial testing (tension and/or compression) of gyratory compacted cylindrical HMAC specimens under temperature controlled conditions. Specimen conditioning and laboratory testing at representative field service temperatures is strongly recommended to simulate environmental temperature conditions.

The CM approach discussed in this interim report encompasses surface energy data analysis and consequently the acronym CMSE is used, with SE denoting surface energy.

CMSE FATIGUE ANALYSIS INPUT AND OUTPUT DATA

Table 4-1 summarizes the general CMSE fatigue analysis input and the expected output data. These parameters and their respective components are discussed in more detail in subsequent sections. Figure 4-2 is a schematic illustration of the CMSE design and analysis system.

Table 4-1. Summary of CMSE Fatigue Analysis Input and Output Data.

Source	Parameter
Laboratory test data (HMAC mixture testing of cylindrical specimens)	- Tensile stress & strain - Relaxation modulus (tension & compression) - Uniaxial repeated direct-tension test data (strain, stress, time, & N) - Anisotropic data (vertical & lateral modulus) - Dynamic contact angle for asphalt SE - Vapor pressure and adsorbed gas mass for aggregate SE
Analysis of laboratory test data	- Tensile strength - Relaxation modulus master-curves (tension & compression) - Non-linearity correction factor - DPSE & slope of DPSE vs. Log N plot - SE for asphalt & aggregates - Healing indices - Healing calibration constants - Creep compliance - Shear modulus - Load pulse shape factor
Field conditions (design data)	- Pavement structure (layer thickness) - Pavement materials (elastic modulus & Poisson's ratio) - Traffic (ESALs, axle load, & tire pressure) - Environment (temperature & moisture conditions.) - Field calibration coefficients - Temperature correction factor
Computer stress-strain analysis	- Design shear strain (γ) @ edge of a loaded tire
Other input parameters	- Reliability level (i.e., 95%) - Crack density - Microcrack length - HMAC brittle-ductile failure characterization - Stress intensity factors - Regression constants - Shear coefficient
OUTPUT	- Paris' law coefficients of fracture (A, n) - Shift factor due to anisotropy (SF_a) - Shift factor due to healing (SF_h) - Fatigue load cycles to crack initiation (N_i) - Fatigue load cycles to crack propagation (N_p) - HMAC mixture fatigue resistance (N_f)

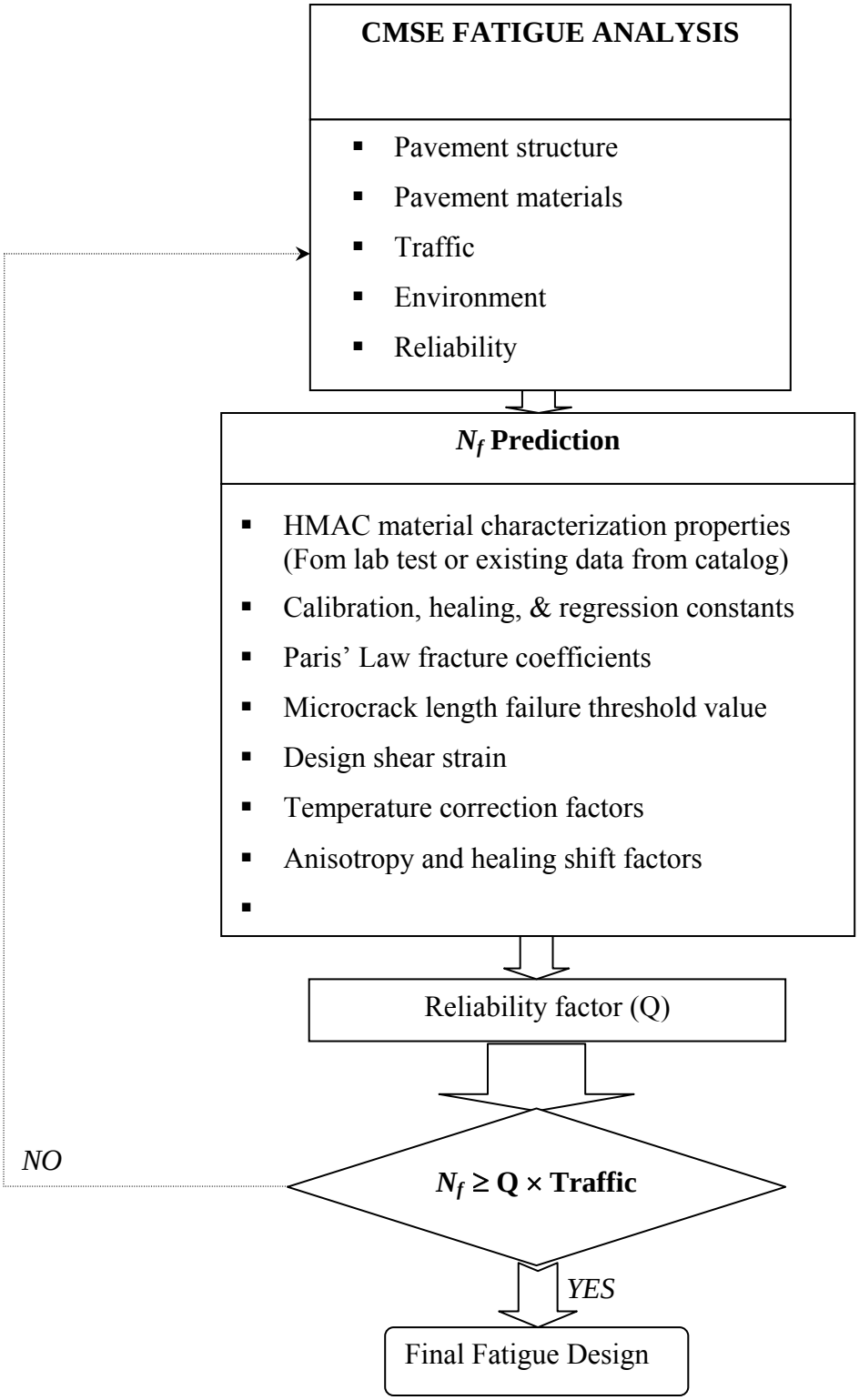

Figure 4-2. The CMSE Fatigue Design and Analysis System.

CMSE FATIGUE FAILURE CRITERIA

For the CMSE approach, fatigue failure is defined as crack propagation through the HMAC layer thickness. In this project, researchers selected a maximum microcrack length of 0.30 inches as the failure threshold value for crack initiation and propagation through the HMAC layer. This 0.30 inches threshold value was selected based on findings of Lytton et al. in their extensive fatigue tests that crack propagation in the HMAC layer begins when microcracks grow and coalesce to form a small crack of approximately 0.30 inches long (*29*).

CMSE FATIGUE ANALYSIS PROCEDURE

Equation 4-1, which relates fatigue life (N_f) to the number of load cycles to crack initiation (N_i) and crack propagation (N_p) as a function of anisotropy (SF_a) and healing (SF_h) shift factors is the fundamental principle of the CMSE approach for fatigue modeling of HMAC mixtures (*29*).

$$N_f = SF_a \times SF_h\left(N_i + N_p\right) \qquad \text{(Equation 4-1)}$$

where:

N_f = Fatigue life or number of load cycles to fatigue failure
SF_a = Shift factor due to anisotropy, ranging between 1 and 5
SF_h = Shift factor due to binder healing effects, ranging between 1 and 10
N_i = Number of load cycles to crack initiation
N_p = Number of load cycles to crack propagation

Each of these terms in Equation 4-1 is discussed in the following subsections.

Shift Factor Due to Anisotropic Effect, SF_a

Anisotropy arises due to the fact that the HMAC material is not isotropic as often assumed. The mixture stiffness (modulus) in the lateral (horizontal) direction is not equal to that in the vertical direction due to the differences in the particle orientation during compaction/construction. During construction, there is always a high compactive effort in the vertical direction relative to other directions. So the material behavior or response to loading and/or the environment is different in different directions. However, most laboratory test protocols measure only the vertical stiffness and assume isotropic behavior.

In the CMSE analysis, SF_a takes care of the anisotropic behavior of the HMAC mixture. Equation 4-2 shows the elastic modular relationship between vertical (E_z) and horizontal (E_x) moduli used in this project. E_z and E_x are measurable parameters from the anisotropic test (*34*).

$$SF_a = \left(\frac{E_z}{E_x}\right)^{1.75} \qquad \text{(Equation 4-2)}$$

where:

E_z = Elastic modulus in vertical direction

E_x = Elastic modulus in lateral or horizontal direction

Shift Factor Due to Healing Effect, SF_h

Due to traffic rest periods and temperature variations, asphalt has a tendency to heal (closure of fracture surfaces), which often results in improvement in the overall HMAC mixture fatigue performance. The CMSE approach takes this into account and relates healing to traffic rest periods and temperature by the following equations (*29*, *33*):

$$SF_h = 1 + g_5\left(\frac{\Delta t_r}{a_{TSF}}\right)^{g_6} \qquad \text{(Equation 4-3)}$$

$$\Delta t_r = \frac{31.536 \times 10^6 \, P_{DL}}{80kN \text{ Traffic ESALs}} \quad \text{(Equation 4-4)}$$

$$g_5 = a(h_o)^{g_6} \quad \text{(Equation 4-5)}$$

$$h_o = \dot{h}_2 + \left(\frac{\dot{h}_1 - \dot{h}_2}{1 + \left[\left(\frac{\dot{h}_1 - \dot{h}_2}{h_\beta} \right) \left(\frac{\Delta t C_{sr}}{a_{TSF}} \right) \right]} \right) \quad \text{(Equation 4-6)}$$

$$\dot{h}_1 = \left(\frac{C_1}{\left[\Delta G_h^{LW} E_c \right]^{\left(\frac{1}{m_c} \right)}} \right) \quad \text{(Equation 4-7)}$$

$$\dot{h}_2 = \left(\left[C_2 \left(\frac{\Delta G_h^{AB}}{E_c} \right) \right]^{\left(\frac{1}{m_c} \right)} + C_3 \right) \quad \text{(Equation 4-8)}$$

$$h_\beta = C_4 \left(\frac{\Delta G_h^{AB}}{\Delta G_h^{LW}} \right) \left(\frac{C_5}{m_c} \right) \quad \text{(Equation 4-9)}$$

where:

Δt_r = Rest period between major traffic loads, s

Δt = Loading time, s

a_{TSF} = Temperature shift factor for field conditions (~1.0)

C_{sr} = Square rest period factor (~1.0)

a, g_5, g_6 = Fatigue field calibration constants

h_0, $\dot{h}_{1-2}$, = Healing rates

h_β = Healing index, ranging between 0 and 1.0

P_{DL} = Pavement design life in years

ESALs = Equivalent single axle loads

$C_{1\text{-}5}$ = Healing constants

E_c = Elastic modulus from compression relaxation modulus master-curve

m_c = Exponent from compression relaxation modulus master-curve

ΔG_h^{AB}, ΔG_h^{LW} =Surface energies due to healing or dewetting, ergs/cm^2

In Equation 4-3, Δt_r represents the field long-term rest period and depends on the pavement design life and traffic expressed in terms of ESALs (*29*). The numerical value of 31.536×10^6 in Equation 4-4 represents the total time in seconds for a 365 day calendar year. The parameter a_{TSF} is a temperature shift factor used to correct for temperature differences between laboratory and field conditions. For simplicity, the research team used an a_{TSF} value of 1.0, but this value can vary depending on the laboratory and field temperature conditions under consideration. C_{sr} represents the shape of the input strain wave rest period during the uniaxial repeated direct-tension test.

As discussed subsequently, the periodic time interval between the input strain waveforms for the uniaxial repeated direct-tension test in this project simulated a square shaped form, with a total duration of 0.9 s. This 0.9 s periodic time interval was considered as the square shaped rest period, so a C_{sr} value of 1.0 was used in the analysis (*36*). If sufficient enough, any rest period to HMAC subjected to repeated loading allows for elastic recovery and subsequent healing, which is a desirable phenomenon in terms of HMAC pavement fatigue performance.

The parameters a, g_5, g_6 , h_0, and $\dot{h}_{1-2}$ are fatigue field calibration constants and healing rates quantifying the HMAC mixture healing properties as a function of climatic location of the pavement structure in question, *SE* due to healing, and HMAC mixture properties (E_c and m_c) obtained from compression relaxation modulus tests. These calibration constants and healing rates also represent the HMAC mixture short-term rest periods and asphalt binder healing rates, both short-term and long-term, respectively (*29*). The parameter h_β is a healing index ranging between 0 and 1.0 that represents the maximum degree of healing achievable by the asphalt binder (*33*).

SE and relaxation modulus tests are discussed in the subsequent sections of this chapter. *SE*, E_c, and m_c are material (asphalt, aggregate, and HMAC mixture) dependent, but also vary with the aging condition of the asphalt and/or HMAC mixture, which has a net impact on SF_h and N_f. As discussed in Chapter 6, this preliminary study has shown that the variation of these parameters (*SE*, E_c, and m_c) with 3 months aging of the asphalt and HMAC mixture at 60 °C

(140 °F) reduced the value of SF_h considerably, particularly the resultant N_f. Analysis procedures for SE, E_c, and m_c are discussed in the subsequent text.

The healing constants C_1 through C_5 were backcalculated from regression analysis as a function of the measured E_c, ΔG_h due to healing, and the healing rates (h_i) using a spreadsheet sum of square error (SSE) minimization technique (29, 30, 33).

Number of Load Cycles to Crack Initiation, N_i

N_i is defined as the number of load cycles required to initiate and grow a microcrack to 0.30 inches in length in the HMAC layer. In the CMSE analysis, N_i is determined according to the following equation as a function of crack density, specimen cross-sectional area, Paris' Law fracture coefficients, and the rate that damage accumulates as indicated by DPSE (29, 30, 34):

$$N_i = \left(\frac{C_{\max}^{(1+2n)}}{A}\right)\left(\left[\frac{4\pi A_c}{b}\right]^n\right)(C_D)^n \qquad \text{(Equation 4-10)}$$

$$n = \left(\frac{1}{m_t}\right) \qquad \text{(Equation 4-11)}$$

$$A = \frac{k}{\sigma_t^2 I_i}\left(\left[\frac{D_1^{(1-m_t)} E_t}{\Delta G_f}\right]^{\left(\frac{1}{m_t}\left[\frac{1}{(n_{BD}+1)}\right]\right)}\right)\int_0^{\Delta t} w^n(t)dt \qquad \text{(Equation 4-12)}$$

$$D_1 = \left(\frac{1}{E_t}\right)\left(\frac{Sin[m_t\pi]}{m_t\pi}\right) \qquad \text{(Equation 4-13)}$$

$$I_i = \frac{2}{(1+n_{BD})} \qquad \text{(Equation 4-14)}$$

$$\int_0^{\Delta t} w^n(t).dt = \int_0^{\Delta t} \left(Sin^{2n}\left[\frac{\pi}{\Delta t} t \right] \right) dt = 0.5042 - 0.1744 \ln(n) \qquad \text{(Equation 4-15)}$$

where:

C_{max} = Maximum microcrack length (~0.30 inches)

A, n = Paris' Law fracture coefficients

A_c = Specimen cross-sectional area

b = Rate of accumulation of dissipation of pseudo strain energy

C_D = Crack density

m_t = Exponent obtained from the tension relaxation modulus master-curve (slope of the log relaxation modulus versus log time graph)

D_1 = Time-dependent creep compliance

E_t = Elastic modulus from tension relaxation modulus master-curve, psi

k = Material coefficient (~0.33)

ΔG_f = Surface energy due to fracture or dewetting, ergs/cm^2

σ_t = Maximum tensile strength

I_i = Dimensionless stress integral factor in crack failure zone, ranging between 1 and 2

n_{BD} = Brittle-ductile factor, ranging between 0 and 1

Δt = Repeated loading time (~0.01 s)

$\int_0^{\Delta t} w^n(t)dt$ = Load pulse shape factor, ranging between 0 and 1

t = Time, s

The parameter C_{max} defines the CMSE failure criterion in terms of the maximum microcrack length at the point of crack initiation and subsequent propagation through the HMAC layer thickness. The crack density (C_D) and rate of accumulation of dissipation of pseudo strain energy (b) are discussed in the subsequent subsections of this chapter. The parameters A and n are Paris' Law fracture coefficients for material fracture properties, which quantifies the HMAC mixture's susceptibility to fracturing under repeated loading. Generally, the smaller the values of the Paris' Law fracture coefficients, the greater the fracture damage resistance.

According to Paris' Law (53) and Schapery's theory (54, 55), the coefficient n can be defined simply as the inverse of the stress (tensile) relaxation rate (m_t) as expressed by Equation 4-11. This assumption is valid for linear visco-elastic HMAC materials under a constant strain-controlled uniaxial direct-tension test (30, 33).

The Paris' Law fracture coefficient A (Equation 4-12), on the other hand, is a function of many parameters including k, D_1, E_t, m_t, n_{BD}, ΔG_f, σ_t, I_i, and $w^n(t)$. Based on Equation 4-10, a small value of A is desirable in terms of HMAC mixture fatigue resistance. Numerical analysis, however, indicated that this coefficient A is very sensitive to n_{BD} and σ_t, if other factors are held constant. The parameter k is a material coefficient relating the length of the fracture process zone ($\propto$) to strain energy and mixture tensile strength. While this k is a measurable parameter, a value of 0.33 was used based on findings of Lytton et al. (29) and the assumption that it ($k \cong 0.33$) does not vary significantly with microcrack length in the fracture process zone.

As expressed by Equation 4-13, the time-dependent creep compliance, D_1, was determined as a function of E_t and m_t. Although an exact value of D_1 can be measured from uniaxial creep tests, this less costly and simple approximation produces a reasonable value that is sufficient enough to use in HMAC mixture characterization analysis.

The numerical integration of $w^n(t)$ with respect to time (t) describes the shape of the input load pulse as a function of material fracture parameter n (Paris' Law fracture coefficient). This integral exhibits a linear relationship with the Paris' Law fracture coefficient A, evident from Equation 4-12, and has a subsequent inverse relationship with N_i. For a haversine shaped input strain waveform for the uniaxial repeated direct-tension test, as was the case in this project, the integral reduces to a simple linear form shown in Equation 4-15, with n as the only variable. Note that material response to loading is not only magnitude dependent but also depends on the shape of the application load form.

As discussed subsequently, a haversine shaped input load form is a close simulation of HMAC material load-response under a moving wheel load (29, 30). The parameters E_t, m_t, ΔG_f, and σ_t are discussed subsequently.

I_i is an elasticity resultant factor due to the integration of the stresses near the microcrack tip over a small region in the microcrack failure zone (*29*, *30*, *33*). As expressed by Equation 4-14, the research team quantified I_i simply as a function of n_{BD} in this project. This brittle-ductile factor n_{BD}, which ranges between 0 for perfectly linear plastic materials and 1.0 for brittle materials, is an age-related adjustment factor that accounts for the brittleness and ductility state of the HMAC mixture in terms of stress-strain response under loading. In this project, unaged HMAC specimens were assumed to exhibit plastic behavior and were subsequently assigned an n_{BD} value of 0.0. All the aged HMAC specimens were assumed to exhibit a brittle-ductile behavior lying somewhere between perfectly plastic and brittle behavior, and were thus assigned an n_{BD} value of 0.5.

Number of Load Cycles to Crack Propagation, *Np*

N_p refers to the number of load cycles required to propagate a 0.30 inch microcrack through the HMAC layer thickness. As expressed by Equation 4-16, N_p is determined as a function of the maximum microcrack length, HMAC layer thickness, shear modulus, Paris' Law fracture coefficients, and a design shear strain (*29*, *30*, *33*).

$$N_p = \left(\frac{d^{\left(1-\frac{n}{2}\right)}}{\left[A(2r)^n (SG)^n (1-nq)\right]} \right) \left(1 - \left[\frac{C_{\max}}{d} \right]^{(1-nq)} \right) \left(\frac{1}{\gamma} \right)^n \qquad \text{(Equation 4-16)}$$

$$S = \frac{(1-\nu)}{(1-2\nu)} \qquad \text{(Equation 4-17)}$$

$$G = E_t \left(\frac{G_{xz}}{E_z} \right) \qquad \text{(Equation 4-18)}$$

where:

A, n = Paris' Law fracture coefficients

r, q = Regression constants for stress intensity factor (~4.40, 1.18) (*29*)

S = Shear coefficient

G = Shear modulus

C_{max} = Maximum microcrack length (~0.30 inches)

d = HMAC layer thickness

γ = Maximum design shear strain at tire edge

ν = Poisson's ratio (~0.33)

G_{xz} = Resilient shear modulus

E_t = Elastic modulus from tensile relaxation modulus master-curve

If the elastic modular ratio G_{xz}/E_z in Equation 4-18 is unknown, Equation 4-19 below can be used to approximate G (*36*). Equation 4-19 is the shear-elastic modulus relationship based on elastic theory.

$$G = \frac{E_t}{2(1+\nu)} \qquad \text{(Equation 4-19)}$$

The parameters A, n, and C_{max} were discussed in the previous subsections, and γ is discussed in the subsequent text. Like N_i, an inverse relationship exists between A and N_p, indicating that a small value of A is desired in terms of HMAC mixture fatigue resistance. The γ is the shear strain and also exhibits an inverse relationship with N_p.

Unlike N_i, d is introduced in N_p because during the microcrack propagation process, for fatigue failure to occur, a microcrack length of a defined threshold value must actually propagate through the HMAC layer thickness. N_i is primarily a fatigue model for microcrack initiation and is independent of the parameter d. Parameters r and q are regression constants that are a function of the stress intensity distribution in the vicinity of the microcrack tip. Values of 4.40 and 1.18 were used, respectively, based on findings of previous work by Lytton et al. (*29*). S is a shear coefficient, which as defined by Equation 4-17, is a function of the Poisson's ratio. E_z and G_{xz} are load-related material shear properties, which quantify the HMAC shear response to traffic loading.

Surface Energies, ΔG_h^{AB}, ΔG_h^{LW}, and ΔG_f

To cause load-induced damage in the form of fatigue cracking or to close up the fracture surfaces (healing), energy must be expended. Surface energy data thus constitute input parameters for the healing, crack initiation, and propagation calculations in the CMSE fatigue analysis. The respective equations for the surface energy data analysis required for the CMSE approach are as follows (*30*, *33*):

$$\Delta G_h^{LW} = -\Gamma_{ij}^{LW} + \Gamma_i^{LW} + \Gamma_j^{LW} \quad \text{(Equation 4-20)}$$

$$\Delta G_h^{AB} = -\Gamma_{ij}^{AB} + \Gamma_i^{AB} + \Gamma_j^{AB} \quad \text{(Equation 4-21)}$$

$$\Delta G_f = \Delta G_f^{LW} + \Delta G_f^{AB} = -\Gamma_{ij}^{LW} + \Gamma_i^{LW} + \Gamma_j^{LW} - \Gamma_{ij}^{AB} + \Gamma_i^{AB} + \Gamma_j^{AB} \quad \text{(Equation 4-22)}$$

$$\Gamma_{ij}^{LW} = \left(\sqrt{\Gamma_i^{LW}} - \sqrt{\Gamma_j^{LW}}\right)^2 \quad \text{(Equation 4-23)}$$

$$\Gamma_i^{AB} = 2\left(\sqrt{\Gamma_i^+ \Gamma_i^-}\right) \quad \text{(Equation 4-24)}$$

$$\Gamma_{ij}^{AB} = 2\left(\sqrt{\Gamma_i^+} - \sqrt{\Gamma_j^-}\right)\left(\sqrt{\Gamma_i^-} - \sqrt{\Gamma_j^-}\right) \quad \text{(Equation 4-25)}$$

$$\Gamma_j^{AB} = 2\left(\sqrt{\Gamma_j^+ \Gamma_j^-}\right) \quad \text{(Equation 4-26)}$$

where:

Γ	=	Surface free energy component of asphalt or aggregate, ergs/cm^2
i,j	=	Subscript “i” for asphalt (healing or fracture) and “j” for aggregate
h,f	=	Subscript “h” for healing and “f” for fracture
LW	=	Superscript “LW” for Lifshitz-van der Waals component
AB	=	Superscript “AB” for Acid-Base component

+	=	Superscript "+" for Lewis acid component of surface interaction
–	=	Superscript "–" for Lewis base component of surface interaction
Γ_{ij}	=	Interfacial surface energy between asphalt and aggregate due to "LW" or "AB" (superscripts) components, ergs/cm^2
ΔG	=	Total surface free energy due to "h" or "f" (subscripts) for "LW" and/or "AB" (superscripts) components, ergs/cm^2

Relaxation Modulus, E_i, Exponent, m_i, and Temperature Correction Factor, a_T

The elastic relaxation modulus ($E(t)$) and exponent (m_i) were determined from relaxation modulus master-curves of log modulus (E) versus log time (t). These master-curves were generated from tension and compression relaxation test data at a reference temperature of 20 °C (68 °F) (*30*). From the relaxation modulus master-curve, a power function of relaxation modulus and loading time was generated as follows:

$$E(t) = E_i \xi^{-m_i} \qquad \text{(Equation 4-27)}$$

$$\xi = \frac{t}{a_t} \qquad \text{(Equation 4-28)}$$

where:

$E(t)$	=	Elastic modulus at time t
E_i	=	Elastic modulus, tension (E_t) or compression (E_c) @ $\xi = 1.0$ s
ξ, t	=	Reduced and actual test time, respectively, s
m_i	=	Stress relaxation rate ($0 \leq m_i < 1$)
i	=	Subscript "t" for tension or "c" for compression

Equation 4-27 is a simple power law relationship that is valid for most HMAC materials at intermediate and/or long times of loading (*30*). The exponent m_i refers to the rate of stress relaxation.

DPSE and Constant, *b*

Researchers determined the constant *b* from a combination of the relaxation modulus test data (E_t and m_t) in tension and the uniaxial repeated direct-tension test data. The constant *b* is defined as the rate of damage (energy dissipation) due to repeated loading that primarily causes fracture at relatively low temperatures (*30*, *35*).

For any selected load cycle, the time-dependent linear visco-elastic stress (under damaged or undamaged conditions) was calculated using the Boltzmann superposition constitutive equation as a function of the relaxation modulus and the uniaxial repeated test data (*30*, *35-37*). A temperature correction factor (a_T) was also introduced into the constitutive equation to normalize the calculated stress to a given reference temperature. In this project, a_T was obtained from relaxation modulus analysis and the selected reference temperature was 20 °C (68 °F). This temperature is a realistic simulation of field service temperatures. The uniaxial repeated direct-tension test was conducted at 30 °C (86 °F), and therefore the calculated stress had to be normalized to 20 °C (68 °F).

Secondly, pseudo strain for damaged conditions was calculated as a function of the normalized calculated linear visco-elastic stress for damaged conditions, the reference modulus (E_R), and $\psi(t)$ (*30*). In the analysis, calculated pseudo strain rather than physically measured strain is used to characterize damage and healing to separate and eliminate the time-dependent visco-elastic behavior of the HMAC material from real damage during the strain controlled fatigue test (*30*).

E_R is the modulus of the undamaged material determined from the first load cycle of the uniaxial repeated direct-tension test. The $\psi(t)$, which is a function of the calculated and measured stress at the first load cycle in an assumed undamaged condition, is introduced primarily to account for any non-linearity of the undamaged visco-elastic material.

Finally, DPSE was then calculated as a product of the measured stress and the calculated pseudo strain for damaged conditions using the double meridian distance method (DMD) for traverse area determination (*30*, *38*). This DPSE is simply the area in the pseudo hysteresis loop of the measured tensile stress versus the calculated pseudo strain plotted as shown in Figure 4-1. The respective equations are shown subsequently.

$$DPSE = \sum\left(\varepsilon_R^d(t)\sigma_m^d(t)\right) \quad \text{(Equation 4-29)}$$

$$\varepsilon_R^d(t) = \psi(t)\frac{\sigma_c^d(t)}{E_R} \quad \text{(Equation 4-30)}$$

$$\Psi(t) = \frac{\sigma_{c(1)}^u(t)}{\sigma_{m(1)}^u(t)} \quad \text{(Equation 4-31)}$$

$$\sigma_c^u(t) \neq \sigma_m^u(t)\,,\ \sigma_c^d(t) \neq \sigma_m^d(t) \quad \text{(Equation 4-32)}$$

$$\sigma_{c(1)}^u(t) = \sigma_{c(1)}^d(t) \neq \sigma_{c(2\ldots N)}^d(t)\ ,\ \sigma_{m(1)}^u(t) = \sigma_{m(1)}^d(t) \neq \sigma_{m(2\ldots N)}^d(t) \quad \text{(Equation 4-33)}$$

$$\sigma_c(t) = \int_0^t E(t-\tau)\frac{\partial\varepsilon(\tau)}{d\tau}\,d\tau \quad \text{(Equation 4-34)}$$

Equation 4-34 is the general uniaxial stress-strain relationship applicable to most linear visco-elastics materials including HMAC (*30*, *35*). For a haversine shaped input strain waveform, Equation 4-34 can be written in the simple approximate numerical-integration form shown in Equation 4-35:

$$\sigma_c(t_{i+1}) = \sum_{k=0}^{k=i+1}\left(C_k\Delta\tau\left[E_\infty + E_1\left(t_{i+1}-t_k\right)^{-m}\right]\right) \quad \text{(Equation 4-35)}$$

Assuming E_∞ is zero, and using E_t and m_t for undamaged conditions and a_T from relaxation modulus analysis, Equation 4-35 reduces to Equation 4-36 shown below:

$$\sigma_c(t_{i+1}) = \sum_{k=0}^{k=i+1}\left(C_k\Delta\tau\left[E_t\left(\frac{(t_{i+1}-t_k)}{a_T}\right)^{-m_t}\right]\right) \quad \text{(Equation 4-36(a))}$$

$$\sigma_c(t_{i+1}) = \Delta\tau E_t \sum_{k=0}^{k=i+1}\left(C_k \left(\frac{(t_{i+1} - t_k}{a_T} \right)^{-m_t} \right) \qquad \text{(Equation 4-36(b))}$$

where:

$\sigma^u_{c(1)}(t)$ = Calculated time-dependent linear visco-elastic tensile stress in an assumed undamaged condition at the first load cycle

$\sigma^d_c(t)$ = Calculated time-dependent linear visco-elastic tensile stress under damaged conditions at any load cycle other than the first

t_{i+1}, t_k = Present and previous time, respectively, s

τ = Loading time history, e.g., 0.0 to 0.10 s at which strains were measured

$\Delta\tau$ = Time increment, s (e.g., 0.005 s)

$E(t-\tau)$ = Tensile relaxation modulus in assumed undamaged condition at time t-τ

$\varepsilon(\tau)$ = Measured strain at previous time,τ

C_k = Mean slope of any segment of the haversine input strain waveform

$\varepsilon^d_R(t)$ = Calculated pseudo strain for damaged conditions

E_R = Reference modulus for assumed undamaged material calculated from the first load cycle

$\psi(t)$ = Dimensionless non-linearity correction factor (NLCF)

$\sigma^u_{m(1)}(t)$ = Measured tensile stress for assumed undamaged condition at the first load cycle

$\sigma^d_m(t)$ = Measured tensile stress for damaged conditions

a_T = Temperature correction factor (from relaxation modulus analysis)

$DPSE$ = Dissipated pseudo strain energy

For a haversine shaped input strain waveform, both the measured and approximate (calculated) stress should exhibit a shape form of the format shown in Figure 4-3.

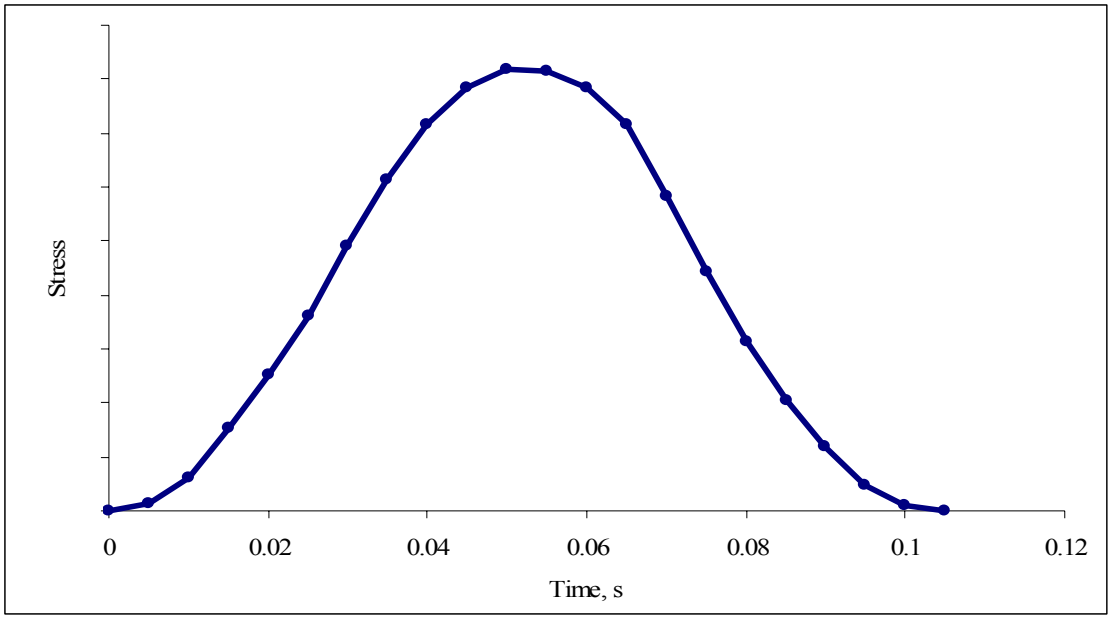

Figure 4-3. Output Stress Shape Form (Measured or Calculated [Approximate]).

DPSE for selected load cycles (N) was then plotted against log N to generate a linear function of the format shown in Equation 4-37. The constant b in Equation 4-37, also defined as the rate of change in DPSE during microcrack growth, is simply the slope of the DPSE versus log N plot, which is the required input parameter for the CMSE fatigue analysis *(30)*.

$$W_R = a + bLog(N) \qquad \text{(Equation 4-37)}$$

where:

W_R = DPSE

a = Constant or DPSE at the first load cycle

b = Slope of W_R-log N plot

N = Load cycle

A plot of DPSE versus log N should exhibit a simple linear graph of the format shown in Figure 4-4.

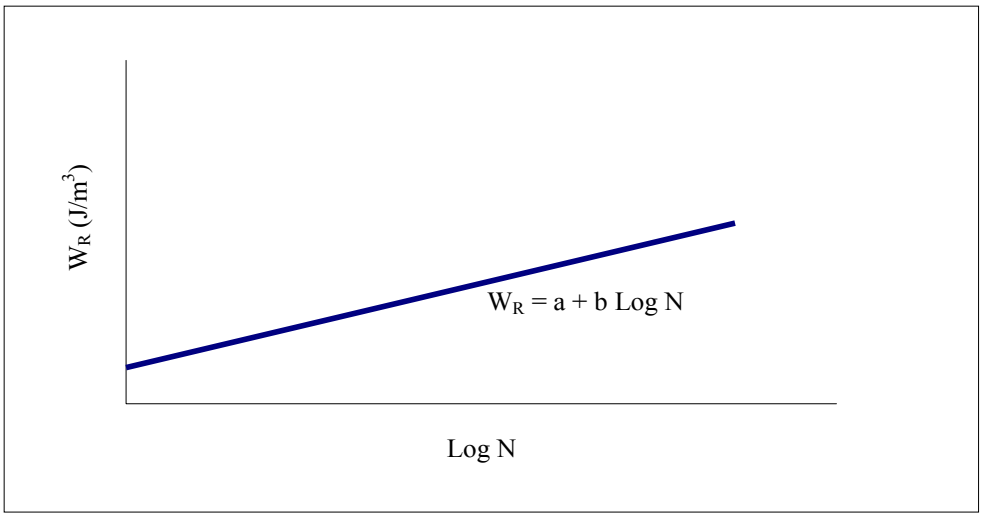

Figure 4-4. Example of W_R – Log N Plot.

The constant *b* is inversely related to the HMAC mixture fatigue resistance. Generally, a comparatively small value of *b* is indicative of a relatively low rate of accumulation of micro fatigue damage and consequently high HMAC mixture fatigue resistance.

Crack Density, C_D

Crack density calculations were based on the cavitation analysis by Marek and Herrin (*39*) assuming a brittle mode of crack failure for the HMAC specimen, as shown in Figure 4-5.

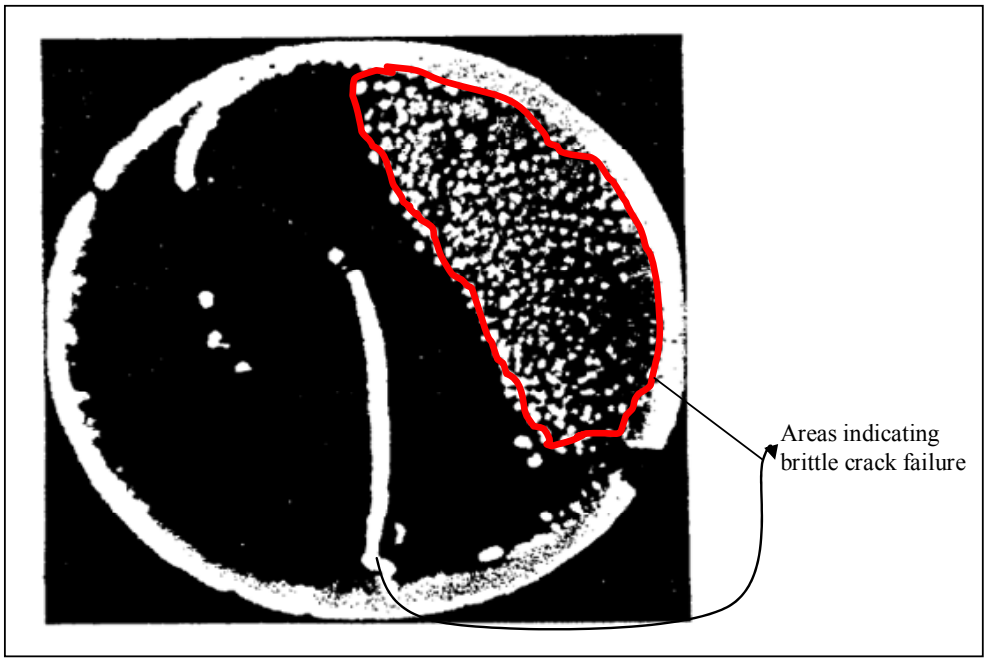

Figure 4-5. Brittle Crack Failure Mode (Marek and Herrin [*39*]).

In their analysis, Marek and Herrin (*39*) used an average microcrack length of 0.015 inches based on 281 HMAC samples. Using these data, the research team calculated microcrack density as a function of the number of cracks per specimen cross-sectional area to be 1,495 in^{-2}. This is the crack density value (1,495 in^{-2}) used for the CMSE fatigue analysis in this project.

Shear Strain, γ

FEM analysis software that takes into account the visco-elastic nature of HMAC is desirable for pavement stress-strain analysis to determine the maximum design shear strain γ at the edge of a loaded tire. If a linear elastic analysis software such as ELSYM5 (*15*) is used, an adjustment to the calculated γ can be made to account for the visco-elastic and plastic nature of HMAC.

Input parameters for the stress-strain analysis include traffic loading (ESALs and the axle and tire configuration), pavement structure and material properties defined as a function of environment (temperature and subgrade moisture conditions), and desired response locations. If linear-elastic conditions are assumed, Equation 4-38 can be used to calculate γ (*36*).

$$\gamma = \frac{\sigma_p}{SG} \qquad \text{(Equation 4-38)}$$

where:

σ_p = Tire pressure, psi (~100 psi)

S = Shear coefficient

G = Shear modulus, psi

VARIABILITY OF FATIGUE LIFE PREDICTED BY THE CMSE APPROACH

As an estimate for variability of fatigue life measured by the CMSE approach, a coefficient of variation *COV* is utilized. The *COV* expresses the standard deviation as a percent of the mean as follows:

$$COV = \frac{100s}{\bar{x}} \qquad \text{(Equation 4-39)}$$

where:

COV = Coefficient of variation

s = Sample standard deviation

$\bar{x}$ = Sample mean, calculated based on replicate measurements of N_f

The *COV* is a measure of relative variation, and it says that the measurements lie, on the average, within approximately *COV* percent of the mean. Replicate N_f obtained by varying the material input parameters such as σ_t, E_i, m_i, and b for the same HMAC mixture based on actual laboratory measured replicate values (different specimens) also provided a reasonable measure of variability and precision of the CMSE approach. The *COV* obtained as a function of these replicate N_f is an indicator of the CMSE approach's N_f prediction capability and repeatability of the associated CMSE laboratory tests.

CMSE LABORATORY TESTS

The required laboratory tests for the CMSE approach of HMAC fatigue analysis include tensile strength, relaxation modulus both in tension and compression, uniaxial repeated direct-tension, and surface energy (*29*, *30*, *33*). These tests are described in this section. For each of these tests, at least two replicate specimens were tested per aging condition.

Tensile Strength Test

The tensile strength test was conducted to determine the HMAC mixture tensile strength (σ_t), which is a required input parameter for CMSE N_f analysis. The test protocol is briefly discussed in the subsequent text.

Test Protocol

The tensile strength test protocol involves applying a continuous increasing tensile load to a cylindrical HMAC specimen (Figure 4-6) at a constant elongation (deformation) rate of 0.05 in/min till failure (break point). This test is destructive. Figure 4-6 shows the loading configuration for and typical results from the tensile strength test.

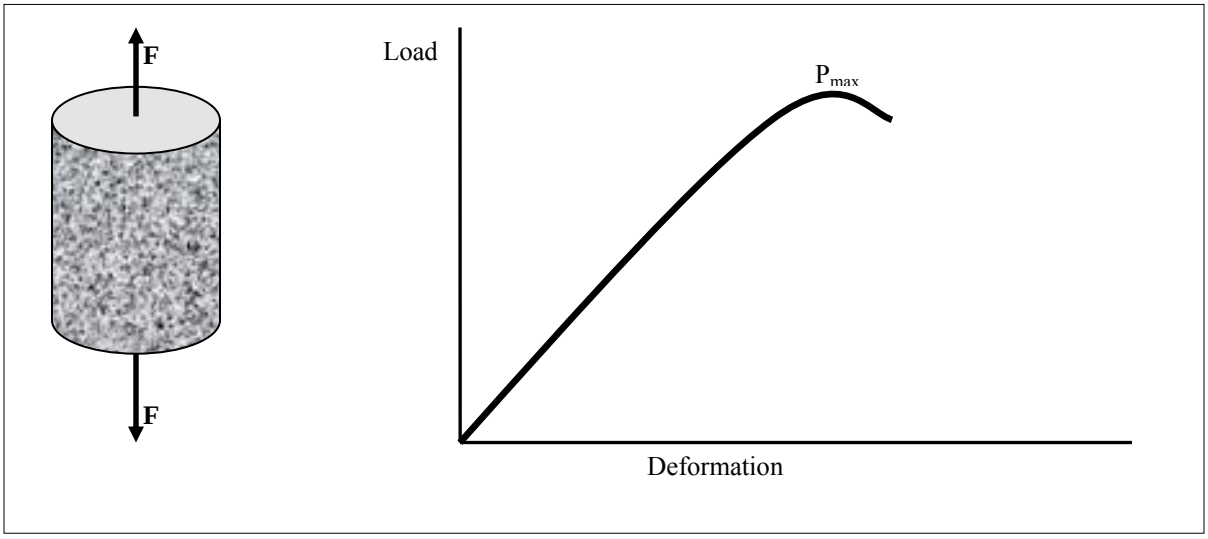

Figure 4-6. Loading Configuration for Tensile Strength Test.

Test Conditions and Data Acquisition

The tensile strength test was conducted in an environmentally controlled chamber at a test temperature of 20±0.5 °C (68±32.9 °F). Specimens were preconditioned to 20 °C (68 °F) for a minimum period of 2 hrs. The temperature was monitored and controlled through a thermocouple probe attached inside a dummy HMAC specimen also placed in the environmental chamber. An MTS equipped with an automatic data measuring system applied the loading. Loading data were measured via the MTS load cell, and deformations were reported via three LVDTs attached vertically to the sides of the specimen. During the test, load, and axial deformation data were captured electronically every 0.1 s. Two replicate specimens were tested per aging condition.

From the captured load data, tensile strength was calculated simply as the maximum tensile load at break divided by the specimen cross-sectional area:

$$\sigma_t = \frac{P_{\max}}{\pi r^2} \qquad \text{(Equation 4-40)}$$

where:

σ_t = Tensile strength, psi

P_{max} = Maximum tensile load at break, kip

r = Radius of cylindrical specimen, inches

Relaxation Modulus Test

The time-dependent elastic modulus ($E(t)$), modulus relaxation rate (m_i), and temperature correction factor (a_T) constitute input parameters for the CMSE fatigue analysis. These material properties were determined from the relaxation modulus test (*30*).

Test Protocol

Relaxation modulus is a strain-controlled test. The test involves applying a constant axial strain to a cylindrical HMAC specimen either in tension or compression for a given time period and then releasing the strain for another given time period, thereby allowing the specimen to rest or relax (elastic recovery). The test loading configuration is shown in Figure 4-7.

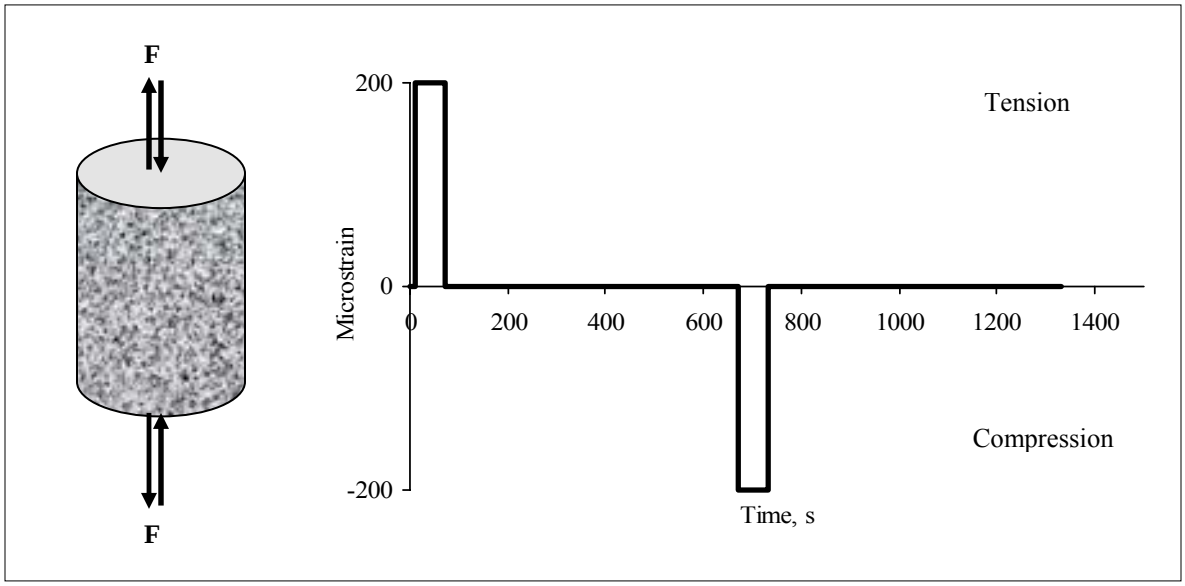

Figure 4-7. Loading Configuration for Relaxation Modulus Test.

As shown in Figure 4-7, the loading sequence consisted of a 200 tensile microstrain sitting for a period of 60 s followed by 600 s rest period, and application of a 200 compression microstrain for 60 s followed by another 600 s rest period (*30*). Researchers selected 200 microstrain because for the HMAC mixtures considered in this project, prior trial testing with microstrains above 200 proved to be destructive while those below 200 were too small to produce meaningful results. A 60 s strain loading time was considered adequate to prevent irrecoverable damage while a 600 s rest period was considered adequate to allow for elastic recovery. The time interval for the strain load application from 0 to +200 or -200 microstrain was 0.6 s, and the input strain waveform was actually a trapezoidal shape.

Test Conditions and Data Acquisition

Testing was conducted in an environmentally controlled chamber at three temperatures: 10, 20, and 30 °C (50, 68, and 86 °F), to facilitate calculation of a time-dependent relaxation modulus master-curve. This master-curve is a graphical representation of the HMAC material properties as a function of temperature and loading time. Note that HMAC material is sensitive to temperature and time of loading.

The temperatures were monitored and controlled at a tolerance of ±0.5 °C (32.9 °F) through a thermocouple probe attached inside a dummy HMAC specimen also placed in the environmental chamber. For each temperature-test sequence, the minimum specimen conditioning time was 2 hrs. The MTS provided the loading while an automated data measurement system captured the data (time, load, and deformation) electronically every 0.5 s. Loading data were measured via the MTS load cell, and deformations were recorded via three LVDTs attached vertically to the sides of the specimen. Three replicate specimens were tested per aging condition.

Figure 4-8 is an example of the output stress response from the relaxation modulus test at a single test temperature of 10 °C (50 °F).

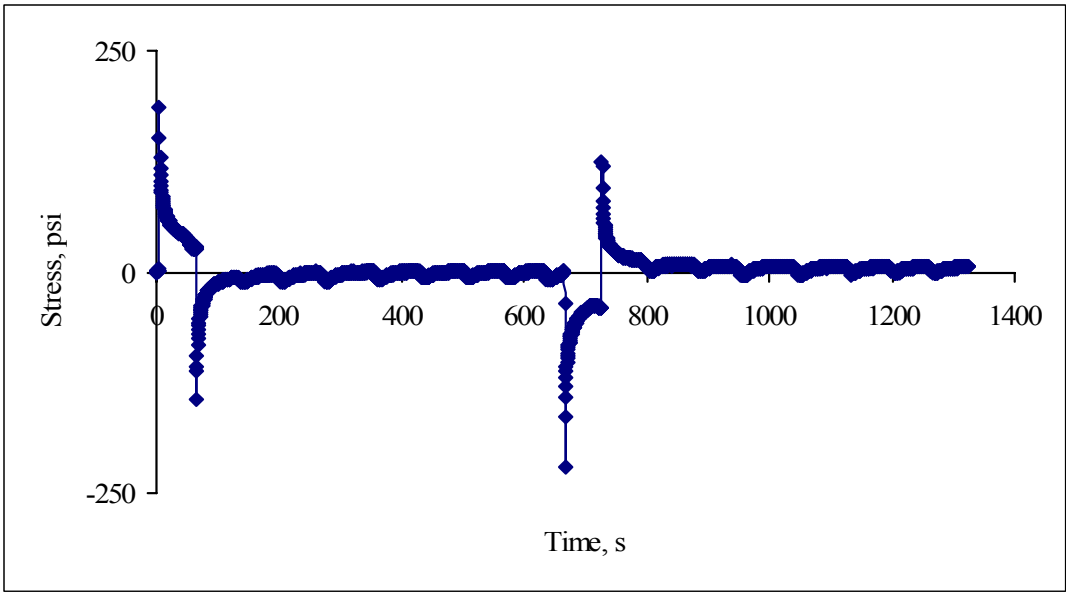

Figure 4-8. Example of Stress Response from Relaxation Modulus Test @ 10 °C (50 °F).

Equation 4-41 was used to calculate the elastic modulus (relaxation) as a function of the measured load (stress) and strain.

$$E = \frac{\sigma}{\varepsilon} = \frac{P}{\pi r^2 \varepsilon} \qquad \text{(Equation 4-41)}$$

where:

E = Elastic modulus

P = Load

ε = Strain

A time reduced-superposition logarithmic analysis (utilizing the SSE method) of the elastic modulus data for each test temperature to a reference temperature of 20 °C (68 °F) generates the required time-dependent relaxation modulus master-curve. This master-curve is represented in the form of a simple power law. By the same logarithmic SSE analysis, temperature correction factors (a_T) are determined, where a_T has a value of 1.0 for the 20 °C (68 °F) reference temperature.

Uniaxial Repeated Direct-Tension Test

The time-dependent tensile stress *($\sigma(t)$)* is an input parameter required to calculate the rate of dissipation of pseudo strain energy (b) that is necessary to calculate N_i. This material property was determined from the uniaxial repeated direct-tension test discussed subsequently.

Test Protocol

Like the relaxation modulus test, the uniaxial repeated direct-tension test was conducted in a strain controlled mode (*30*). An axial direct tensile microstrain of 350 was applied repeatedly to a cylindrically HMAC specimen at a frequency of 1 Hz for a total of 1,000 load cycles. The input strain waveform was haversine shaped.

The actual loading time was 0.1 s with a 0.9 s rest period between load pulses. Thus, a complete load cycle including the rest period was 1.0 s. Figure 4-9 shows the loading configuration.

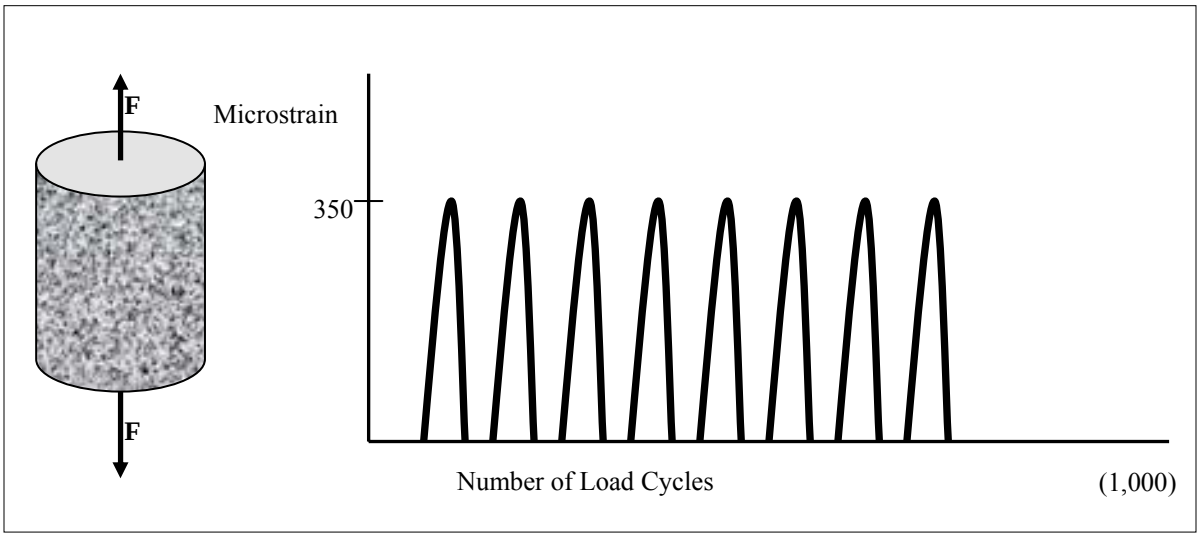

Figure 4-9. Loading Configuration for Uniaxial Repeated Direct-Tension Test.

The haversine shaped input strain waveform is representative of the field load pulse developed under moving wheel loads of commercial vehicles on interstate highways (*30*). A relatively high input strain magnitude of 350 microstrain was selected because this value (350 microstrain) was considered substantial enough to induce cumulative micro fatigue damage (microcracking) within the HMAC specimen during the test. In this test, while micro fatigue damage is desirable, an appropriate input strain level must be selected that will allow the test to continue to an appreciable number of load cycles to capture sufficient data that will allow for calculation of the *b* parameter needed in the CMSE analysis. For this project, testing was terminated at 1,000 load cycles, during which time sufficient data had been captured for DPSE analysis and subsequent calculation of the constant *b*.

Test Conditions and Data Acquisition

The haversine input strain waveform was supplied by the MTS, and axial deformations were measured via three LVDTs. Data (time, load, and deformations) were captured electronically every 0.005 s (to capture sufficient data for DPSE analysis). The test was conducted in an environmentally controlled chamber at a test temperature of 30±0.5 °C (86±32.9 °F). The minimum conditioning period for the specimens was 2 hrs. The temperature was monitored and controlled through a thermocouple probe attached inside a dummy HMAC specimen also placed in the environmental chamber.

Three replicate cylindrical HMAC specimens that had previously been subjected to a series of relaxation modulus tests at 10, 20, and 30 °C (50, 68, and 86 °F) were used for this test for each aging condition. It should be noted that the relaxation modulus test was assumed to be non-destructive. However, the uniaxial repeated direct-tension test is a destructive test since some micro damage occurs within the HMAC specimen even though damage may not be physically visible. Figure 4-10 is an example of the stress response from the uniaxial repeated direct-tension test at 30 °C (86 °F). The measured stress ($\sigma(t)$), strain ($\varepsilon(t)$), and the time (t) are the required input parameters for CMSE fatigue analysis to calculate DPSE.

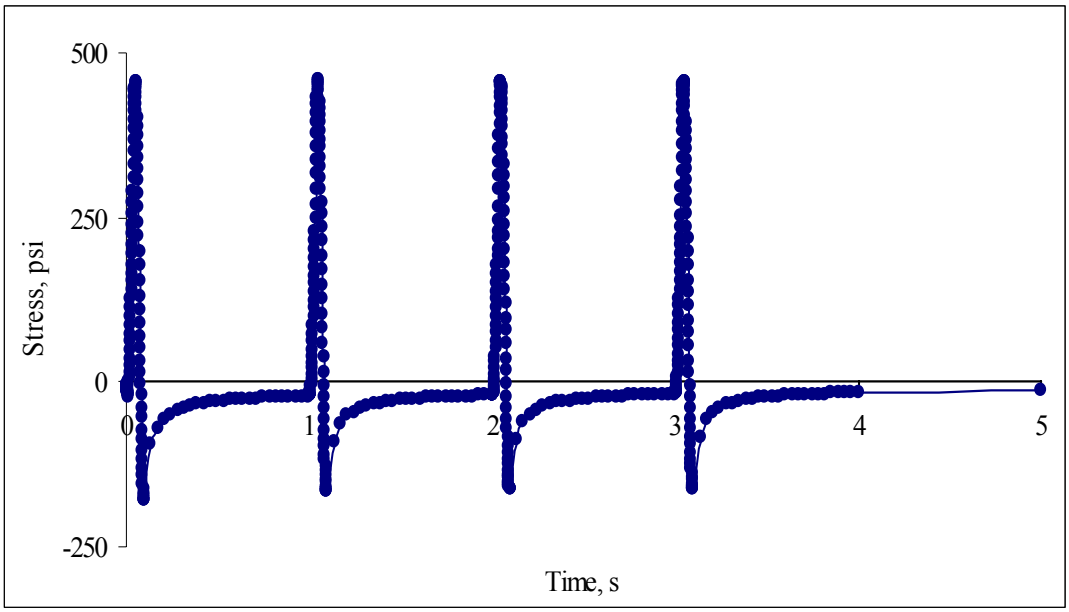

Figure 4-10. Stress Response from Uniaxial Repeated Direct-Tension Test @ 30 °C (86 °F).

Surface Energy Measurements for Asphalt

The surface energy measurements for the asphalts in this project were completed using the Wilhelmy plate method (*30*, *33*). Compared to other methods such as the drop weight, Du Nouy ring, pendant drop, Sessile drop, capillary rise, and maximum bubble pressure, the Wilhelmy plate method is relatively simple and does not require complex corrections factors to the measured data (*30*, *33*).

The contact angle between asphalt and any liquid solvent can be measured using the Wilhelmy plate method. This method is based on kinetic force equilibrium when a very thin plate is immersed or withdrawn from a liquid solvent at a very slow constant speed as illustrated in Figure 4-11 (*40*).

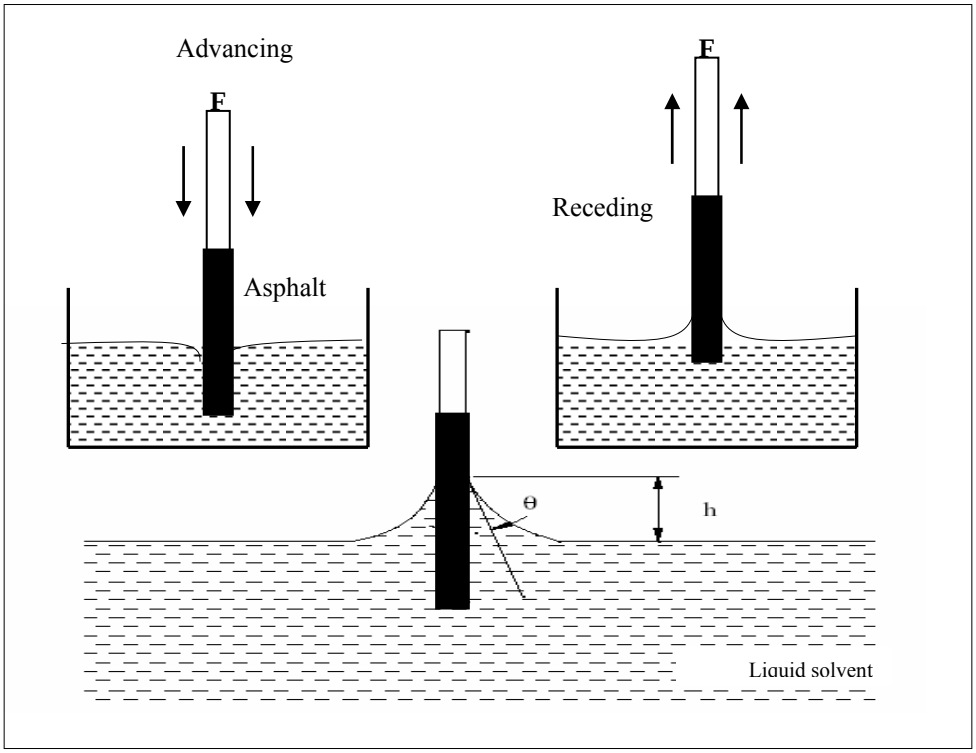

Figure 4-11. Loading Configuration for the Wilhelmy Plate Method (*30*, *33*, *40*).

The dynamic contact angle between asphalt and a liquid solvent measured during the immersing process is called the advancing contact angle, while the dynamic contact angle during the withdrawal process is called the receding contact angle.

The advancing contact angle, which is a wetting process, is associated with the fracture process, while the receding angle is associated with the healing mechanism. The total surface free energy and its components for asphalt are calculated from these advancing and receding contact angles. The surface free energy calculated from the advancing contact angles is called the surface free energy of wetting or healing, while the surface free energy computed from the receding contact angle is called the surface free energy of dewetting or fracturing.

Test Protocol and Data Acquisition

To complete the Wilhelmy plate test, approximately 0.65 g of hot-liquid asphalt (PG 64-22) heated to about 144 °C (291.2 °F) was coated onto glass plates 50 mm (2 inches) in length by 25 mm (1 inch) in width with a 0.15 mm (0.006 inches)thickness. By dipping the glass plate into a mass of hot-liquid asphalt to a depth of about 15 mm (0.6 inches), a thin asphalt film of approximately 1 mm (0.039 inches) thickness was created on the glass plate after allowing the excess asphalt to drain off (*30*, *33*).

As shown in Figure 4-11, the actual test protocol involves an automatically controlled cycle (s) of immersion and withdrawal (receding) processes of the asphalt coated glass plates into a liquid solvent to a depth of about 5 mm (0.2 inches) at an approximate uncontrolled ambient temperature of 20±2 °C (68±36 °F). The temperature is not tightly controlled in this test because previous research has indicated that the measurable contact angle, and consequently the surface free energy are not very temperature sensitive (*30*, *33*).

Prior to testing, the asphalt-coated glass plate must be vacuumed for about 12 hrs in a diseccator to de-air the asphalt. Three test asphalt samples are required per test per three liquid solvents, and thus a total of nine samples were used. Distilled water, formamide, and glycerol were the three selected liquid solvents used in this project because of their relatively large surface energies, immiscibility with asphalt, and wide range of surface energy components. Table 4-2 lists the surface energy components of these three liquid solvents (distilled water, formamide, and glycerol) (*30*, *33*).

Table 4-2. Surface Energy Components of Water, Formamide, and Glycerol.

Solvent	Surface Free Energy Components (ergs/cm^2) (*30*, *33*)				
	Γ_L	Γ_L^{LW}	Γ_L^+	Γ_L^-	Γ_L^{AB}
Distilled water	72.60	21.60	25.50	25.50	51.00
Formamide	58.00	39.00	2.28	39.60	19.00
Glycerol	64.00	34.00	3.60	57.40	30.00

During the test, the loading force for the immersion and receding processes was provided by an automatically controlled Dynamic Contact Analyzer (DCA) balance shown in Figure 4-12. Data (dynamic contact angle) were measured and captured electronically via the WinDCA software. Figure 4-13 is an example of the measured dynamic advancing and receding contact angles at 20±2 °C (68±36 °F).

Figure 4-12 The DCA Force Balance and Computer Setup - Wilhelmy Plate Test.

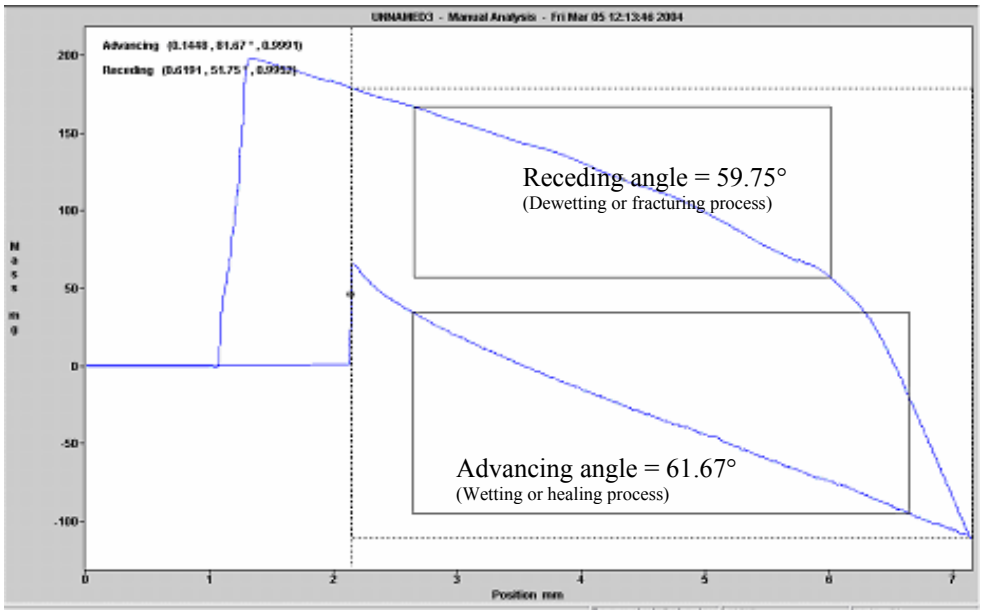

Figure 4-13. Example of the DCA Software Display (Advancing and Receding).

For clarity, the vertical axis title in Figure 4-13 is "mass" in mg with a scale of -100 to 200 mg, and the horizontal axis title is "position" in mm with a scale of 0 to 7 mm.

Asphalt Surface Energy Calculations

Equation 4-42 is the force equilibrium equation resulting from the immersion (advancing) or the withdrawal (receding) processes during the Wilhelmy plate test. Based on the Young-Dupre theory and the assumption that asphalt equilibrium film pressure is zero, Equation 4-42 reduces to Equation 4-43 (*33*).

$$\Delta F = P_t \Gamma_L Cos\theta - V\rho_L g + V\rho_{Air} g \qquad \text{(Equation 4-42)}$$

$$\Gamma_{L_i}\left(1 + Cos\theta_i\right) = 2\sqrt{\Gamma_i^{LW}\Gamma_{L_i}^{LW}} + 2\sqrt{\Gamma_i^{-}\Gamma_{L_i}^{+}} + 2\sqrt{\Gamma_i^{+}\Gamma_{L_i}^{-}} \qquad \text{(Equation 4-43)}$$

where:

F = Applied force

P_t	=	Perimeter of the asphalt coated glass plate
θ	=	Dynamic contact angle between asphalt and the liquid solvent, degrees (°)
V	=	Volume of immersed section of glass plate
ρ	=	Density (subscript "L" for liquid solvent and "Air" for air)
g	=	Acceleration due to gravity
Γ	=	Surface free energy, ergs/cm^2

The dynamic contact angle θ (°) is the measurable parameter, advancing (wetting) or receding (dewetting). Γ_{Li}^{LW}, Γ_{Li}^{+}, and Γ_{Li}^{-} are surface free energy components of the liquid solvent. Γ_i^{LW}, Γ_i^{+}, and Γ_i^{-} are the three unknown components of the asphalt surface free energy from Lifshtz-van der Waals forces, Lewis base, and Lewis acid, respectively, that need to be determined. Mathematically, three liquid solvents of known surface free energies must be used to solve Equation 4-43 for the three unknown parameters Γ_i^{LW}, Γ_i^{+}, and Γ_i^{-}. Algebraically, Equation 4-43 can easily be transformed into a familiar matrix form of simple linear simultaneous equations expressed by Equation 4-44 (*33*):

$$\begin{bmatrix} a_{11} & a_{12} & a_{13} \\ a_{21} & a_{22} & a_{23} \\ a_{31} & a_{32} & a_{33} \end{bmatrix} \begin{bmatrix} x_1 \\ x_2 \\ x_3 \end{bmatrix} = \begin{bmatrix} Y_1 \\ Y_2 \\ Y_3 \end{bmatrix} \qquad \text{(Equation 4-44)}$$

$$a_{1i} = 2\frac{\sqrt{\Gamma_{L_i}^{LW}}}{\Gamma_{L_i}},\ a_{2i} = 2\frac{\sqrt{\Gamma_{L_i}^{+}}}{\Gamma_{L_i}},\ a_{3i} = 2\frac{\sqrt{\Gamma_{L_i}^{-}}}{\Gamma_{L_i}} \qquad \text{(Equation 4-45)}$$

$$x_1 = \sqrt{\Gamma_i^{LW}},\ x_2 = \sqrt{\Gamma_i^{-}},\ x_3 = \sqrt{\Gamma_i^{+}} \qquad \text{(Equation 4-46)}$$

$$Y_i(x) = 1 + Cos\theta_i \qquad \text{(Equation 4-47)}$$

The solution of Equation 4-44 provides the surface free energy components of the asphalt required for the CMSE fatigue analysis.

Surface Energy Measurements for Aggregate

The surface energy measurements for the aggregates were not made for the analysis presented in this interim report. The results in Chapter 6 are based on estimates shown in Table 4-3 that were obtained by previous measurements in other research projects (*30, 33*). Actual measurements are planned as subsequent work in this project, and the measurements and associated analysis procedure are discussed in Chapter 8.

Table 4-3. Surface Energy Component Estimates for Aggregate in Bryan Mixture.

Material	**Surface Free Energy Components (ergs/cm^2) (*30, 33*)**		
	Γ_j^{LW}	Γ_j^+	Γ_j^-
Bryan Aggregate (limestone)	87.0	0.4	286

CHAPTER 5
BINDER AGING EFFECTS

Asphalt oxidation is a major contributor to age-related pavement failure (*41*). Through oxidation, the binder becomes stiffer and more brittle and thus less able to sustain, without damage, the deformations of flexible pavements. This project investigates the role that this binder embrittlement plays in the phenomenon of fatigue resistance.

This chapter includes further discussion of 1) binder oxidation and embrittlement in both laboratory and pavement aging, 2) the objectives of binder measurements in understanding pavement fatigue resistance, and 3) the experimental methodology used in this work to evaluate binder aging and to relate it to HMAC mixture properties.

As elaborated in Chapter 2, the term "binder" is used synonymously with the term "asphalt" for terminology preferences in respect of the asphalt chemical properties and some material characterization tests.

BINDER OXIDATION AND EMBRITTLEMENT

As briefly introduced above, binders experience hardening and embrittlement over time that reduces the performance of flexible pavements. The process is relentless and thus, over enough time, can destroy the pavement. The constancy of the hardening rate over time and the depth to which oxidation occurs, based on recent pavement data, are surprising and at the same time critical to understanding pavement durability for both unmodified and modified binders.

As binders oxidize, carbonyl (– C=O) groups are formed that increase the polarity of their host compounds and make them much more likely to associate with other polar compounds. As they form these associations, they create less soluble asphaltene materials, which behave like solid particles. This composition change, taken far enough, results in orders-of-magnitude increases in both the asphalt's viscous and elastic stiffness properties. The end result is a material that increases its stress greatly with deformation (high elastic stiffness) and simultaneously cannot relieve the stress by flow (high viscosity), leading to a pavement that is very brittle and susceptible to fatigue and thermal cracking.

The Maxwell model is a very simple way of explaining, in a qualitative sense, the essence of the impact of this elastic stiffening and viscosity increase on elongational flow of asphalt. The model is that of an elastic spring in series with a viscous dashpot element as shown in Figure 5-1.

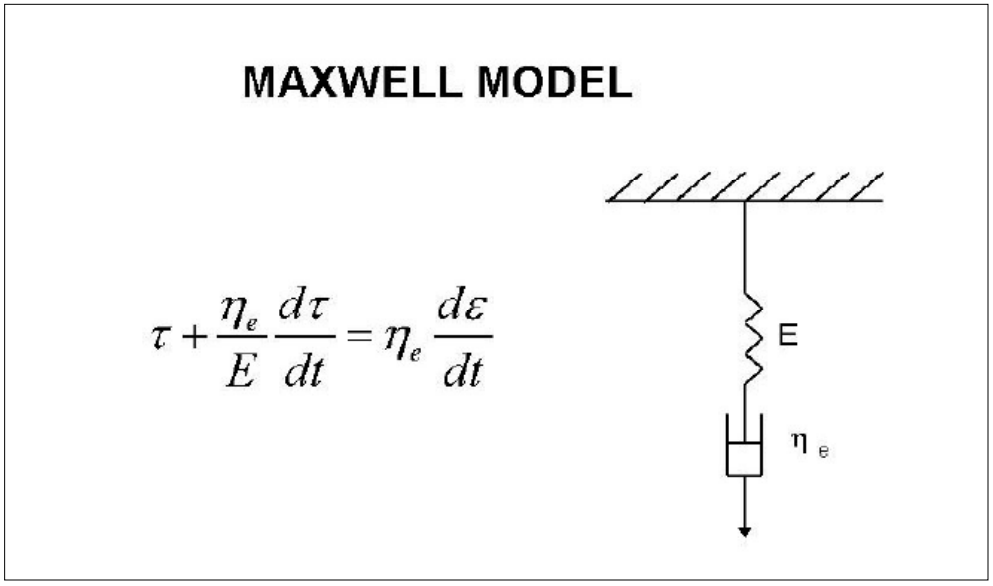

Figure 5-1. The Maxwell Model.

The stress that builds in the combined element is the result of the balance between the elastic modulus and the viscosity. Upon elongation, the stress versus elongation response rises in response to the elastic spring but then goes through a maximum value before decaying over time in response to viscous flow. The value of the maximum stress depends upon the relative values of the elastic modulus and the viscosity. The lower their values, the higher the maximum stress; the higher the values, the lower the maximum stress. If the maximum stress exceeds the failure stress of the material, then failure occurs.

This Maxwell model is very simple and certainly is too simple to quantitatively characterize asphalt materials, but it still captures the basic elements that are important to understanding binder failure that occurs due to oxidation and embrittlement. As asphalts oxidize, they harden, a process that simultaneously increases its elastic stiffness and its viscosity.

Consequently, in the context of the Maxwell model, with aging and consequent hardening, a binder cannot take as much deformation without building to a stress level that results in its failure stress being exceeded. So, as binders age and harden, their ductilities decrease dramatically. The binder ductility for a newly constructed pavement may be of the order of 30 cm (15 °C, 1 cm/min) (11.8 inches [59 °F, 0.39 inches/min]) where as the binder ductility of a heavily aged pavement will be much lower, down to 3 cm (1.18 inches) or less.

Literature reports emphasize the importance of a binder's ductility to pavement durability. Several studies report that a value of the 15 °C (59 °F) ductility at 1 cm/min (0.39 inches/min) in the range of 2 to 3 cm (0.79 to 1.18 inches) corresponds to a critical level for age-related cracking in pavements (*41*,*42*).

This embrittlement of binders has been captured with the discovery of a correlation between binder ductility (measured at 15 °C, 1 cm/min) (59 °F, 0.39 inches/min) and binder Dynamic Shear Rheometer (DSR) properties (elastic dynamic shear modulus [G'], viscous dynamic shear modulus [G"] and dynamic viscosity [η'] equal to G"/ω [ω is angular frequency]) shown in Figure 5-2. A very good correlation exists between binder ductility and G'/(η'/G') (or, equivalently G'/[(G"/ω)/G']), demonstrating the interplay between elastic stiffness and ability to flow in determining binder brittleness, as discussed above in the context of the Maxwell model.

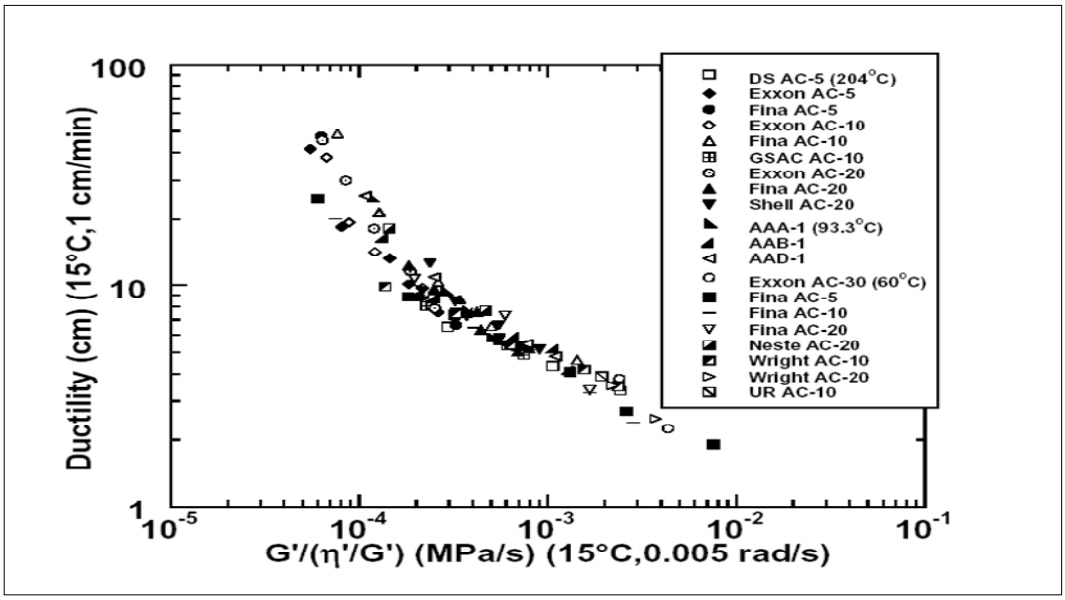

Figure 5-2. Correlation of Aged-Binder Ductility with the DSR Function G'/(η'/G') for Unmodified Binders.

This correlation is depicted on a "map" of G' versus η'/G' (Figure 5-3), which tracks a pavement binder as it ages in service (*42-44*). This particular binder is from SH 21 between Bryan and Caldwell but represents the trends seen for all conventional binders. On this type of plot, with increased aging, a binder moves, over time, from the lower right toward the upper left as the result of increases in both the elastic stiffness and viscosity (but note that G' increases more than viscosity, i.e., G"/ω, because movement is toward the left with smaller values of η'/G'). Note also the dashed lines that represent lines of constant ductility, calculated from the correlation of Figure 5-2 below 10 cm (3.9 inches).

Recent evidence suggests that pavement binders age at surprisingly constant rates and to surprising depths. Figure 5-3 illustrates this conclusion from Glover et al.'s work contained in Research Report FHWA/TX-03/1872-2 (*13*), through measurements on SH 21 between Bryan and Caldwell; all data shown in this figure are from a single station, #1277. This highway was constructed from July 1986 to July 1988 in three, 2 inch lifts. The solid symbols (with the exception of the solid diamond) are binder measurements from cores taken from the third lift down from the surface of the pavement, as originally constructed. With each lift being 2 inches thick, this bottom lift had 4 inches of pavement material on top of it. (Note: In 2000, this pavement had a chip seal and overlay placed on top of it, burying the original lifts even more.) Yet, even buried this deeply, its binder moves across the DSR "map" in a relentless fashion and at about the same pace as the top lift (open symbols). Binder from the 1989 bottom lift has an estimated ductility of 20 cm (7.87 inches) at 15 °C (59 °F). By 1996, it was reduced by aging to 5.6 cm (2.2 inches), and by 2002, it was less than 5 cm (1.97 inches). Meanwhile, the top lift binder's ductility was estimated to be 16 cm (6.3 inches) in 1989, 4.5 cm (1.77 inches) in 1996, and about 4 cm (1.57 inches) in 2002. The march across the DSR map was not that different for the top lift compared to the bottom lift. Binder from the middle lift, taken in 1989 and 1992, is also shown and tracks well with the other lifts. Note that the rolling thin-film oven test (RTFOT) plus pressure aging vessel (PAV) laboratory-aged binder matches the 1992 pavement-aged binder, suggesting that for this pavement, RTFOT plus PAV is approximately equivalent to hot-mix and construction aging plus four years of field pavement aging.

These results are rather remarkable and strongly suggest, as noted above, that oxidative aging rates are remarkably constant over time and, beyond the very top portion of the pavement, proceed at remarkably uniform rates, at least to several inches below the surface of the pavement. Note that the literature reports that ductility values in the range of 2 to 3 cm (0.79 to 1.18 inches) for 15 °C (59 °F) at 1 cm/min (0.39 inches/min) appear to correspond to a critical level for age-related cracking. Thus, the top-left corner of the pavement aging figure (Figure 5-3) is a suspect region for pavement performance. While this region has not yet been verified conclusively to be a critical zone, recent pavement data including several Long Term Pavement Performance (LTPP) pavements are consistent with this preliminary conclusion.

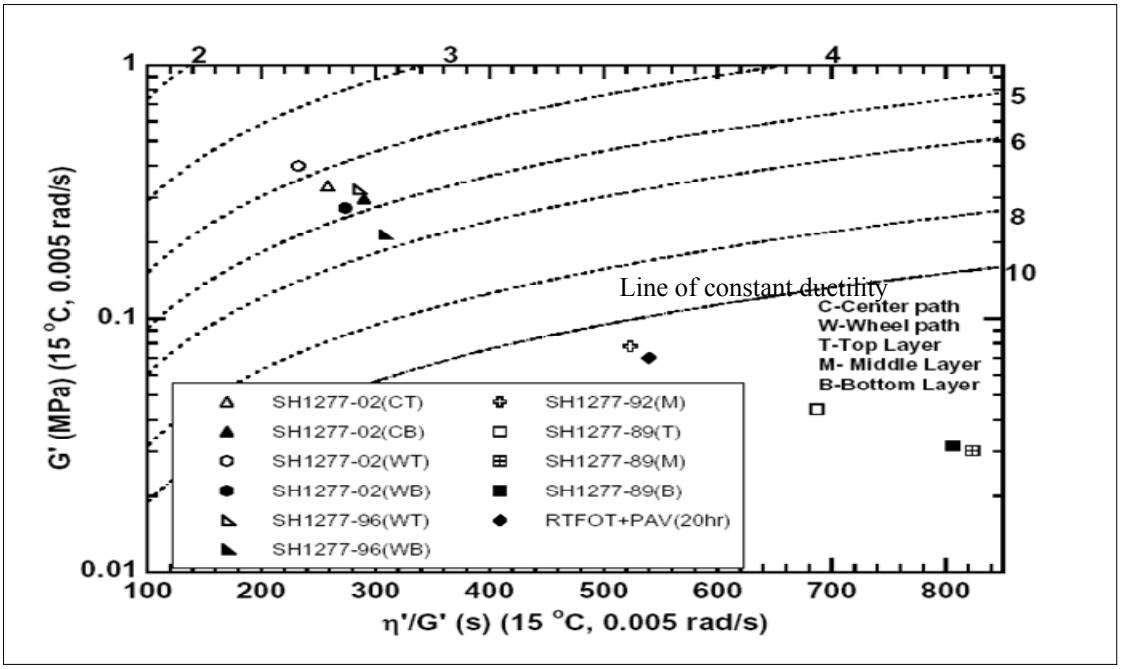

Figure 5-3. Binder Aging Path on a G' versus η'/G' Map (Pavement-aged Binders) (*13*).

Clearly, binder properties change drastically over the life of a pavement. These changes result in a dramatic decrease in flexibility and occur continuously throughout its service lifetime. It is the objective of this project to investigate how these changes impact the fatigue resistance of HMAC pavements. Ultimately, the objective is to be able to predict reductions in pavement fatigue resistance from laboratory measurements of binder oxidation and embrittlement.

METHODOLOGY

Changes in binder properties with aging are to be related to changes in mixture properties with the objective of learning how to predict changes in mixture (and ultimately pavement) fatigue lives due to binder stiffening. To this end, a PG 64-22 unmodified binder was used in a basic mixture (denoted as the Bryan mixture). This binder was tested in both aged and unaged conditions as discussed subsequently. The HMAC mixture was aged and also tested as discussed in Chapters 2, 3, and 4. The results from all of these tests are presented in Chapter 6.

Binder Aging

Two different methods of accelerated aging were used in this project. A stirred air flow test (SAFT), which stimulates the hot mix process, was used for short-term aging comparisons (*45*, *46*). An environmental room at 60 °C (140 °F) and atmospheric pressure and 50 percent relative humidity was used for long-term aging comparisons. Aging at 60 °C (140 °F) is used as an approximation to field aging.

Neat (original) binder was aged by both of these means and subsequently tested; binder in compacted mixtures was aged in the 60 °C (140 °F) room and had to be extracted and recovered before testing.

Extraction and Recovery Method

An effective extraction and recovery process is necessary to compare the properties of mix-aged binder with those of the original binder. The process used in this project consisted of two parts: 1) the extraction process, and 2) the filtration and recovery process.

At a mixture binder content of about 5 percent by mass, approximately 150 g of HMAC mixture were needed to obtain approximately 7 g of binder. The mixtures were broken into small pieces with a hammer before extracting the binder from the HMAC specimens.

Toluene and ethanol were used for the binder extraction process. A total of three successive washes were used in the extraction process. For the first wash, 100 mL of toluene was used to extract binder from the aggregate by contact for 20 minutes. The second and third washes, also for 20 minutes each, used a 15 weight percent ethanol-toluene solution.

The washes were filtered two times using a new doubled coffee filter each time. The filtered solution was then distributed among six 15 mL con type tubes (approximately 12 mL solution per tube) and centrifuged at about 3000 rpm for 10 minutes to remove aggregate from the solution.

The binder was recovered from the solvent with a Buchi, RE 111 rotovap. During removal of the solvent, the bath temperature was kept at 100 ^{o}C (212 °F) to avoid hardening or softening of the asphalt in dilute solution. When no more solvent could be detected visually dripping from the condenser, the temperature was increased to 173.9 ^{o}C (345 °F) to ensure sufficient solvent removal.

The extraction and recovery procedure took from 3 to 4 hours for each specimen. Two replicates were extracted and recovered for each mixture, and the properties of the recovered binders were compared to each other. When inconsistencies occurred in these recovered binder properties, additional replicates were extracted, up to four replicates total for a given mixture (*47*).

BINDER TESTS

Binder tests conducted included size exclusion chromatography, dynamic shear rheometry, ductility, and fourier transform infrared spectroscopy. These tests are discussed in the subsequent text, and results are presented and discussed in Chapter 6.

Size Exclusion Chromatography (SEC)

After extraction and recovery, the binder was analyzed using SEC to ensure complete solvent removal. Test samples were prepared by dissolving 0.2 ± 0.005 g of binder in 10 mL of tetrahydrofuran (THF). The sample then was sonicated for 30 minutes to ensure complete dissolution and filtered through a 0.45µm Polytetrafluoroethylene (PTFE) syringe filter.

Samples of 100 μL were injected into 1000, 500, and 50 Å columns in series with THF carrier solvent flowing at 1.0 mL/min. The chromatograms of binders obtained from the same replicate should overlay each other. If there was any solvent residue in the binder, there was a peak located at 38 minutes on the chromatogram *(48)*.

Dynamic Shear Rheometer

The rheological properties of the binder were measured by a Carri-Med CSL 500 Controlled Stress DSR Rheometer.

The rheological properties of interest were the complex viscosity (η) measured at 60 °C (140 °F) and 0.1 rad/s (approximately equal to the low-shear rate limiting viscosity) and the storage modulus (G') and the dynamic viscosity (η'), both at 45 °C (113 °F) and 10 rad/s measured in a frequency sweep mode. A 2.5 cm (0.98 inches) composite parallel plate geometry was used with a 500 mm (19.5 inches) gap between the plates.

These rheological properties were used to understand how the physical properties of the binder changed with time. DSR measurements also were important for deciding whether the binder was changed in some way by the extraction and recovery process (*46*-*48*). If two extraction and recovery processes yielded binders with matching SEC chromatograms but significantly different complex viscosities, then at least one of the binders was suspected of having undergone solvent hardening or softening.

Ductility

Ductilities for long-term aged original binder, 3 month aged in a 60 °C (140 °F) room after SAFT for this interim report, were measured at 15 °C (59 °F) and an extensional speed of 1 cm (0.39 inches) per minute in accordance with ASTM D113-86 *(49)*. The ductility sample, which had been made in a mold, had a 3 cm (1.18 inches) initial gauge length and a tapered throat. The ductility was taken as the amount of extension in centimeters of the asphalt specimen when the binder fractured at the tapered throat.

Fourier Transform Infrared Spectroscopy (FTIR)

Carbonyl area (CA) was measured using a Galaxy 5000 FTIR spectrometer with an attenuated total reflectance, ATR zinc selenide prism *(47)*. CA is the area under the absorption band from 1650 to 1820 cm^{-1} (4231 to 4667 $inches^{-1}$) and relates directly to the oxygen content in the asphalt binder, and thus increases in CA are used to quantify oxidative aging *(50, 51)*.

CHAPTER 6
RESULTS AND ANALYSIS

This chapter presents preliminary results for the Bryan mixture (PG 64-22 binder plus limestone aggregate), analyzed at a typical 95 percent reliability. In this analysis, laboratory fatigue life was defined as the predicted HMAC mixture fatigue resistance without inclusion of any shift factors to simulate field conditions and environmental exposure. Field fatigue life was then calculated as a function of the field shift factors and the predicted HMAC laboratory fatigue life. Throughout this chapter and Chapter 7, the units of fatigue life (laboratory or field) are defined and expressed in terms of the number of allowable load repetitions to fatigue failure. Note that the fatigue failure criterion is different for each fatigue analysis approach (ME and CMSE) as discussed previously in Chapters 3 and 4, respectively.

Note that during this reporting period, both laboratory testing and N_f analysis for 0 and 3 months aging conditions had been completed for the CMSE approach but not for the ME approach. Consequently, only results available at the report time are presented for the ME approach. These include 0 months BB testing, 0 months laboratory N_f analysis, and 3 months BB testing for the lower test strain level.

ME PRELIMINARY FATIGUE RESULTS

The ME preliminary fatigue results, including the BB laboratory test results and the predicted HMAC fatigue resistance, are discussed in this section.

BB Laboratory Test Results

Table 6-1 is a summary of the BB fatigue test results conducted at two strain levels (374 and 468 microstrains) at 20 °C (68 °F) and 10 Hz frequency for 0 months aging. Note that although the researchers obtained relatively low *COVs* (Tables 6-1 and 6-2) with this preliminary analysis, high variability can often be expected in BB testing depending on the degree of precision exercised during the specimen fabrication process, handling and storage, and temperature control during testing.

Table 6-1. BB Laboratory Test Results (0 Months).

Specimen	Test Microstrain	AV (%)	Average Test Temperature (°C) (°F)	Load Cycle to Failure (*N*)
(a) Low test strain level (374 microstrain)				
BBB20011	374	7.1	20.46 (68.83)	131,000
BBB20012	374	7.2	19.96 (67.93)	120,000
BBB20013	374	7.5	20.35 (68.63)	130,000
Mean		7.3	20.26 (68.46)	127,000
Standard deviation (Stdev)		0.2	0.26 (0.47)	6,083
COV		2.9%	1.30% (0.69%)	4.79%
(b) High test strain level (468 microstrain)				
BBB20021	468	7.0	20.35 (68.63)	51,000
BBB20022	468	7.2	20.54 (68.97)	46,000
BBB20023	468	6.7	19.80 (67.64)	55,000
Mean		7.0	20.23 (68.41)	50,667
Stdev		0.2	0.38 (0.69)	4,509
COV		3.2%	1.90% (1.01%)	8.90%

In Table 6-1, *N* refers to the number of laboratory load cycles or repetitions to fatigue failure during the BB test. Fatigue failure as defined in Chapter 3, is the point of 50 percent reduction in the initial HMAC flexural stiffness measured at the 50th load cycle (*11*, *12*).

The N-ε_t Empirical Relationship

Figure 6-1 represents a plot of the average laboratory *N* versus ε_t on a log-log scale. Based on Figure 6-1, an empirical fatigue relationship of the power form expressed by Equation 6-1 was derived for the Bryan HMAC mixture, for 0 months aging condition.

$$N = 1 \times 10^{-9} \varepsilon_t^{-4.0984} \qquad \text{(Equation 6-1)}$$

with: $k_1 = 1 \times 10^{-9}$ and $k_2 = 4.0984$

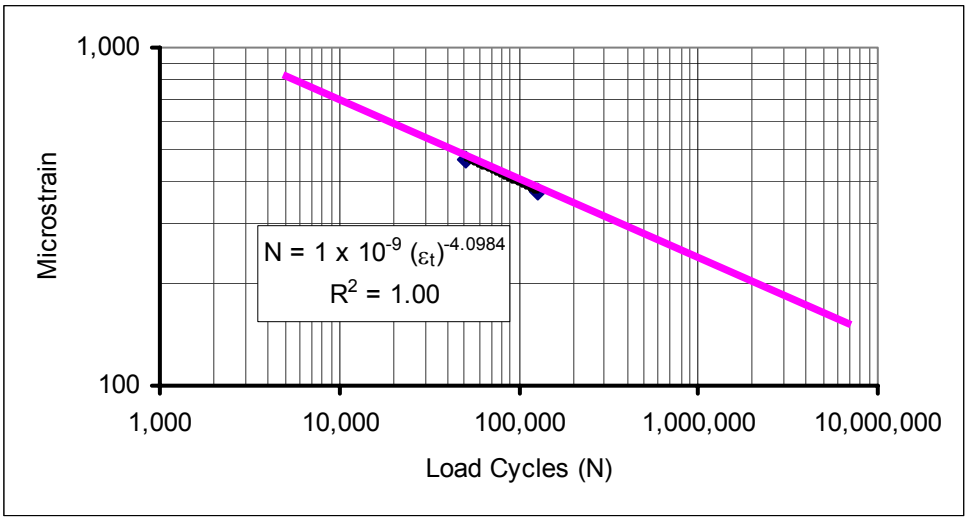

Figure 6-1. Load Cycles (*N*) versus Tensile Microstrain (ε_t) - ME.

Note that the fatigue results in Figure 6-1 were based on two test strain levels. For a better fatigue relationship and subsequent improvements in predicting N_f, more data points (collected at more than two test strain levels) are recommended, with the recognition that BB testing is time consuming.

HMAC Mixture Fatigue Resistance

The estimated laboratory N_f and its prediction interval based on a design ε_t of 157 microstrain are shown in Table 6-2. These results were determined with statistical software, the least square regression line, and *Ln* normal back-transformation at 95 percent reliability.

Table 6-2. HMAC Mixture Fatigue Resistance – ME (0 Months).

Parameter	**Value (1×10^6)**
Estimated laboratory N_f	4.48
Lower 95% laboratory prediction interval	2.13
Upper 95% laboratory prediction interval	9.46
Stdev	1.46
COV	32.68%

CMSE PRELIMINARY FATIGUE RESULTS

Table 6-3 through 6-5 summarize the CMSE laboratory test results and the HMAC mixture fatigue lives obtained at 0 and 3 months aging, respectively. In Tables 6-4 and 6-5 laboratory fatigue life is represented by ($N_i + N_p$) and field fatigue life by N_f. N_f is simply a product of the shift factors (SF_a and SF_h) and the laboratory fatigue life ($N_i + N_p$) (Chapter 4).

The average estimated laboratory HMAC mixture fatigue resistance and predicted field fatigue life for 0 months aged specimens were 6.31×10^6 and 69.22×10^6 allowable load repetitions. The average fatigue lives for the 3 months aged HMAC mixture were 2.42×10^6 and 18.93×10^6 allowable load repetitions for the laboratory and field fatigue lives, respectively.

Table 6-3. CMSE Tensile Strength Results.

Specimen	AV (%)	Aging Condition @ 60 °C (140 °F)	Tensile Strength @ break, psi	Tensile Microstrain @ Break
BCM-TS0001	7.0	0 months	103.16	1,300.06
BCM-TS0031	7.0	3 months	81.13	429.44

Table 6-4. CMSE Laboratory Test Results (0 Months).

Specimen	Laboratory Test Parameters					Shift Factors		Fatigue Life (1×10^6)	
	E_t, psi	E_c, psi	m_t	m_c	b	SF_a	SF_h	Lab ($N_i + N_p$)	Field (N_f)
BCMSE0001 (7.0% AV)	200,997	301,860	0.38	0.35	0.73	1.63	6.73	6.03	66.15
BCMSE0002 (6.8% AV)	215,203	277,580	0.42	0.37	0.69	1.63	6.73	6.59	72.29
Mean	208,100	289,720	0.40	0.36	0.71	1.63	6.73	6.31	69.22
Stdev	10,045	17,169	0.03	0.01	0.03	0.00	0.00	0.4	4.34
COV	4.83%	5.93%	7.50%	3.93%	3.98%	0.0%	0.0%	6.28%	6.27%

Table 6-5. CMSE Laboratory Test Results (3 Months).

Specimen	Laboratory Test Parameters					Shift Factors		Fatigue Life (1×10^6)	
	E_t, psi	E_c, psi	m_t	m_c	b	SF_a	SF_h	Lab ($N_i + N_p$)	Field (N_f)
BCMSE0031 (7.1% AV)	631,632	669,797	0.37	0.32	1.33	1.65	5.64	2.22	20.67
BCMSE0032 (6.9% AV)	719,568	750,245	0.39	0.34	1.16	1.65	3.84	2.62	17.18
Mean	675,600	710,021	0.38	0.33	1.25	1.65	4.74	2.42	18.93
Stdev	62,180	56,885	0.01	0.01	0.12	0.00	1.27	0.28	2.47
COV	9.20%	8.01%	3.72%	4.29%	9.66%	0.0%	26.85%	11.69%	13.04%

The laboratory test parameters, shift factors, and fatigue lives shown in Tables 6-3 through 6-5 were obtained consistent with the calculations and analysis procedure described in Chapter 4. Parameters m_t, m_c, b, SF_a, and SF_h are unitless constants while fatigue life, as discussed previously, is expressed in terms of the allowable number of load repetitions to fatigue failure.

COMPARISON OF FATIGUE LIVES – ME VERSUS CMSE

Figure 6-2 shows a comparison of the HMAC laboratory mixture fatigue resistance in terms of *Lab* N_f magnitude obtained at 0 months aging for both the ME and CMSE approaches. For this interim report, the ME field fatigue life for 0 months aging was not analyzed and thus only laboratory fatigue lives could be compared for the two approaches. For 3 months aging, BB testing for the ME approach was only completed for the lower test strain level (374 microstrain), and thus both laboratory and field N_f analysis could not be completed and are not presented in this interim report.

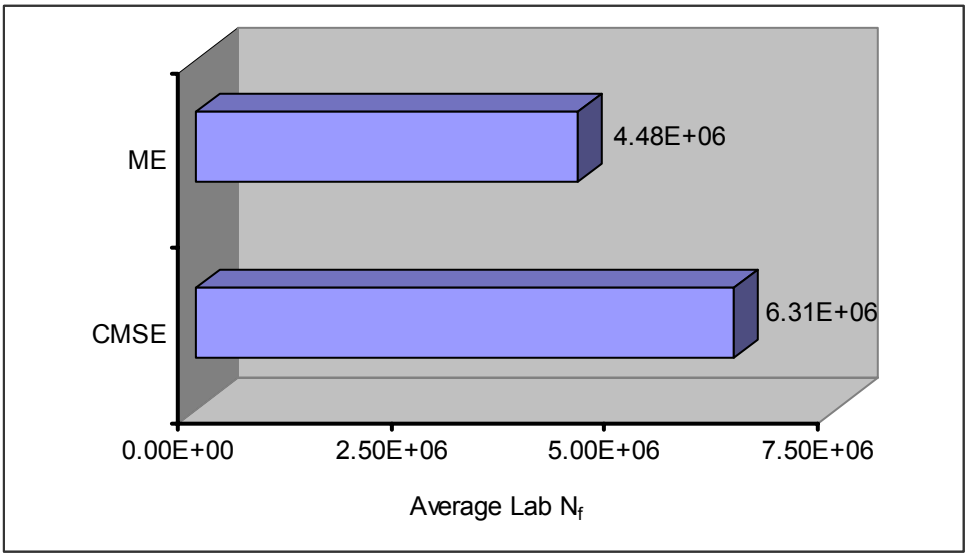

Figure 6-2. Laboratory Fatigue Life – ME versus CMSE.

Based on this preliminary analysis and using the CMSE approach as the benchmark, Figure 6-2 indicates that the two approaches are comparable and indicate that both approaches can predict HMAC mixture fatigue resistance. However, the ME approach exhibited a relatively high variability with a *COV* of 32.68 percent compared to 6.27 percent for the CMSE approach (Tables 6-2 and 6-4). Because of the absence of actual field data, the CMSE results from previous research were used as a benchmark for comparison purposes (*5*, *35*, *52*, *53*).

EFFECTS OF HMAC AGING AT 60 °C (140 °F) FOR THREE MONTHS

In this interim report, three months aging at 60 °C (140 °F) was completed for both the CMSE and ME approaches. However, laboratory testing and analysis (both laboratory and field N_f) was completed only for the CMSE approach. For the ME approach, both BB testing and laboratory N_f analysis was completed for 0 months. For 3 months aging, BB testing was only completed for the lower test strain level (374 microstrain), and thus both laboratory and field N_f analysis could not be completed. Nonetheless, the flexural stiffness and dissipated energy results obtained from BB testing at the lower strain level (374 microstrain) for both 0 and 3 months aging conditions are presented.

Flexural Stiffness and Dissipated Energy – ME Repeated Flexural Loading

Figures 6-3 and 6-4 show the effects of 3 months aging at 60 °C (140 °F) under flexural BB fatigue testing at 20 °C (68 °F) for the 374 test microstrain.

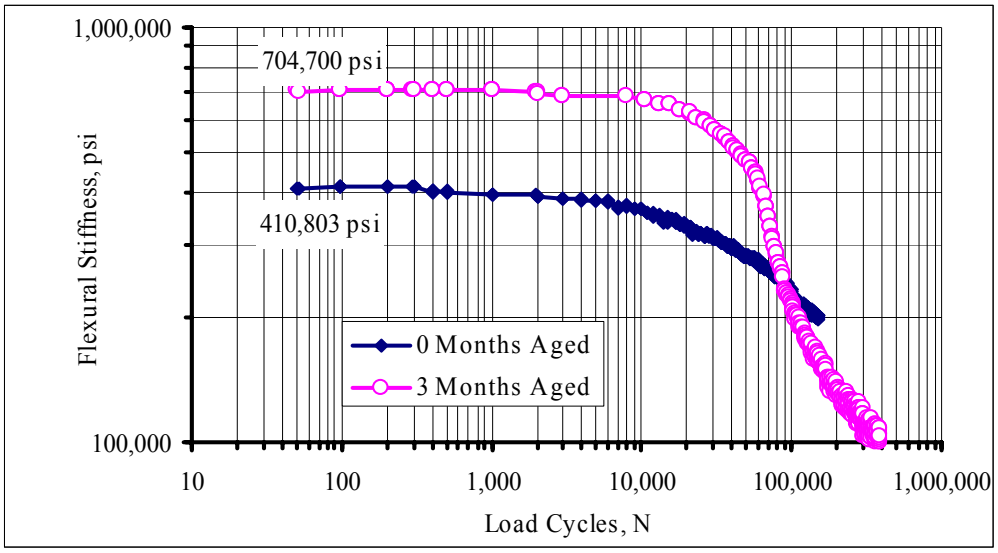

Figure 6-3. Flexural Stiffness, psi (374 Test Microstrain).

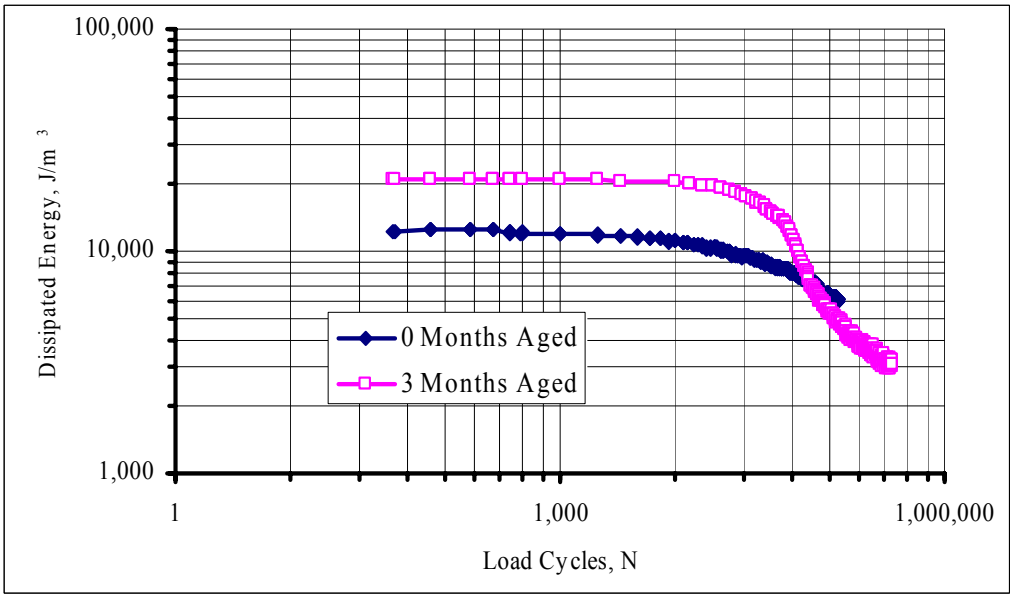

Figure 6-4. Dissipated Energy, J/m^3 (374 Test Microstrain).

Figures 6-3 and 6-4 show that the rate of decrease of stiffness and energy dissipation was higher for the 3 months aged beam specimens compared to the 0 months specimens. This is indicative that the aged specimens accumulated damage at a much faster rate. Due to aging, the 3 months aged beam specimens exhibited a higher initial stiffness (approximately 704,700 psi versus 410,803 psi) measured at the 50th load cycle, and subsequently required a relatively high amount of energy to induce and initiate damage. But once damage was initiated, subsequent damage progressed at a more accelerated rate compared to the 0 months aged specimens.

With regard to the number of laboratory load cycles to fatigue failure (failure criteria is described in Chapter 3), for the same input 374 microstrain level, the 0 months aged specimen required approximately 131,000 load repetitions to reach the failure point while the 3 months aged specimens sustained only about 71,400 (Figure 6-3). This reduction in the number of sustainable laboratory load cycles to fatigue failure is approximately 50 percent, indicating that aging has a very significant effect on the HMAC mixture fatigue resistance.

Tensile Stress and Strain at Break – CMSE Tensile Loading

Figure 6-5 shows an example of the effect of aging the HMAC mixture at 60 °C (140 °F) in terms of tensile stress and strain at break under tensile loading at 20 °C (68 °F). This result is representative of two individual test specimens, aged for 0 and 3 months, respectively.

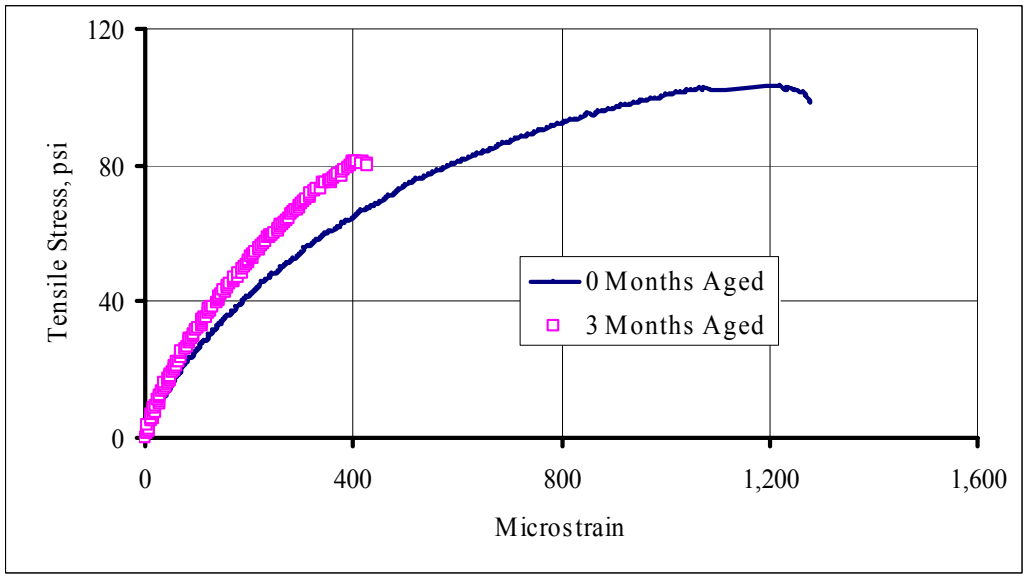

Figure 6-5. Tensile Stress, psi.

Figure 6-5 indicates that as the HMAC ages, as expected, it becomes more brittle and thus easy to break under tensile loading at a lower failure strain. The stress at break for the 0 months aged specimen (103.16 psi) is approximately 21 percent more than that of the 3 months aged specimen (81 psi). While this stress difference may be within the expected variability of the test, the change in the strain at break is significantly larger: 1300 microstrains versus 429 microstrains, indicating a difference of about 67 percent and a loss in ductility with aging.

The average slope of the 3 months aged HMAC graph was calculated by fitting a linear trend line in the elastic region to be approximately 2.2 times (0.19 versus 0.90) that of the 0 months aged specimen. This steep slope is evidence that although the 3 months aged specimen breaks at a relatively lower stress level, the resistance to deformation is relatively high due to brittle behavior compared to the more elastic 0 months aged specimen. For the same amount of applied loading or stress, there was more deformation or strain in the 0 months specimen compared to the 3 months aged specimen as shown by the shape of the stress-strain curve in Figure 6-5.

Relaxation Modulus – CMSE Tensile Loading

Figure 6-6 is an example of a plot of the relaxation modulus master-curves, versus reduced time on a log-log scale, for 0 and 3 months aged HMAC specimens under tensile loading.

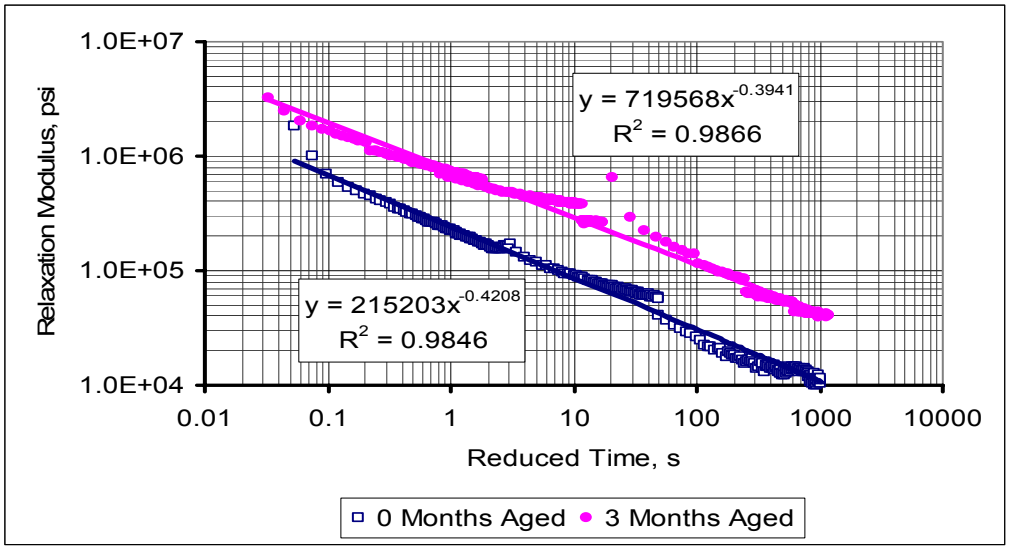

Figure 6-6. Relaxation Modulus, psi – Tension.

In Figure 6-6, the relaxation modulus increased significantly after aging due to HMAC hardening from oxidation of the binder. Due to this stiffening effect as a result of aging, the rate of stress relaxation (m_i) or *m-value* indicated by the power exponents in Figure 6-6 also decreased. For example, m_i for 0 months and 3 months aging was 0.42 and 0.39, respectively.

For both aging conditions, the *m-values* were relatively higher in tension compared to those in compression as evident from Tables 6-4 and 6-5, but vice versa for the relaxation modulus (E_i). This difference in E_i values (higher in compression than in tension) indicate that a relatively higher load was required to sustain a 200 microstrain strain in compression than in tension and indicates the anisotropic nature of HMAC.

Dissipated Pseudo Strain Energy – CMSE Uniaxial Repeated Direct-Tensile Loading

Figure 6-7 is an example of a plot of the DPSE versus log *N* during RDT testing at 30 °C (86 °F) with the test data normalized to 20 °C (68 °F). This DPSE was calculated as a function of the measured time-dependent tensile stress ($\sigma(t)_m$) during RDT testing and the pseudo strain (PS) discussed in Chapter 4.

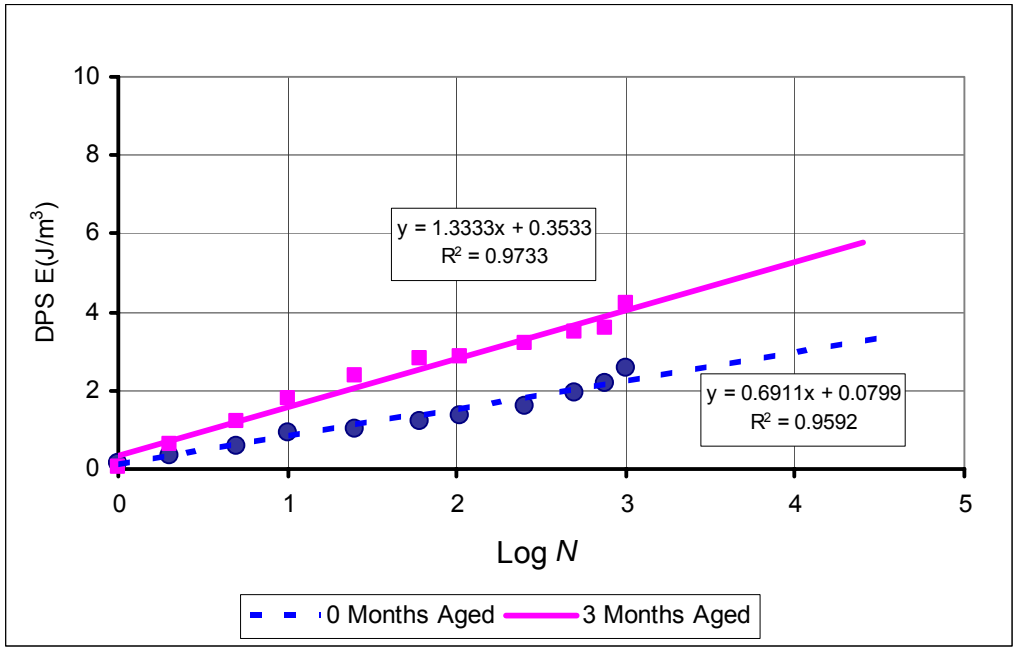

Figure 6-7. Dissipated Pseudo Strain Energy, J/m^3.

The slope (b) of the plot of DPSE versus Log N is representative of the rate of HMAC fatigue damage under uniaxial repeated direct-tension loading. Figure 6-7 shows that the rate of damage for the 3 months aged specimen was relatively higher compared to the 0 months aged specimen. The slope, b of the 3 months graph was approximated to be 1.9 times that of the 0 months graph. Thus the rate of damage after aging was approximately 1.9 times that prior to 3 months aging.

Microcrack Growth Prediction - CMSE

A backcalculation of the microcrack length using the CMSE equations discussed in Chapter 4 with the assumption that no damage occurs during the first load cycle of the uniaxial repeated direct-tension test, predicted the microcrack growth plotted in Figure 6-8. At any load cycle, microcrack length after aging was predicted to be approximately 2.7 times that of the 0 months aged specimens.

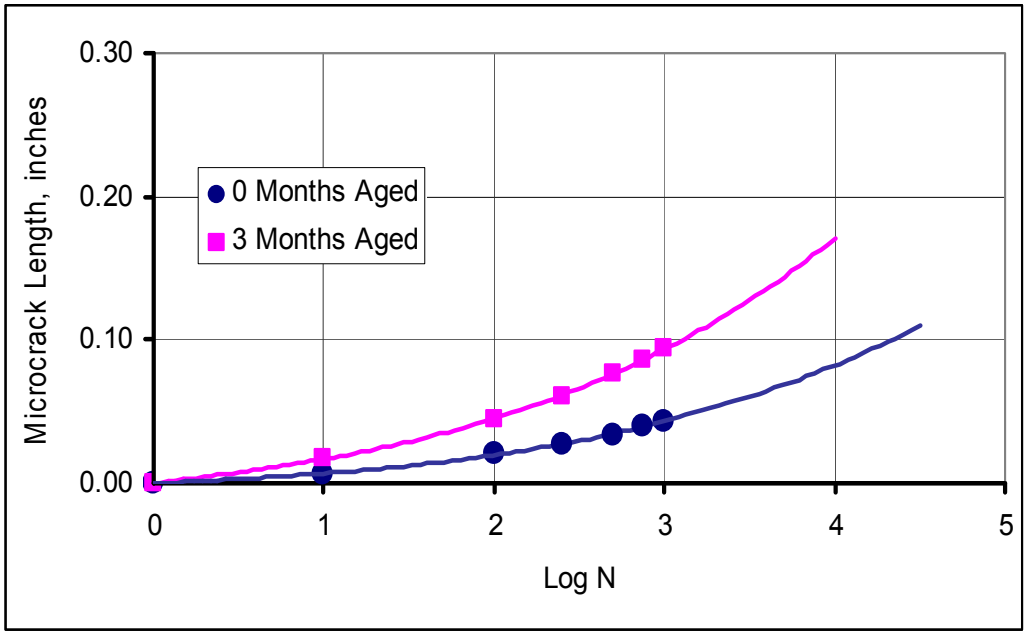

Figure 6-8. Microcrack Growth Prediction, inches.

A linear approximation of the slopes indicated that the microcrack in the aged specimen was growing at a rate of approximately two times that of the 0 months aged specimens. This predicted rate of microcrack growth does not differ significantly from the 1.9 rate of damage approximated in Figure 6-7 (i.e., 3 months versus 0 months aging) based on the DPSE analysis. This behavior is expected because as the HMAC ages, it loses both its cohesive and adhesive properties and thus becomes more susceptible to microcracking under tensile loading.

Healing Effect - CMSE

As discussed in Chapter 4, the asphalt in the HMAC mixture is known to elastically recover and heal during rest periods. In most cases, this healing effect has a net result of improving the HMAC mixture fatigue performance. Figure 6-9 compares the effects of aging on the HMAC mixture's healing potential.

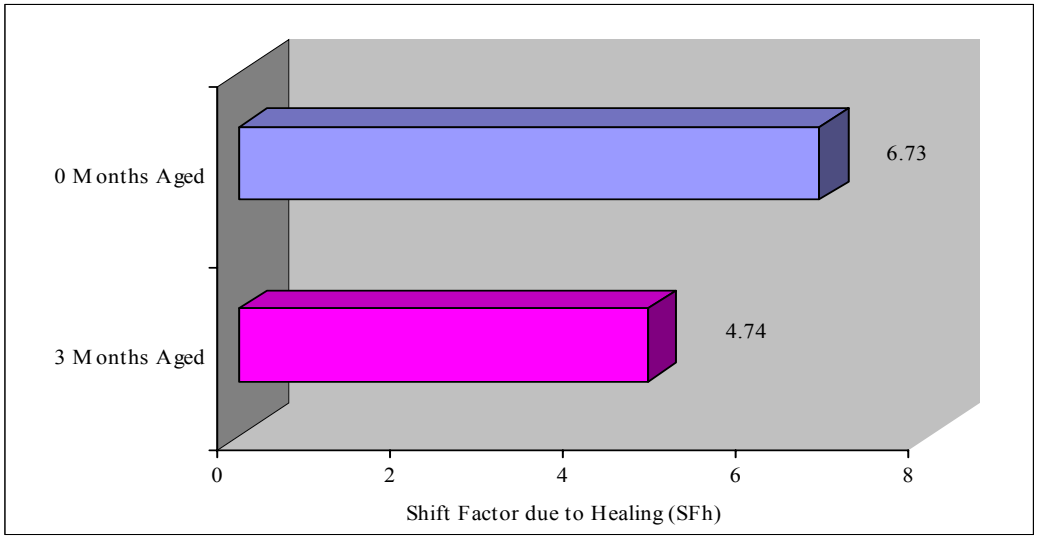

Figure 6-9. Calculated Shift Factor Due to Healing.

As the HMAC ages, the asphalt loses its elastic properties, and subsequently its healing potential decreases. This reduction in healing potential is clearly evident in Figure 6-9, which shows a decrease of approximately 30 percent after 3 months of aging at 60 °C (140 °F). Since the shift factor due to healing is a multiplicative factor in the CMSE fatigue analysis, N_f will subsequently decrease as aging progresses.

Fatigue Life - CMSE

Table 6-6 and Figure 6-10 compare the HMAC fatigue life after 3 months of laboratory aging at 60 °C (140 °F) with that after 0 months aging based on the CMSE analysis.

Table 6-6. CMSE Field Fatigue Life Analysis (Bryan Mixture).

Parameter	Aging Condition @ 60 °C (140 °F)	
	0 Months	3 Months
Estimated laboratory fatigue life ($N_i + N_p$)	6.31×10^6	2.42×10^6
Shift factors ($SF_a \times SF_h$)	10.97	7.82
Predicted field fatigue life ($N_f = (SF_a \times SF_h) \times (N_i + N_p)$)	69.22×10^6	18.93×10^6

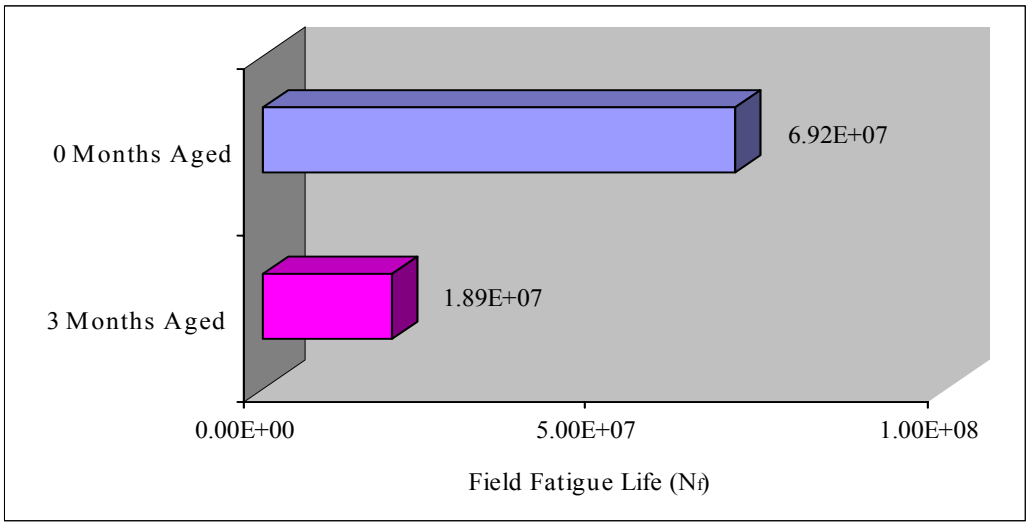

Figure 6-10. HMAC Field Fatigue Life – CMSE.

Table 6-6 shows a decline in N_f (both laboratory and field) with aging. This decrease in fatigue life as indicated by the reduction in N_f magnitude is evidence that aging has a significant effect on HMAC mixture fatigue performance. The rate of this N_f decline with aging and the effect of the shift factors is, however, yet to be explored with different mixtures and more aging conditions.

BINDER TEST RESULTS AND EFFECTS OF AGING

In this interim report, four aged-binder conditions are reported on a single PG 64-22 binder; two conditions are neat binders at two aging conditions, and two are aged binders recovered from laboratory mixtures. Neat binder was aged in a HMAC simulation, the SAFT to give one condition of aging (designated PG-64S). Then this binder was further aged in the 60 °C (140 °F) environmental room in thin films (approximately 1 mm [0.039 inches] thick) for 3 months to obtain a second aging condition (PG-64-3M). Two more conditions were obtained by aging the Bryan C mixture. The mixture was prepared using the STOA protocol and then compacted; this method produced one aging condition (Bryan-0M). The second condition was obtained by aging the compacted laboratory mixture in the environmental room for 3 months beyond STOA conditioning (Bryan-3M). Note that the 0 months and 3 months refer to environmental room aging beyond STOA so that 0 months aging still has a significant condition of aging beyond SAFT aging.

The binders in the compacted mixes were extracted and recovered according to the procedure outlined in Chapter 5. SEC was used to check whether the solvent residues exist in the binder. SEC chromatograms for recovered binders from Bryan mixtures are shown in Figure 6-11 and show that the recovered binders did not have solvent residue, which, if present, would significantly affect the rheological properties. They also show that the asphaltene peak, centered at about 23 minutes of retention time, increased with aging, a common result.

The aged binders were characterized by DSR and FTIR measurements, given in Table 6-7. Aging increases carbonyl area (oxygen content), viscosity, and the elastic modulus, but decreases the ductility. The calculated ductility shown in Table 6-7 is an estimate based on the measured DSR values and the correlation discussed in Chapter 5, Figure 5-2, below 10 cm (3.9 inches) ductility.

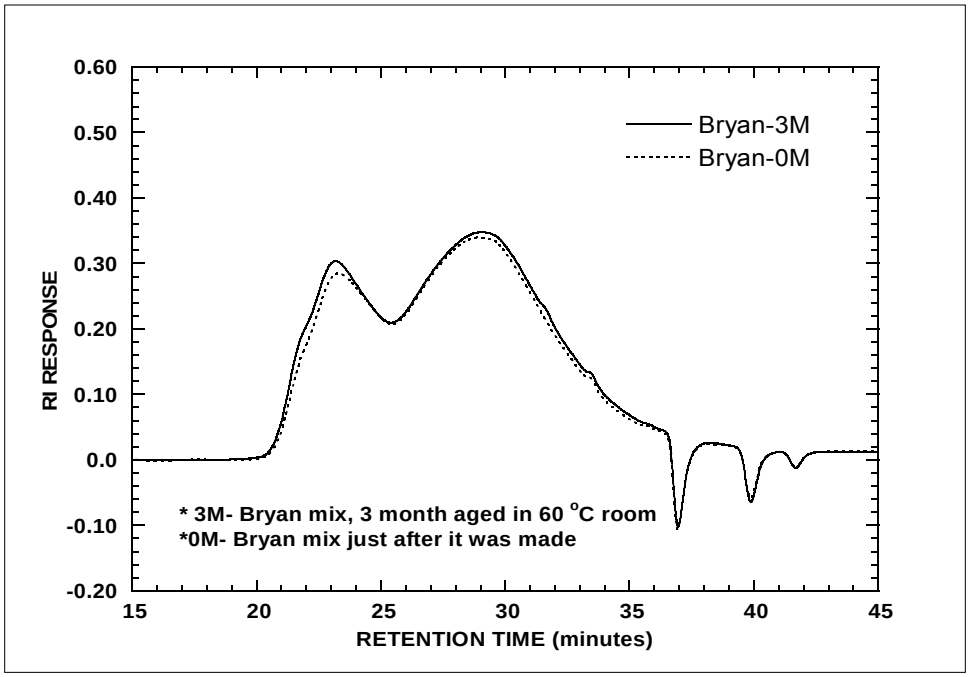

Figure 6-11. SEC Chromatogram for Recovered Binders from Bryan Mixtures (°F = 32 + 1.8(°C)).

Table 6-7. DSR Properties and Carbonyl Areas of Original and Recovered Binders (°F = 32 + 1.8(°C)).

Name[a]	η* (poise) 60 °C (0.1 rad/s)	G' (MPa)	η' (MPa*s) @0.005rad/s	Calculated Ductility (cm)[b]	η'/G' (s)	G'/(η'/G') (MPa/s)	Carbonyl Area
PG64S	10,500	0.02062	9.97	N/A	483.4	4.265E-05	0.62014
PG64-3M	45,760	0.09695	30.18	8.03	311.3	3.114E-04	0.85708
Bryan-A	38,200	0.07023	23.21	9.50	330.5	2.125E-04	0.79807
Bryan-B	31,640	0.06468	22.48	10.07	347.5	1.861E-04	0.76020
Bryan-C	28,910	0.05811	20.99	10.74	361.3	1.608E-04	0.76150
Bryan-D	28,320	0.06060	22.11	10.59	364.9	1.661E-04	0.75768
Bryan-0MA	36,900	0.07052	23.33	9.49	330.8	2.132E-04	0.80709
Bryan-0MB	38,200	0.06962	22.93	9.52	329.3	2.114E-04	0.80709
Bryan-3MA	81,000	0.1731	45.66	5.78	263.8	6.560E-04	0.92662
Bryan-3MB	75,000	0.1489	40.20	6.24	270.0	5.516E-04	0.91857

[a] PG64S: SAFT aged original binder; PG64-3M: 3 month aged in 60 °C room after SAFT; Bryan-A, B, C, D, 0MA, 0MB are recovered binders after mixtures were made; Bryan-3MA, -3MB are the replicates of recovered binders after mixtures were aged for 3 months in a 60 °C room; [b] Based on the correlation of Figure 5-2, for ductilities below 10 cm

Figure 6-12 presents the data of Table 6-7 in a DSR map (G' versus η'/G') of the various aged samples. The circles are the laboratory-aged binders; the open circle is SAFT-aged, and the solid circle is SAFT plus 3 months aging in the 60 °C (140 °F) environmental room. Lines of constant ductility are also shown in the graph based on the correlation in Figure 5-2 below 10 cm (3.9 inches). These lines correspond to the calculated ductility values shown in Table 6-7. The triangles are the binders recovered from aged mixtures; the open triangles are from the STOA-conditioned mixtures with 0 months additional aging, and the solid triangles are STOA compacted mixtures plus 3 months additional aging of the compacted mixtures in the 60 °C (140 °F) environmental room.

A number of observations about these results are appropriate. First, the data all form a consistent path across the DSR map, suggesting that the same oxidation mechanisms and physical responses occur, independent of whether the aging is as a neat binder in thin films or occurs in contact with aggregate. This result is consistent with comparisons of neat binder and mixture or pavement aging reported previously (*13*). Second, STOA aging produces a binder that is aged well beyond the HMAC production process, more like HMAC (RTFOT or SAFT aging) plus PAV based on previous information (Figure 5-3 of this report) (*13*).

In the remainder of the project, SAFT plus PAV aging will be conducted to obtain a more precise comparison with this specific binder. A third observation is that three months aging in 1mm (0.039 inches) films in the environmental room occurs at a faster rate than aging in compacted mixtures (0.022 versus 0.012 ln(MPa/s)/day). This is not unexpected, as access to oxygen in the compacted mixtures is limited to diffusion into pores and then into the asphalt films coated on the aggregate. In addition, SAFT aging (and some time afterwards) is still in the initial jump period, which has a higher aging rate. More data are needed to more fully assess thin film binder aging rates versus compacted mixture aging rates.

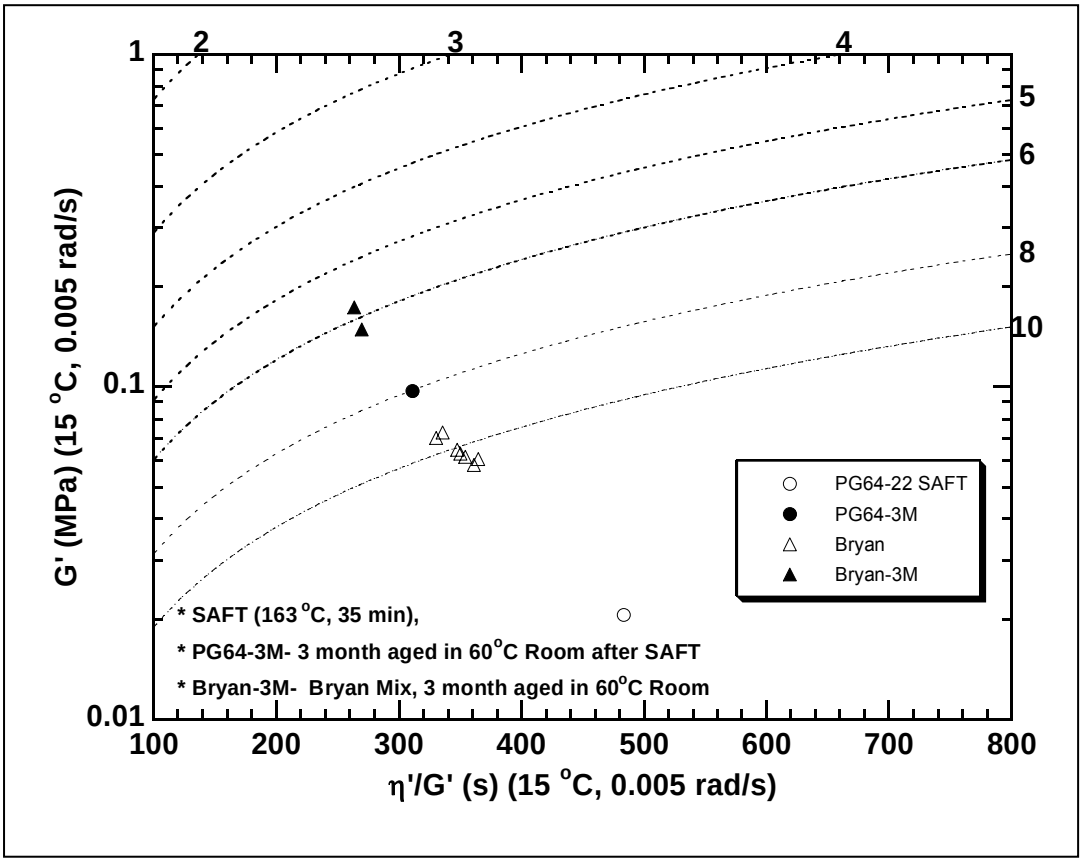

Figure 6-12. Movement of Binder across the DSR Map (°F = 32 + 1.8 (°C)).

THE IMPACT OF BINDER AGING ON FATIGUE RESISTANCE

The previous sections demonstrate that mixture fatigue resistance is decreased significantly by binder aging. Also, they quantify changes in binder properties that accompany this decline of fatigue life. Figure 6-13 shows the dependence of field fatigue life (Figure 6-5) on the binder DSR function G'/(η'/G') (Table 6-6) in a way similar to the dependence of ductility on the same function, shown previously in Figure 5-2. In Figure 6-13, the acronym AASHTO-PP2 refers to STOA described in Chapter 2.

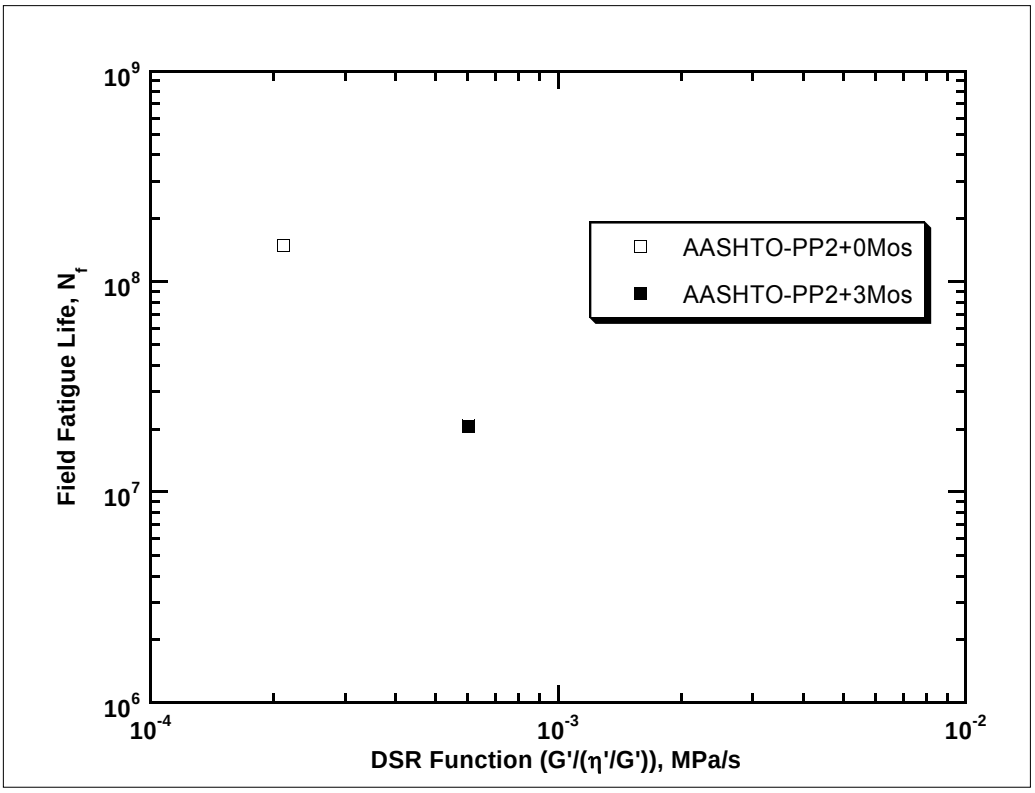

Figure 6-13. Mixture Field Fatigue Life versus Binder DSR Function.

Another data point at 6 months aging in the environmental room (after STOA) is essential to beginning to confirm, or reject, this relationship; data at still longer aging times will provide even better statistical correlations. The point at 6 months aging will be obtained later in this project.

Future data will allow for a better understanding of the effect of binder aging on fatigue life. Tests with the same mix design using other binders would give evidence as to whether such a relationship is universal with unmodified binders, as is the ductility correlation for aged binders. It is expected that a different correlation would exist for different mix-designs, and as a hypothesis, a family of correlations might be found, shifted with respect to each other and very likely with different slopes, for different mix designs. As additional data are obtained, these correlations and others will be assessed. Understanding the impact of binder aging on fatigue is essential to designing fatigue resistant mixtures and extending pavement performance.

CHAPTER 7
SUMMARY

This chapter summarizes the preliminary findings contained in this interim report, including the effects of HMAC and binder aging. A comparative analysis of the ME and CMSE fatigue analysis approaches is also presented.

HMAC MIXTURE FATIGUE RESISTANCE

The laboratory HMAC mixture fatigue resistance obtained by both the ME (4.48×10^6) and CMSE (6.31×10^6) approaches in terms of N_f magnitude are comparable. However, the ME approach exhibited a relatively high variability with a *COV* of 32.68 percent compared with 6.27 percent for the CMSE approach.

EFFECTS OF AGING ON HMAC MIXTURE PROPERTIES

Table 7-1 is a summary of the HMAC mixture properties and fatigue response to 3 months of accelerated aging at 60 °C (140 °F) based on CMSE testing. These changes in HMAC properties and a substantial decrease in fatigue life, as evident in Table 7-1, indicate that aging has a significant effect on HMAC mixture fatigue resistance and should be taken into account during fatigue design and analysis.

Compared to the 0 months aged HMAC specimens, the 3 months aged HMAC specimens exhibited lower values of ε_f, m_i, σ_t, and SF_h and higher values of E_i, A, and b, respectively. These changes in material characteristic properties are indicative that aging reduces HMAC mixture's resistance to fatigue damage and ability to heal, which is evident from a decrease in N_f after aging.

Table 7-1. Effects of Aging on HMAC Properties and N_f Based on CMSE Testing

Material Property	Unit	Aging Condition @ 60 °C (140 °F)		Trend with Aging	Effect on N_f
		0 Months	3 Months		
Tensile stress @ break, σ_t	psi	103.16	81.06	Decrease	Reduce
Failure tensile strain @ break, ε_f	in/in	1,300.06	429.44	Decrease	
Relaxation modulus (tension), E_t	psi	208,100	289,720	Increase	
Relaxation modulus (compression), E_c	psi	675,600	710,020	Increase	
Stress relaxation rate (tension), m_t	Unitless	0.40	0.38	Decrease	
Stress relaxation rate (compression), m_c	Unitless	0.36	0.33	Decrease	
Rate of damage (DPSE), b	Unitless	0.71	1.25	Increase	
Rate of microcrack growth	Unitless	0.37	0.79	Increase	
Shift factor due to healing, SF_h	Unitless	6.73	4.74	Decrease	
Fracture coefficient, A	Unitless	6.27×10^{-8}	16.00×10^{-8}	Increase	
Fatigue life (N_f)	Allowable load repetitions	69.22×10^6	18.93×10^6	Decrease	

EFFECTS OF AGING ON BINDER PROPERTIES

Asphalt mixtures consist of aggregate and binder. In service, binder oxidizes, resulting in compositional and physical changes. The physical property changes are very significant in that over a lifetime, binders can stiffen by orders of magnitude, decreasing their flexibility accordingly. These binder changes are the primary source of mixture physical property changes and must be considered when investigating mixture long-term performance and fatigue.

Previous work has investigated aging and the impact on binder properties; this project is the first effort to quantify mixture property changes, including fatigue, that occur because of binder oxidative hardening. One goal of this binder aging work is to be able to incorporate knowledge of binder aging into a mixture fatigue design and analysis process.

Binder stiffening with aging is manifested in increases in the dynamic elastic shear modulus (G') and dynamic shear viscosity (η'). Tracking these changes on the DSR map of G' versus η'/G' gives a valuable perspective on binder aging and the consequent changes in ductility, which the literature shows correlates with age-related cracking. AASHTO-PP2 short-term aging appears to correspond, roughly, to RTFOT plus PAV aging, based on the limited data to date. The binder in compacted mixtures ages readily in a 60 °C (140 °F) environmental room and follows the same track on the DSR map as binder aged in the absence of aggregate. The resulting binder stiffening in mixtures is reflected in stiffer mixture properties, including E_t, the elastic stiffness in tension, which increases and m_t, the stress relaxation rate in tension, which decreases (Table 7-1). This binder stiffening results in decreases in the (field) fatigue life calculated using the CMSE approach (Table 7-1).

Correlations between predicted fatigue life and binder DSR properties are being investigated and could provide the basis for predicting changes in field fatigue life due to aging and thus the basis for a design test that combines mixture durability with binder aging. Such a procedure will be evaluated for the ability to distinguish different mix designs in their ability to accommodate aging with minimal loss of fatigue life.

ME VERSUS CMSE

Table 7-2 is a comparative review of the ME and CMSE approaches in terms of equipment requirements, testing protocols, specimens, data analysis, and variability of the results based on the observations and findings made for this interim report.

Table 7-2. Preliminary Comparison of ME and CMSE Approaches.

Item	Detail	ME	CMSE
Equipment	Requirements	MTS + *BB* + LVDT +TC + TP	MTS + LVDT +TC + TP
	Handling	Difficult (heavy)	Easy
Testing	Machine setup	Complicated	Easy
	Procedure	Difficult	Easy
	Time	Long (~5 hrs)	1 hr (at most)
	Other tests	None	SE & AN
Specimen	Fabrication	Difficult (sawing)	Easy
	Compaction	kneading compactor	SGC
	Time	45 hrs	40 hrs
	Handling & storage	Extreme care required	Easy
	Air voids (COV)	4.84%	1.05%
	Aging effects	Relatively high (SVR=1.93)	Moderate (SVR = 1.33)
Analysis	Procedure & steps	Easy & straightforward	Somewhat complicated
	Complexity	Simple & straightforward	Many complex equations & constants
	Cracking	Indirectly incorporated in shift factors	Directly incorporated
	Healing effect		
	Rest periods		
	Anisotropic effect		
	Visco-elastic effect		
	Binder aging effects	Not directly accounted for	Not directly accounted for in current CMSE version
	Failure criteria	50% stiffness reduction	0.30 inches microcrack growth and propagation through HMAC layer
	Other computations	Design tensile strain	Design shear strain
Results	Variability	Relatively high	Low
	COV	32.68%	6.28%

Legend: ME = Mechanistic Empirical, BB = Bending Beam, CMSE = Calibrated Mechanistic with Surface Energy, SE = Surface Energy, AN = Anisotropic,
MTS = Material Testing System, LVDT = Linear Variable Differential Transducer,
TC = Temperature Chamber, TP = Temperature Probe, SVR = Surface Area to Volume Ratio

Test Equipment

Compared to the CMSE, Table 7-2 shows that the ME approach requires additional equipment for the BB test. This BB device can be costly, and the device is also difficult to handle because of weight. Additionally, the BB device lacks the advantage of versatility because it can be used only for third-point loading BB fatigue testing. Most HMAC characterization laboratory tests use cylindrical specimens like the CMSE approach.

Testing Procedure

Laboratory test time for both approaches is comparable. The many auxiliary CMSE tests such as AN and SE equate to BB testing in terms of time and cost. However, the equipment setup and test procedure are relatively complex for BB testing and require a comparatively higher degree of precision. With the CMSE approach, testing of cylindrical specimens require proper alignment along the axis of loading to prevent the induction of undesirable moments that can lead to erroneous results.

Specimens

Beam specimens for BB testing are comparatively difficult to fabricate, time consuming to make, and require delicate handling and storage. Improper handling and/or storage can easily induce residual stresses within the specimen, which can have a negative impact on the results. Because of their relatively high SVR, the beam specimens tend to expose a large surface area to oxidative aging compared to the CMSE cylindrical specimens. Also, the shape of the specimens and the linear compaction procedure makes it difficult to adequately control the AV, as evident from the high *COV* shown in Table 7-2. All these factors produce final results with a relatively higher variability.

The BB specimens require the linear kneading compactor for compaction. Unlike the SGC, many HMAC characterization laboratory tests do not utilize kneading compaction. Therefore, use of the kneading compactor for fabrication of only beam specimens can be viewed as costly because the compactor is limited in its application in the laboratory.

Analysis and Results

Although the ME analysis procedure is comparatively simple and straightforward and does not require a lot of input data, the approach does not directly account for the many factors such as healing and anisotropy that have a direct impact on HMAC mixture fatigue performance. The ME fatigue failure criterion (50 percent reduction in initial stiffness) may also not be a good indicator of the remaining fatigue life of HMAC. In addition, the tie between fatigue crack area on an in situ pavement structure or crack length through the HMAC layer thickness and 50 percent stiffness reduction is also not well defined (*11*, *12*).

In comparison, the CMSE approach takes into account many factors that affect HMAC mixture fatigue performance including healing, anisotropy, visco-elasticity, crack initiation, and crack propagation. As a result, the analysis appears complex because of the utilization of numerous equations and constants, particularly if the calculations are done manually. However, this type of analysis is necessary to adequately model the HMAC mixture fatigue resistance by analyzing and directly incorporating all the influencing factors. Moreover, these numerical calculations can easily be simplified to input data if a simple spreadsheet analysis program is developed for the computations including predicting HMAC mixture fatigue resistance.

In both approaches (ME and CMSE), however, binder aging is not directly incorporated. In the case of the CMSE approach, an aging shift (SF_{ag}) is being developed and will possibly be incorporated in the final CMSE version that will be presented in the final report. Also, the CMSE failure criterion needs to be reviewed to establish the adequacy of assuming that one microcrack (0.30 inches) initiating and propagating through the HMAC layer thickness is representative of the fatigue cracking process in the entire HMAC pavement structure. The current CMSE approach is calibrated with this generalized hypothesis. Additional data is thus needed to validate this hypothesis and/or modify the calibration.

Preliminary results indicated a relatively high variability in the ME approach with a *COV* of 4.84 percent for the AV and 32.68 percent for laboratory N_f. The CMSE *COVs* were 1.05 percent and 6.27 percent for AV and laboratory N_f, respectively.

CONCLUDING REMARKS

In summary, this preliminary research illustrates that both the ME and CMSE approaches can predict the HMAC mixture fatigue resistance based on the assumption that the CMSE approach provides a benchmark that in previous research predicted field performance (*5*, *35*, *52*, *53*). The fatigue results obtained were comparable.

The effect of aging was demonstrated as detrimental to the fatigue performance of HMAC mixtures in terms of a declining N_f magnitude. Thus this process (aging) must be taken into account during fatigue design and analysis. Based on the test conditions considered in this project, these preliminary results showed that aging reduces the HMAC mixture's resistance to fracture damage and its ability to heal.

A preliminary comparison of the ME and CMSE approaches showed that although the ME analysis procedure is simple and straightforward, there is a relatively high variability in both the mixture AV and the final N_f results. The input data for the CMSE approach are more comprehensive and require numerous auxiliary tests. But this bulk input data which can easily be reduced in a simple analysis, are necessary to account for the HMAC properties that directly affect fatigue performance. These factors are not all directly accounted for with the ME approach. Variability in both the AV and final N_f results were relatively low compared to the ME approach.

As discussed in Chapter 8, research for this project is still ongoing to: (1) further investigate the effects of binder aging on the HMAC mixture fatigue properties, (2) review other fatigue analysis approaches including that recommended in the proposed NCHRP 1-37A 2002 Pavement Design Guide, and (3) investigate the applicability and validity of the CMSE fatigue analysis approach.

CHAPTER 8
CURRENT AND FUTURE WORK

The tasks discussed in this chapter are currently ongoing and/or planned for the near future and will be presented in the final research report. Due to the publication process, laboratory testing for some of these tasks is actually already complete, and the data are currently being analyzed. The tasks discussed in this chapter actually represent the current status of TxDOT Project 0-4468 as of April 7, 2004.

MATERIALS – THE YOAKUM MIXTURE

In addition to the TxDOT Type C limestone mixture obtained from the Bryan District, researchers will also evaluate the fatigue properties of another mixture from the Yoakum District. This mixture is a 12.5-mm Superpave mixture designed with crushed river gravel and a PG 76-22 asphalt (5.6 percent by weight of aggregate). This mixture was used on US Highway 59 near Victoria and is considered a rut resistant mixture. This type of mixture was selected to examine its fatigue properties consistent with the title and motivation of this project.

The aggregate and asphalt were collected from the Fordyce Materials plant and Eagle Asphalt (Marlin Asphalt), Inc., respectively. In addition to the crushed river gravel, this mixture uses 14 percent limestone screenings and 1 percent hydrated lime. Table 8-1 and Figure 8-1 show the combined gradation of the Yoakum river gravel.

Aggregate batching, mixing, STOA, compaction, and specimen preparation for different laboratory tests with this mixture follow a similar procedure used for the Bryan mixture as discussed in Chapter 2. However, the mixing and compaction temperatures are consistent with the TxDOT Tex-205-F and Tex-241-F test specifications for PG 76-22 asphalt (9). These temperatures are 163 °C (325 °F) and 149 °C (300 °F) for mixing and compaction, respectively, utilizing the same compactors discussed in Chapter 2 for cylindrical and beam HMAC specimens.

The target compaction AV is 7±0.5 percent for all HMAC specimens including the Yoakum mixture. For HMAC specimen sawing, coring, volumetric analysis, handling, storage, and aging, researchers followed the procedures discussed in Chapter 2.

Table 8-1. 12.5 mm Superpave Gravel Aggregate Gradation.

Sieve Size	TxDOT Specification		Percent Passing
	Upper	Lower	
19.00	100	--	100.0
12.50	100	90	94.6
9.50	90		81.0
4.75			54.4
2.36	58	28	32.9
1.18			22.4
0.60			16.2
0.30			11.0
0.15			7.6
0.075	10	2	5.5

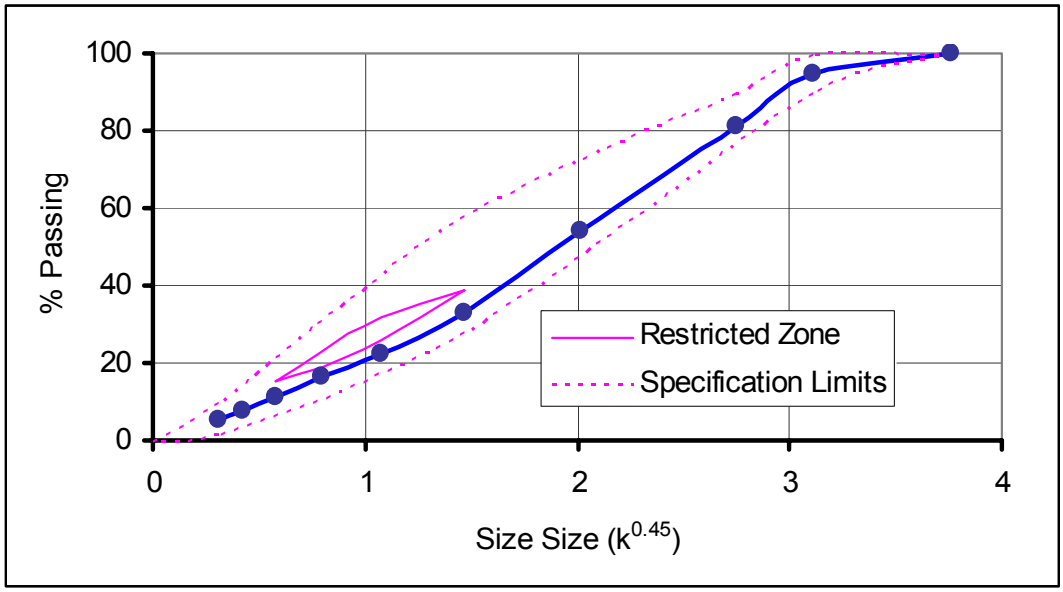

Figure 8-1. Gravel Aggregate Gradation Curve for Rut Resistant 12.5 mm Superpave Mixture.

PAVEMENT STRUCTURES, TRAFFIC, AND ENVIRONMENTAL CONDITIONS

Table 8-2 is a list of the selected TxDOT pavement structures and associated traffic that are being considered in this project. These pavement structures represent actual material properties and layer thicknesses that are commonly used on TxDOT highways in Texas (*14*).

Researchers plan to present the fatigue results for all of these pavement structures in the final report. The results discussed in Chapter 6 are only for the first pavement structure.

Table 8-2. Selected Pavement Structures and Traffic

PS #	Material type, layer thickness, and elastic modulus				Traffic ESALs	% Trucks
	Surfacing	Base	Subbase	Subgrade		
1	HMAC, 6 inches, 500,000 psi	Flex, 14 inches, 28,000 psi	None	9,000 psi	5,000,000	25
2	HMAC, 2 inches, 500,000 psi	Flex, 10 inches, 60,000 psi	Lime stabilized, 6 inches, 35,000 psi	12,400 psi	1,399,000	23.7
3	HMAC, 2 inches, 500,000 psi	Asphalt stabilized, 7 inches, 500,000 psi	Flex, 8 inches, 24,000 psi	Silt-clay, 9,600 psi	7,220,000	13
4	HMAC, 2 inches, 500,000 psi	Flex, 6 inches, 50,000 psi	Stabilized subgrade, 5 inches, 30,000 psi	10,000 psi	390,000	10.7

In addition to the above pavement structures, the research team also intends to analyze the highway pavement sections (US 290, SH 47, and US 59) where the Bryan and Yoakum mixtures were actually used (*6*, *54*). Results will be presented in the final report.

The environmental condition considered in this interim report was wet-warm. The research team also plans to consider the dry-cold (DC) environment, and the results will be reported in the final report (*14*). WW and DC are the two extreme Texas weather conditions the research team considered to have a significant impact on HMAC mixture fatigue performance.

LABORATORY TESTING AND AGING CONDITIONS

Ongoing and planned laboratory tests include BB, CM, binder mixture (BM), anisotropic, SE measurements, and binder tests.

BB Testing and HMAC Aging Conditions

The BB test and HMAC fatigue analysis procedure are described in Chapter 3. BB testing and analysis with 0 months aging specimens for Bryan and Yoakum mixtures are complete. BB testing of the 3 months aged specimens for the Bryan mixture is also complete, and the data are currently being analyzed. The research team will conduct the test with 3 and 6 months aged specimens for the Yoakum mixture following the same procedure and thereafter analyze the results. Preparation of HMAC specimens for 3 and 6 months aging is complete, and the specimens are now being aged in an environmental room at 60 °C (140 °F). Results from different aging conditions will enable the researchers to explore the relationship between binder and mixture aging and use this relationship to predict mixture fatigue lives based on binder testing.

CMSE Testing and HMAC Aging Conditions

The CMSE laboratory tests and fatigue analysis procedure for HMAC are discussed in Chapter 4. These tests include tensile strength (TS), uniaxial relaxation modulus (RM), and uniaxial repeated direct-tension. The research team completed CMSE testing with 0 months aged for both HMAC mixtures and 3 months aged specimens for the Bryan mixture. Currently RM and RDT tests for the Yoakum mixture for 3 months aged specimens are underway. TS testing for the 3 months aged Yoakum specimens is already complete, and the data are currently being analyzed. Similar testing will be conducted with 6 months aged specimens. Specimen preparation for 6 months aging is already complete, and the specimens are currently being aged in an environmental room at 60 °C (140 °F). The data analysis procedure will be essentially the same as that discussed in Chapter 4.

Test results from these specimens will be used to analyze the fatigue life of the aged specimens and predict the fatigue performance of HMAC at different points during the pavement service life. In addition, the results will allow investigation of the relationship between binder and mixture aging. This relationship is critical if aging is to be included in mixture fatigue design and analysis through accelerated binder aging and testing.

BM Testing and HMAC Aging Conditions

The objective of the BM tests is to measure the effect of laboratory aging of a compacted specimen on its relaxation modulus. The BM test protocol is similar to the CMSE relaxation modulus test described in Chapter 4, except that with BM testing the same HMAC specimen is repeatedly tested at different aging conditions. This test is being performed with both mixtures (Bryan and Yoakum) at 0 and 3 months aging conditions with three replicate specimens for each mixture. Again, the same specimen tested at 0 months aging is subjected to a second relaxation modulus test after subsequent aging for 3 additional months.

The research team has already prepared specimens and completed the first testing sequence of 0 months aging for both mixtures (Bryan and Yoakum). The data are currently being analyzed. The same specimens are currently being aged in an environmental room at 60 °C (140 °F). The second sequence of testing will occur after 3 months of aging as soon as the specimen aging process is complete.

AN Testing and HMAC Aging Conditions

The modulus of HMAC is an important input parameter used in predicting fatigue performance. HMAC is not an isotropic material. The objective of this AN test is to measure the variation of HMAC modulus in the vertical (E_z) and horizontal (E_x) directions. These values are input parameters for CMSE fatigue analysis. Primarily, AN testing will be conducted to determine the shift factor due to anisotropy (SF_a) discussed in Chapter 4. The AN test protocol is not yet finalized, but researchers are planning to use repeated compressive loading on a cylindrical specimen along its longitudinal axis and measure the strain both in axial and radial directions. Analysis of the results will produce the required E_z and E_x modulus values.

The AN test will be performed for both the mixtures (Bryan and Yoakum) with 0 and 3 months aged specimens on three replicate specimens at one test temperature of 20 °C (68 °F). Trial testing is already complete, and data analysis is underway.

Since this test will probably be destructive in nature, separate specimens were fabricated for 0 and 3 months aging conditions. The 3 months HMAC specimens are currently aging at 60 °C (140 °F) in an environmental temperature-controlled room.

SE Measurements for Asphalt and Aging Conditions

Surface energy of asphalt and aggregate are used as input parameters for the CMSE procedure. For the CMSE procedure, the research team is testing the binder samples at two different aging conditions, 0 and 3 months aging, respectively.

The surface energy of the two asphalts (PG 64-22 and PG 76-22) have already been measured for both unaged (original) and after 3 months aging with the Wilhelmy plate method described in Chapter 4. Complete test results will be presented in the final report.

SE Measurements for Aggregate

Surface energy of aggregates is calculated based on the spreading pressure of reference liquid vapors (with known surface energy values) onto the aggregate surface. The spreading pressure can be calculated using an isotherm, which is a plot of the adsorbed mass versus the vapor pressure.

A typical test procedure for measuring surface energy of aggregate involves the measurement of the mass of vapor adsorbed onto the aggregate surface at different vapor pressure levels of the reference liquid. The adsorbed mass is typically measured for 8 to 10 different vapor pressure levels until the maximum saturated vapor pressure of the reference liquid (at the test temperature) is reached. The measured adsorbed mass can then be plotted against the vapor pressure of the liquid to generate the isotherm, which can then be used to calculate the specific surface area and the spreading pressure using the Brunauer, Emmett, and Teller (BET) and Gibbs free energy equations (*30*, *33*).

Typically, isotherms for three reference liquids (water, Methyl Propyl Ketone 74 [MPK], and n-hexane) are required to be able to calculate all three components of surface energy. The Universal Sorption Device (USD) is comprised of a Rubotherm magnetic suspension balance system, computer, Messpro (computer software), temperature control unit, high quality vacuum, vacuum regulator, pressure transducer, solvent container, and a vacuum dissector (*30*, *33*). The USD is a very sensitive magnetic suspension balance capable of measuring mass to the order to 10^{-5} gm. The magnetic suspension allows the sample to be suspended in a cell that is physically separate from the balance, and thus the cell and the sample can be subjected to a vacuum or very low pressures.

The recently modified USD integrates the measurement of mass and control of pressure and degassing operations using software controlled by a single computer. This software can be used to run the entire test procedure without the intervention of an operator for any given solvent. The software also takes into account a buoyancy correction for the suspended mass, a correction for zero point drift, and an equilibrium analysis tool that estimates whether the adsorption for a given vapor pressure level has reached equilibrium or not in real time. Once the test is complete, the degassing sequence is automatically initiated in preparation for the next test.

The software also has a built-in analysis tool that does all the calculations required based on the BET and the Gibbs free energy equations, providing the user the end results such as the spreading pressure, isotherm, and specific surface area. The developed software and hardware controls are intended to automate the system and minimize human interference and resulting errors in the test procedure. The overall testing efficiency is improved due to relatively shorter testing times and the fact that tests can also be run overnight without the operator present.

Binder Testing and Aging Conditions

Tests of the binder for the Bryan mixture continue. Aging the compacted mixture beyond the 3 months conditions obtained to date is essential to assess correlations between mixture fatigue life and binder properties. Additionally, binder tests for the Yoakum mixture are proceeding. Test protocols and data analysis procedures for these binder tests were described in Chapter 5. Work that remains is summarized in Tables 8-2 and 8-3. Compacted mixture tests of 0, 3, and 6 months aged specimens are planned.

FATIGUE ANALYSIS APPROACHES

Results from the proposed NCHRP 1-37A 2002 Pavement Design Guide are not contained in this interim report but will be presented in the final research report. In addition, researchers plan to complete a CM fatigue analysis procedure without the inclusion of SE data. These two approaches are discussed briefly in this section.

Proposed NCHRP 1-37A 2002 Pavement Design Guide with Dynamic Modulus Testing

The proposed NCHRP 1-37A 2002 Pavement Design Guide (M-E Pavement Design Guide) adopts a ME approach for the structural design of asphalt pavement (*56*). The basic inputs for pavement design include environment, material, and traffic data. There are two major aspects of ME based material characterization: pavement response properties and major distress/transfer functions. Pavement response properties are required to predict states of stress, strain, and displacement within the pavement structure when subjected to external wheel loads. These properties for assumed elastic material behavior are the elastic modulus and Poisson's ratio. The major distress/transfer functions for asphalt pavements are load-related fatigue fracture, permanent deformation, and thermal cracking.

The new design guide suggests a hierarchical system for materials characterization. This system has three input levels. Level 1 represents a design philosophy of the highest practically achievable reliability, and Levels 2 and 3 have successively lower reliability. The Level 1 design procedure requires a dynamic modulus value for HMAC and a complex shear modulus for unaged asphalt as input parameters.

Input Data

For Level 1 fatigue analysis, M-E Pavement Design Guide software requires the DM of an HMAC mixture measured over a range of temperatures and frequencies (5 temperatures × 6 frequencies), and complex shear modulus (measured with the DSR) of asphalt measured over a range of temperatures. The binder data are used in the software to predict mixture aging using the global aging model (*56*).

Output Data

The M-E Pavement Design Guide software predicts the percentage of fatigue cracking (along with other distresses) at any age of the pavement for a given structure and traffic level. The failure criteria can be set in two ways: setting the limit of percentage of cracks for a given number of traffic loads or determining the number of traffic loads in terms of ESALS to reach a certain percentage of cracks at a certain age of the pavement.

DM Testing Protocol

The DM test is not a new test for paving materials. A typical test is performed over a range of different temperatures by applying sinusoidal loading at different frequencies to a confined or unconfined sample. Typical parameters obtained from this test are the complex modulus (E*) and the phase angle (δ). The complex modulus E* is a function of the storage modulus E′ and loss modulus E″. The magnitude of the complex modulus is represented as the dynamic modulus shown in Equation 8-1.

$$|E^*| = \frac{\sigma_0}{\varepsilon_0} \qquad \text{(Equation 8-1)}$$

where:

|E*| = Dynamic modulus

σ_0 = Axial stress

ε_0 = Axial strain

In this project, tests were conducted in accordance with AASHTO Designation: TP 62-03 Standard Method of Test for Determining Dynamic Modulus of Hot Mix Asphalt Concrete Mixtures at 25, 10, 5, 1, 0.5, and 0.1 Hz and -10, 4.4, 21.1, 38, and 54.4 °C (14, 40, 70, 100, and 130 °F) test temperatures (*57*). The stress level for measuring the DM was chosen in order to maintain the measured resilient strain within 50 to 150 microstrains. The order for conducting each test was from lowest to highest temperature and highest to lowest frequency of loading at each temperature to minimize specimen damage.

Data generated were used to plot a master-curve using the sigmoidal curve fitting function as illustrated by Equation 8-2 (*56*).

$$\log(|E^*|) = \delta + \frac{\alpha}{1 + e^{\beta - \gamma \log(\xi)}} \qquad \text{(Equation 8-2)}$$

where:

|E*| = Dynamic modulus

ξ = Reduced frequency

δ = Minimum modulus value

α = Span of modulus values

β = Shape parameter

γ = Shape parameter

Specimen Preparation

Specimens for DM testing were fabricated, sawed, and cored to 150 mm (6 inches) in height, 100 mm (4 inches) diameter, and 7±0.5 percent AV consistent with the HMAC specimen preparation procedure discussed in Chapter 2 for cylindrical HMAC specimens. For each mixture (Bryan and Yoakum), three replicate specimens with three LVDTs glued on each specimen were used for the test.

The research team has already completed dynamic modulus testing with 0 months aged Bryan and Yoakum HMAC mixture specimens. Binder complex shear modulus testing with the DSR for the PG 64-22 (Bryan) and PG 76-22 (Yoakum) asphalts is also complete. There is no plan for further testing with aged HMAC specimens or asphalt samples. The research team is currently analyzing the results for predicting fatigue performance using the currently available version of M-E Pavement Design Guide software.

CM without SE Measurements

The complete CMSE analysis procedure involves the determination of the surface energies of both asphalt and aggregate. Determination of these parameters is a time consuming process. Therefore, to improve the practicality of the CMSE approach, researchers will attempt to predict fatigue life using the CM procedure without using SE as an input parameter. This analysis will be performed with both mixtures (Bryan and Yoakum) at different aging conditions including 0, 3, and 6 months aging conditions.

TIMEFRAME - LABORATORY TESTING AND DATA ANALYSIS

Tables 8-3 and 8-4 are a summary list of the number and types of tests remaining and ongoing and the estimated dates of completion for laboratory testing and data analysis, respectively as of 04/07/2004.

Table 8-3. HMAC and Component Material Tests Remaining and Ongoing (TxDOT Project 0-4468 Status as of 04/07/2004).

Approach	Test Type	Materials	Aging Conditions @ 60 °C (140 °F)	# of Tests Remaining
ME	BB	Bryan mixture Yoakum mixture	6 months 3 & 6 months	6 12
CMSE & CM	TS	Bryan mixture Yoakum mixture	6 months 6 months	2 2
	RM & RDT	Bryan mixture Yoakum mixture	6 months 3 & 6 months	3 6
	SE	Limestone aggregates Gravel aggregates	0 months 0 months	3 3
	AN	Bryan mixture Yoakum mixture	0 & 3 months 0 & 3 months	6 6
BM	RM	Bryan mixture Yoakum mixture	3 months 3 months	3 3
Asphalt binder	DSR	Bryan binder Yoakum binder Recovered Bryan binder Recovered Yoakum binder	6 months 6 months 3 & 6 months 3 & 6 months	1 1 4 4
	Ductility Test	Bryan binder Yoakum binder	0 & 6 months 0 & 6 months	4 4
	FTIR	Bryan binder Yoakum binder Recovered Bryan binder Recovered Yoakum binder	6 months 6 months 3 & 6 months 3 & 6 months	1 1 4 4
	SEC	Bryan binder Yoakum binder Recovered Bryan binder Recovered Yoakum binder	0, 3, 6 months 3 & 6 months 3 & 6 months 3 & 6 months	3 2 4 4

Table 8-4. Estimated Timeframe for Lab Testing and Data Analysis (TxDOT Project 0-4468 Status as of 04/07/2004).

Approach	Date of Expected Completion					
	Testing & Aging Condition @ 60 °C (140 °F)			Data Analysis & Aging Condition @ 60 °C (140 °F)		
	0 months	3 months	6 months	0 months	3 months	6 months
AASHTO	08/2003	N/A	N/A	04/2004	N/A	N/A
ME	10/2003	05/2004	7/2004	12/2003	5/2004	08/2004
CMSE	11/2003	04/2004	6/2004	04/2004	5/2004	07/2004
CM	11/2003	04/2004	6/2004	04/2004	5/2004	07/2004
BM	02/2004	06/2004	N/A	04/2004	7/2004	N/A
Binder Testing	12/2003	04/2004	07/2004	03/2004	05/2004	07/2004

TIMEFRAME – PRELIMINARY FATIGUE ANALYSIS PROTOCOL.

Table 8-5 lists the timeframes researchers envisage recommending a preliminary fatigue analysis approach based on the analysis stages indicated in the table.

Table 8-5. Timeframe for Recommending a Preliminary Protocol.

Approaches Considered	Expected Date
ME & CMSE based on 0 months aging	End of April 2004
ME, CMSE, & CM based on 0 and 3 months aging	End of May 2004
ME, CMSE, & CM based on 0, 3, and 6 months aging & NCHRP 1-37A Guidance	Mid August 2004

TIMEFRAME – DELIVERABLE PRODUCTS

Table 8-6 summarizes the present status of the deliverable products of Project 0-4468 as of 04/07/04.

Table 8-6. Project 0-4468 Product Status.

Product	Description	Submittal Date	Comment
Phase I: Financial Year 03 & 04 (FY03/04)			
R1	Interim Research Report 0-4468-1	05/31/04	Preliminary findings
P1	Product 0-4468-P1: Database of fatigue lives of commonly used TxDOT HMAC mixtures	10/31/04	Based on 2 HMAC mixtures; Basic & Rut Resistant. R2 to include P1 & P2
P2	Product 0-4468-P1: Recommended fatigue analysis system	10/31/04	
R2	Research Report 0-4468-2	10/31/04	
Phase II: Financial Year 05 (FY05) (With Modification)			
P1	Database as in Phase I above	10/31/05	With modification & additional HMAC mixtures. R3 to include P3 & P4 and updates of P1 & P2
P3	Fatigue analysis workshop materials	10/31/05	
P4	Instruction for fatigue analysis workshop	10/31/05	
R3	Research Report 0-4468-3	10/31/05	
PSR	Project Summary Report	10/31/05	Summary of work accomplished, findings, recommendations, & conclusions

The FY05 modification with additional HMAC mixture characterization by the recommended fatigue analysis approach from FY03/04 is necessary to:

- provide confidence in the selected fatigue analysis approach,
- populate the database of fatigue lives of commonly used TxDOT HMAC mixtures, and
- provide additional data to sufficiently incorporate the effects of binder aging in the selected fatigue analysis approach.

The proposed six to eight additional FY05 HMAC mixtures that will be tied to the FY03/04 mixtures will include the following materials:

- Mixtures: Superpave
- Binders: PG 64-22, PG 70-22, & PG 76-22
- Aggregates: gravel

Laboratory testing and subsequent data analysis will be similar to the FY03/04 protocol consistent with the selected and recommended fatigue analysis approach. The proposed FY05 duration will be approximately 12 months with a budget estimate of $100,000.00.

CLOSURE

Upon completion of the tasks discussed in this chapter, the following objectives of the project will be achieved:

- A fatigue mix-design and analysis system to ensure adequate performance under specified environmental and loading conditions in a particular pavement structure will be evaluated and recommended.
- Fatigue resistance of commonly used TxDOT HMAC mixtures will be evaluated and compared with a subsequent establishment of a database of fatigue lives of these HMAC mixtures. However, research reports R1 (this interim report) and R2 (to be submitted by 10/31/2004) will include only two HMAC mixtures (Basic [Chapter 2] and Rut Resistant [this chapter]).
- The effects of binder aging on HMAC mixture properties and fatigue resistance will be realized, and a procedure to account for the effects of aging is being investigated and possibly incorporated in the recommended fatigue analysis approach.

REFERENCES

1. Deacon, J. A., J. S. Coplantz, A. A. Tayebali, and C. L. Monismith, "Temperature Considerations in Asphalt-Aggregate Mixture Analysis and Design," *Transportation Research Record* 1454, pp. 97-112 (1994).

2. Superpave Models Team, *Simple Performance Test: Test Results and Recommendations Interim Task C Report*, NCHRP 9-19 Superpave Support and Performance Models Management, Project Deliverable Subtask C.3, Arizona State University: College of Engineering and Applied Sciences, Department of Civil and Environmental Engineering (2000).

3. Witczak, M., *Chapter 2: Material Characterization*, Draft NCHRP 1-37A Report, Arizona State University: College of Engineering and Applied Sciences, Department of Civil and Environmental Engineering (2001).

4. Kim, Y. R., H-J Lee, and D. N. Little, "Fatigue Characterization of Asphalt Concrete Using Viscoelasticity and Continuum Damage Theory," *Journal of the Association of Asphalt Paving Technologists*, Vol. 66, pp. 520-569 (1997).

5. Kim, Y. R., H-J Lee, Y. Kim, and D. N. Little, "Mechanistic Evaluation of Fatigue Damage Growth and Healing of Asphalt Concrete: Laboratory and Field Experiments," *Proceedings of the 8th International Conference on Asphalt Pavements*, Seattle, Washington, August 10-14, pp. 1089-1107 (1997).

6. Texas Department of Transportation (TxDOT), Bryan District Laboratory. HMACP Mixture Design used on US 290 and SH 47: Unpublished Internal Laboratory Test Report. Bryan, Texas (2002).

7. AASHTO PP6-94, Standard Practice for Grading or Verifying the Performance Grade of an Asphalt Binder (1996).

8. AASHTO TP5-98, Standard Test Method for Determining the Rheological Properties of Asphalt Binder Using a Dynamic Shear Rheometer (DSR) (1998).

9. *Pocket Facts*. TxDOT Test Specification Manuals. (http://manuals.dot.state.tx.us) Accessed May 2003 (2003).

10. AASHTO Designation: PP2. Standard Practice for Short and Long Term Aging of Hot Mix Asphalt, *AASHTO Provisional Standards*, Washington, D.C., June Edition (1994).

11. AASHTO TP8-94, Standard Test Method for Determining the Fatigue Life of Compacted Hot-Mix Asphalt (HMA) Subjected to Repeated Flexural Bending (1996).

12. Asphalt Institute, AI Research, Determination of Threshold Strain Level for Infinite Fatigue Life in Asphalt Mixtures. Interim Report for the Asphalt Alliance (2002).

13. Glover, C.J., R.R.Davison, C.H.Domke, Y. Ruan, P. Juristyarini, D.B. Knorr, and S.H. Jung. Development of a New Method for Assessing Asphalt Binder Durability with Field Validation. Technical Research Report FHWA/TX-03/1872-2 (2003).

14. Freeman, T. *Flexible Pavement Database.* Texas Transportation Institute. Ongoing Research Project 187-06, College Station, Texas (2004).

15. Ahlborn, G. "ELSYM5, Computer Program for Determining Stresses and Deformations in Five Layer Elastic System." University of California, Berkeley (1969).

16. Park, D. W. "Characterization of Permanent Deformation in Asphalt Concrete Using a Laboratory Prediction Method and an Elastic-Viscoplastic Model." Ph. D. Dissertation, Texas A&M University, College Station, Texas (2004).

17. Epps, A. L., J. T. Harvey, and C. L. Monismith, "Performance Characteristics of Mixes Containing Asphalt Cements and Crumb Rubber Modified Binders," presented at the Symposium on Asphalt, Number One Thermoplastic Polymer as part of the 217th American Chemical Society Meeting, Anaheim, California, March 23 (1999).

18. Harvey, J., T. Hoover, W. Nokes, N. F. Coetzee, and F. Rust, "CalTrans Accelerated Pavement Test (CAL/APT) Program – Test Results: 1994-1997," *Journal of the Association of Asphalt Paving Technologists*, Vol. 67, pp. 644-689 (1998).

19. Harvey, J. T., J. A. Deacon, A. A. Tayebali, R. B. Leahy, and C. L. Monismith, "A Reliability-Based Mix Design and Analysis System for Mitigating Fatigue Distress," *Proceedings of the 8th International Conference on Asphalt Pavements*, Seattle, Washington, August 10-14, pp. 301-323 (1997).

20. Monismith, C., J. Deacon, and R. Leahy, "Asphalt/Binder-Aggregate Mix Design and Analysis - A Performance-Based Approach," *Proceedings of the International Symposium on Recent Developments in Soil and Pavement Mechanics,* Rio de Janeiro, Brazil, June 25 - 27 (1997).

21. Tayebali, A., J. Deacon, J. Coplantz, J. Harvey, and C. Monismith, *Fatigue Response of Asphalt-Aggregate Mixes*, SHRP-A-404, Washington, D.C.: Strategic Highway Research Program, National Research Council (1994).

22. Harvey, J. T., J. A. Deacon, B. W. Tsai, and C. L. Monismith, *Fatigue Performance of Asphalt Concrete Mixes and Its Relationship to Asphalt Concrete Pavement Performance in California*, RTS-65W485-2, University of California, Berkeley: Asphalt Research Program, CAL/APT Program, Institute of Transportation Studies (1996).

23. Walubita, L., F. Hugo, and A. Epps, *Performance of Rehabilitated Lightweight Aggregate Asphalt Concrete Pavements under Wet and Heated Model Mobile Load Simulator Trafficking: A Comparative Study with the TxMLS*, Center for Transportation Research Report No.1814-3, Austin, Texas: The University of Texas at Austin (2000).

24. van de Ven, M., A. d. F. Smit, and R. Krans, "Possibilities of a Semi-Circular Bending Test," *Proceedings of the 8th International Conference on Asphalt Pavements*, Seattle, Washington, August 10-14, pp. 939-950 (1997).

25. Tayebali, A.A., J. A. Deacon, J.S. Coplantz, J.T. Harvey, and C. L. Monismith. Fatigue Response of Asphalt Aggregate Mixes. SHRP A-003 (1992)

26. Jianlong, Z., and L. Francken, "A Research on the Dissipated Energy Density of Bituminous Mixtures and Overlay," *Proceedings of the XIIIth World Meeting of the International Road Federation*, Toronto, Canada, June 16-20 (1997).

27. Little, D., R. Lytton, D. Williams, C. W. Chen, Y. R. Kim, and H. J. Lee, *Fundamental Properties of Asphalts and Modified Asphalts: Task K – Microdamage Healing in Asphalt and Asphalt Concrete, Final Report, Volume I: Microdamage and Microdamage Healing – Project Summary Report*, Washington, D.C.: Federal Highway Administration (1998).

28. Little, D., R. Lytton, Z. Si, D. Xin, and Y. R. Kim, *Crack Phenomenology: Formation and Healing - Task K Findings, Interim Report*, College Station, Texas: Texas Transportation Institute (2000).

29. Lytton, R. L., J. Uzan, E. G. Fernando, R. Roque, D. Hiltunen, and S. Stoffels, *Development and Validation of Performance Prediction Models and Specifications for Asphalt Binders and Paving Mixes*, SHRP-A-357, Washington, D.C.: Strategic Highway Research Program, National Research Council (1993).

30. Si, Z. “Characterization of Microdamage and Healing of Asphalt Concrete Mixtures.” Ph.D. Dissertation, Texas A&M University, College Station, Texas (2001).

31. Lytton, L.L. “Characterizing Asphalt Pavements for Performance,” *Transportation Research Record* 1723, pp. 5-16 (2000).

32. Good, R. J., and C. J. Van Oss, “The Modern Theory of Contact Angles and the Hydrogen Bond Components of Surface Energies, *Modern Approaches to Wettability*, M. E. Schrader and G. Loeb, eds., New York: Plenum Press (1992).

33. Cheng, D. “Surface Free Energy of Asphalt-Aggregate System and Performance Analysis of Asphalt Concrete based on Surface Free Energy.” Ph.D. Dissertation, Texas A&M University, College Station, Texas (2002).

34. Kim. S.H., D.N. Little, E. Masad, and R. L. Lytton. “Determination of Anisotropic Moduli Considering Aggregate Particle Shape and Gradation in Unbound Granular Layer” *Paper Presented at the 83rd Annual Meeting of the TRB*, Washington D.C., January (2004)

35. Daniel, J. S., and Y. R. Kim, “Development of a Simplified Fatigue Test and Analysis Procedure Using a Viscoelastic, Continuum Damage Model,” to be presented at the Annual Meeting of the Association of Asphalt Paving Technologists, March 18-20 (2002).

36. Lytton, R.L. “CVEN 689, Special Topics in Micromechanics of Civil Engineering” Graduate Civil Engineering Course offered in Fall 2001, Texas A&M University, College Station, Texas (2001)

37. Wen, H., and Y. R. Kim, “A Simple Performance Test for Fatigue Cracking of Asphalt Concrete Based on Viscoelastic Analysis of Indirect Tensile Testing and Its Validation Using WesTrack Asphalt Mixtures,” presented at the 81st Annual Meeting of the Transportation Research Board, Washington, D.C., January 13-17 (2002).

38. *Pocket Facts*. Traverse Area Determination: Double Meridian Distance Method http://www.tpub.com/content/engineering/14070/css/14070_136.htm Accessed April 2004 (2004).

39. Marek, C.R., and M. Herrin, "Tensile Behavior and Failure Characteristics of Asphalt Cements in Thin Films," *Proceedings of the Association of Asphalt Paving Technologists*, Atlanta, Georgia, February 26-28, pp 386-421 (1986).

40. Maugis, D. *Contact, Adhesion and Rupture of Elastic Solids.* Springer, New York, pp. 3-12 (1999).

41. Liu, M., et al. *The Kinetics of Carbonyl Formation in Asphalt.* Aiche Journal, Vol. 42, pp. 1069-1076 (1996).

42. Welborn, J.Y., *Physical Properties as Related to Asphalt Durability: State of the Art.* Transportation Research Record No. 999, pp. 31-36 (1984).

43. Kandhal, P.S., and Koehler, W.C. *Significant Studies on Asphalt Durability: Pennsylvania Experience.* Transportation Research Record No. 999, pp. 41-50 (1984).

44. Ruan, Y., R.R. Davison, and C.J. Glover, *An Investigation of Asphalt Durability: Relationships between Ductility and Rheological Properties for Unmodified Asphalts.* Petroleum Science and Technology, pp. 231-254 (2003).

45. Vassiliev, N.Y., R.R. Davison, and C.J. Glover, *Development of a Stirred Airflow Test Procedure for Short-Term Aging of Asphaltic Materials.* Bituminous Binders, pp. 25-32 (2002).

46. Vassiliev, N.Y., et al., *Air Blowing of Supercritical Asphalt Fractions.* Industrial & Engineering Chemistry Research, pp. 1773-1780 (2001).

47. Stegeman, J.R., et al., *Compositional and Physical Properties of Asphalt Fractions obtained by Supercritical and Solvent Extraction.* Fuel Science & Technology International, pp. 767-794 (1992).

48. Davison, R.R., et al., *Size Exclusion Chromatography of Asphalts.* Chromatographic Science Series, pp. 211-247 (1995).

49. ASTM D 113 – 86. "Standard Test Method for Ductility of Bituminous Materials", Annual Book of ASTM Standards, 04.03, ASTM, Easton, Maryland, 23 (1994)

50. Jemison, H.B., et al., *Application and use of the ATR, FTIR Method to Asphalt Aging Studies.* Preprints - American Chemical Society, Division of Petroleum Chemistry, pp. 490-495 (1990).

51. Liu, M., et al., *Oxygen uptake as Correlated to Carbonyl Growth in Aged Asphalts and Asphalt Corbett Fractions.* Industrial & Engineering Chemistry Research, pp. 466-467 (1998).

52. Uzan, J., "Asphalt Concrete Characterization for Pavement Performance Prediction," *Journal of the Association of Asphalt Paving Technologists*, Vol. 65, pp. 573-607 (1996).

53. Paris, P., and Erdogan, F. "A Critical Analysis of Crack Propagation Laws". Journal of Basic Engineering, Vol. 85, pp. 528-534 (1963).

54. Schapery, R. A. "Correspondence Principles and a Generalized J-Integral for Large Deformation and Fracture Analysis of Viscoelastic Media." *Int. J. Fracture*, Vol. 25, pp.195-223 (1984).

55. Schapery, R.A. Theory of Crack Growth in Viscoelastic Media, Technical Report No. 2, Mechanics & Materials Research Center, Texas A&M University, College Station, Texas (1973).

56. *Pocket Facts.* NCHRP 1-37A Pavement Design Guide. 2002 Design Guide. http://www.2002designguide.com/ http://www.trb.org/mepdg/ http://www4.trb.org/trb/crp.nsf/All+Projects/NCHRP+1-37 Accessed December (2003).

57. AASHTO Designation: TP 62-03. Standard Method of Test for Determining Dynamic Modulus of Hot Mix Asphalt Concrete Mixtures. Washington D.C. (2003).